Effect of the number of ribs on the aircraft wing gross weight.

by
Tomas Marczi

A thesis submitted to the Faculty of Engineering,
at the University of Glasgow
in fulfilment of the requirements for the degree of

Master of Science

University of Glasgow
Department of Aerospace
Engineering
June 2002

Acknowledgment

I would like to thank the BAE Systems and Dr. Smrcek for the great opportunity to study at the University of Glasgow, what I consider as an extremely valuable professional and life experience. I also want to thank Mrs. and Mr. Black for their care and time, which they spent with me helping to improve my English.

Summary

The aim of the project is to develop a calculation process for the influence of the number of uniformly distributed ribs along the span of a two spar wing on the wing gross weight. The project is mainly concerned with the preliminary design of an Ultra Light Aircraft (ULA) or Very Light Aircraft (VLA) wing structure, when the structures engineers have no clear conception of the dimensions and detailed layout of the wing's internal structure. The developed calculation process is presented on one simple wing model. The estimation of the influence of the number of uniformly distributed ribs on the wing gross weight is based on the calculation of the minimum dimensions of the wing's internal structure components. The solution process is then adapted to in the structure calculation for three different spar load ratios and three different spar boom shapes.

The project will be presented in four main parts: (i) Description of Model Used (Idealization), (ii) Aerodynamic Load Calculation, (iii) Minimal Structure Dimensions Calculation and (iv) Results Analysis.

The first part of the project addresses the complicated calculation of the minimum dimensions of the wing structure. The analysis of the dependences between the internal wing structure dimensions and the appropriate simplifications used in the minimum dimensions calculation procedure are explained.

The second part of the paper is concerned with the aerodynamic loading of the wing. Here the aerodynamic conditions are defined, from which the aerodynamic load distribution along the wing span is calculated. Also the analysis and extension of the German BVF method (chapter 9.1) for the chordwise pressure distributions is described.

Using the comparison of wings according to their weight, the third part of the project calculates the minimum dimensions of the wing structure components. For these calculations, the equations of stress/strength equilibrium and geometric characteristics were combined to give the minimum dimensions. During the investigation of spar and boom geometry, an extension of the Gerard Method (E.F. Bruhn, 1973) (used for crippling stress calculations) was developed with the results are presented in the Appendix.

The results of the investigation of the influence of the number of ribs uniformly distributed along the wing span are analysed and presented in the last part of the paper. An assessment is also made of the influence of aircraft weight on the calculation process and the resulting minimum dimensions. In addition, CFD and FEM calculations of one of the wing model layouts was performed for comparison purposes.

Table of Contents

Notation

a	- Longer dimension of thin plate
a_D	- Width of lower flange of rib
a_U	- Width of upper flange of rib
A_{Bcom}, $A_{Boom\ minimum}$	- Boom's cross-sectional area
A_{Eff_Skin}	- Cross-sectional area of skin's effective width
A_{Eff_Web}	- Cross-sectional area of web's effective width
A_{ef_RUSK}	- Cross-sectional area of skin's effective width of upper rib's flange
A_{ef_RLSK}	- Cross-sectional area of skin's effective width of lower rib's flange
A_L	- [L] bar cross-sectional area
A_{RU}	- Cross-sectional area of upper rib's flange
A_{RL}	- Cross-sectional area of lower rib's flange
b	- Aerodynamic chord of the wing section; in chapter "Weight Optimisation Analysis" dimension of non-symmetrical [L] bar
$b(z)$	- Wing sections' aerodynamic chord distribution along the wing span
b_H, b_D	- Boom's dimension (upper, lower), see Figure 4.2
B, B_H, B_D	- Boom's dimension (upper, lower), see Figure 4.2
b_k	- Flap's length
b_s	- Shorter side dimension of thin plate
c^{α}_{Loo}	- Slope of the linear part of the lift line
$c^{\alpha}_{L}(z)$	- Distribution of the gradient of the linear part of the lift line along the wing span
$c_{L\delta}$	- Lift coefficient of wing section with tilted flap
$c_{L\,z0}$	- Lift coefficient at the wing root section (BVF method adjustment)
$c_{L\,z1}$	- Lift coefficient at the examined wing span station
c_{T0}	- Zero lift torque moment coefficient
E	- Young's modulus
E_F	- Young's modulus of the front spar
E_R	- Young's modulus of the rear spar
$f_L(\Theta)$	- Function used in the calculation process of BVF method (defines the chordwise pressure distribution "caused" by the resulting lift force; the resulting pressure force is acting in 0.28% of the wing section's chord

	length; see Figure 9.1)
$f_T(\Theta)$	- Function used in the calculation process of BVF method (defines the chordwise pressure distribution with zero resulting force, which gives the torque moment along the point in 28% of the wing section chord length – $[c_{T0}]$ torque moment; see Figure 9.1)
$f_\delta(\Theta,\phi)$	- Function used in the calculation process of BVF method (defines the chordwise pressure distribution with zero resulting force, which characterizes modification of the torque moment along the point in 28% of the wing section's chord length "caused" by the flap deviation; see Figure 9.1)
$\mathbf{f}^*$	- axial force in FEM bar elemnt
F	- Boom's axial force
F_D	- Axial force of lower boom
F_H	- Axial force of upper boom
F_{RS}, F_{RL}, M_B	- Forces and moment of equilibrium in [B-B] section of the rib (Figure 4.9)
F_{RU}, F_{RL}	- Axial forces in the rib's flanges in [B-B] section of the rib (Figure 4.9)
F_1, F_2	- Spars' shear forces
g	- Gerard's coefficient – number of flanges which compose the composite section (E.F. Bruhn, 1973)
G	- Shear modulus
h_{ef}	- Spar's effective height
h_{ef_F}	- Front spar's effective height
h_{ef_R}	- Rear spar's effective height
H_I	- Spar's height
H_R	- Rib's height
H, H_H, H_D	- Boom's dimension (upper, lower), see Figure 4.2 or Figure 4.3
h, h_H, h_D	- Boom's dimension (upper, lower) , see Figure 4.2 or Figure 4.3
i	- Radius of gyration
I_z, I_{zT}	- Moment of inertia
I_F	- Moment of inertia of the front spar cross-section
I_R	- Moment of inertia of the rear spar cross-section
$\mathbf{k}^*$	- Member stiffness matrix
k_s	- Buckling coefficient which depends on the edge boundary conditions and model plate aspect ratio (a/b)
k_T	- Correction coefficient used in the adjustment of BVF method

L	- Aerodynamic lift
m	- Number of stations selected (according to the Figure 3.3, m = 7)
M_T	- Aerodynamic torque moment
M_o	- Bending moment
M_z	- Torque moment
p	- Aerodynamic pressure
$p_{(x)}$	- Chordwise pressure distribution
q	- Dynamic pressure
q_{F1}, q_{F2}	- Shear flows caused by spars' shear forces F_1, F_2
q_{FW}	- Shear flow of front spar's web
q_{RW}	- Shear flow of rear spar's web
q_p	- (general) shear flow
q_s	- Skin's shear flow
q_T	- Torque moment shear flow
q_1, q_2, q_3, q_4	- Rib's shear flows
R_{1x}, R_{1y}, R_{3x}, R_{3y}	- Reaction forces from leading and trailing part of rib
s_1, s_2, s_3	- Developed length of the skin
t	- (general) thin plate thickness
t_f	- Flange thickness
t_w	- Web thickness
t_L	- [L] bar's thickness
t_s, t_{s1}, t_{s2}, t_{s3}	- Skin's thickness
t_{RibW}	- Rib's web thickness
t_{RH}	- Thickness of upper rib's flange
t_{RD}, t_{RD_min}	- Thickness of lower rib's flange
t_W, t_{FW}, t_{RW},	- Web's thickness
T_y	- Shear force
T_1, T_2, T_3	- Aerodynamic forces acting on the particular parts of rib
$\mathbf{u}^*$	- Member joint displacement
U, U_1, U_2	- Cross-sectional area of wing's torque cell
v_{oo}	- Air flow speed
w, w_{Eff_Skin}	- Skin's effective width
w_{RS}	- Skin's effective width of upper rib's flange
w_1, w_{Eff_Web}	- Web's effective width
x^*	- Chordwise position, in which the pressure is calculated

x_L - Chordwise position of lift force

x_1, x_2, x_3 - Positions of forces T_1, T_2, T_3

x_OEO - Position of shear center

x_Spar - Spars' distance

x_B - Distance of [B-B] section of the rib (Figure 4.9)

y_T, $y_T{}^*$, y_{TH}, $y_{TH}{}^*$, y_{TD}, $y_{TD}{}^*$ - Distance of boom's center of gravity (upper, lower)

y_U, y_L, y_{U_B}, y_{L_B} - Distance from centroidal axis (Figure 4.9)

z - Selected span station at which the circulation value is desired; station distance from the root section

z_1 - Location of the vortices causing decrease of the circulation

Z - Section Modulus

α_{oo} - Geometric angle of attack

α_i - Induced lift angle of attack

α_{eff} - Effective angle of attack ($\alpha_{eff} = \alpha_{oo} - \alpha_i$)

$\alpha_{eff}(z)$ - Distribution of the aerodynamic angle of attack along the wing span

γ - Non-dimensional circulation (expressed by Multhopp)

Γ - Circulation

δ - Angle of flap deviation

Θ_v - Multhopp's angle defined the station spanwise position

Θ - Geometric coefficient used in the BVF method (depends on the ratio [x*/b])

ϕ - Geometric coefficient used in the BVF method (depends on the ratio [b_k/b])

ν - Identifying subscripts of a particular span station where the circulation is to be found (according to the Figure 3.3, "ν" is any number from one to seven)

μ - Poisson's ratio

η - The span stations

η_δ - Lift efficiency coefficient used in the BVF method

ρ_∞ - The free flow's air density

π - Ludolf's constant

σ_{Boom} - Boom's stress

σ_{CR} - Boom's crippling stress

σ_{FRC}	- Rib's flange stress
σ_U	- Ultimate stress
σ_Y	- Yield stress
τ, τ_{CR}	- Critical buckling shear stress of thin plate

Abbreviation:

UL	- Ultra Light
ULA	- Ultra Light Aircraft
VL	- Very Light
VLA	- Very Light Aircraft
MDO	- Multidisciplinary Design Optimisation

Notation in presented graphs:

UF_Boom	- Upper Boom of Front Spar
LF_Boom	- Lower Boom of Front Spar
UR_Boom	- Upper Boom of Rear Spar
LR_Boom	- Lower Boom of Rear Spar
F_Web	- Front Spar Web
R_Web	- Rear Spar Web
Skin	- Skin except the trailing sections of the wing
Ribs	- Ribs except the trailing section

1 Introduction

When the first attempts to fly were made, it was realized that weight plays the most significant role in the design of flight vehicles. Lighter-than-air flight vehicles were the first successful solution to man's attempts to overpower earth's gravity. However, aerostats have only limited usefulness hence man's attempt to conceptualise heavier-than-air flying machines.

As a consequence, the airplane's weight becomes one of the most important parameters; by the late 1930's most of the major aircraft companies had separate weight engineering staffs. At that time the aeronautical engineering specialty of weight engineering, or mass properties was established, which predicts and controls the weight and centre of gravity of new aircraft designs. However, the relations between the size, design or arrangements of the parts of the airplane structures and the aircraft weight were investigated even before, as shown by E. Everling (1923) or Ch.W. Hall (1924).

After World War II, new materials and jet engines were developed, which allowed aircraft speeds to increase. Due to these new developments, aircraft weight prediction became even more complicated. The requirements that emphasized the impact of dynamic pressure and aerodynamic flutter then also had to be considered (Spearman L. M., 1994).

Weight prediction plays one of the most important roles, before and during aircraft design. Thus, the weight prediction and weight calculation have to be done at all stages of the aircraft design. The design process, from the conceptual stage to the detail design stage, can be graphically expressed as a converging iterative spiral shown in Figure 1.1 (Fielding J.P.,1999). Here it can be seen that the parameter "WEIGHTS" occurs in all stages of the design of a new aircraft.

Previous work in the investigation of the effect of the number of ribs on the wing gross weight was undertaken by A.F. Zahm (1920) and J.A. Newlin (1930). However, their work has related to that time wooden wing design with linen cover. Since the metal aircraft have been produced, the weight estimation methods were improved and have started to deal with whole parts of the airplane or aircraft structure. This is clearly seen specially at the comprehensive analysis made by F.R. Shanley (1952) followed by intriguing approach to structure weight estimation presented by W.E. Caddell (1969) and later used and extended by E. Torrenbeek (1972). The modern methods used in the present time based on the Multidisciplinary Design Optimization (MDO), statistical techniques and response surface modeling methodologies. Comprehensive analysis of these techniques has been presented by A.A. Giunta (1997). However, none of the above have considered UL aircraft wing and the relationship between the boom geometry, spar load ratio and wing gross weight according to the number of ribs. These

relationships can be used in the preliminary design stage for making decision about the particular wing layout, quick estimation of wing weight or checking the reasonability of estimates obtained trough other methods.

In the presented thesis the method is developed for estimation of optimum layout of the rectangular, two-spar wing in the preliminary stage of UL aircraft design. The calculation was done for three different spar load ratios and three different boom geometries. The main variable in the calculation process has been the number of ribs and dependent variables have been all dimensions of internal structure components. The presented thesis is continuation of author's previous research (Marczi T., 2001).

For the accurate prediction of an aircraft weight, it is useful to know the relationship between the aircraft structural components according to the components' weight. The weight estimation error would have a far-reaching effect and could be the main reason for an unsuccessful design. It is obvious that the design of a structure with optimal weight is a difficult and long - winded process. If the weight of some structure component is increased for some reason, it means adding weight elsewhere, which leads to increased airplane gross weight.

According to J.E. Younger (1942), the weight of geometrically similar bodies varies as the cube of their corresponding dimensions. If a cubical block is doubled in size, that is, if each edge is doubled in length, its volume and weight will be eight times the volume and weight of the original block. Likewise, an airplane doubled in size will be eight times as heavy, assuming, of course, that geometrical similarity is maintained. An airplane doubled in size, however, has only four times the wing area.

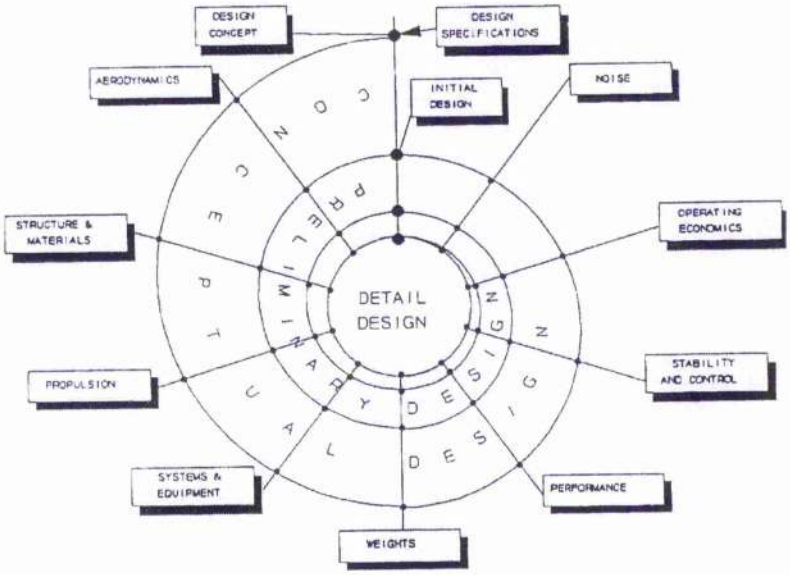

Figure 1.1 – The design spiral (source: Fielding J.P., 1999)

The estimation of the weight of a conceptual aircraft is a critical part of the design process. The general weight analysis usually deals with large portions of the structure (Shanley F.R., 1952; Raymer D.P., 1999), such as the wing, fuselage, landing gear, control surfaces, etc. In the case of treating large structures as a unit, the situation is more complex, since the loads and allowable stresses may both vary throughout the length or the body under consideration. However, the presented project is focused on the more particular parts of the airplane structure.

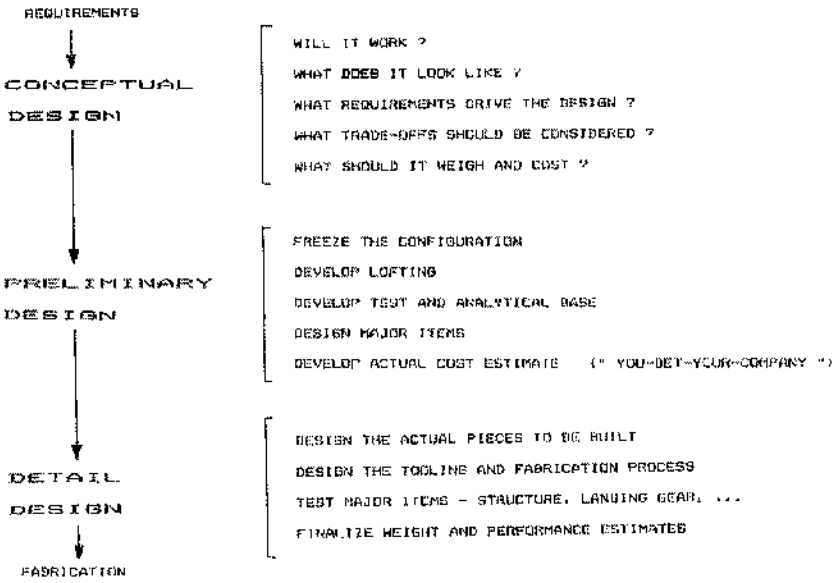

Figure 1.2 - The phases of aircraft design (sorce: D.P. Raymer, 1999)

As Figure 1.1 shows, the Aircraft design can be broken into three major phases: Conceptual Design, Preliminary Design and Detailed Design. The Figure 1.2 explains what is involved in the particular design stages. In the preliminary stage of the airplane design the major changes are over. The configuration arrangement can be expected to remain about as shown on current drawings, although minor revisions may occur. However, the particular dimensions of the wing internal structure components are still unknown. The main purpose of this project is to develop a method for the numerical calculation of the minimum (preliminary) dimensions of the wing structure in the preliminary stage of a UL or VL airplane design. Then, to calculate several wing layouts, differing only in the number of ribs used. The ribs of the wings involved in the calculation are distributed uniformly along the wing span. Due to the relation of minimum dimensions to the minimum weight of the structure, it is possible to compare those wings according to their weight. Such comparisons will illustrate the influence of the number of ribs uniformly distributed along the wing span on the wing gross weight. Since the number of ribs in

this analysis is the prime variable, the wing structure is calculated for the number of ribs increasing from two to fifty on half the wing span. Obviously a number of ribs such as fifty is used for academic purposes only; a real wing structure of a UL or VL aircraft would not have as many.

In order to investigate the ribs' influence on the wing gross weight, the wing internal structure design (Figure 1.3), wing geometry (P.S.Zink et al., 1999) (Figure 1.4), and the shape of particular wing internal structure components need to be involved in the investigation. Also the span load affects the wing structural weight (S.Iglesias, 2001) and can be involved in the investigation. The solution of such a task with so many variables results in lengthy calculations with a huge number of variables, as well as a large number of possible solutions.

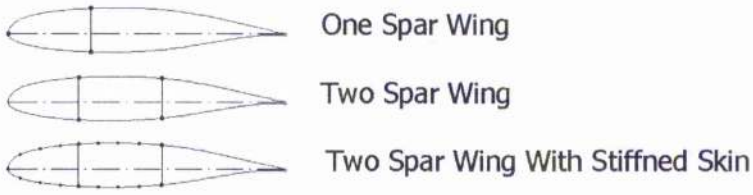

Figure 1.3 - Wing internal structure layout

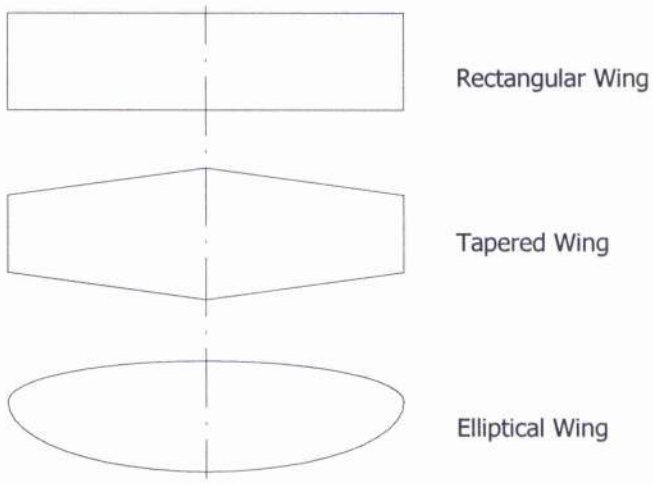

Figure 1.4 – Typical wing geometry.

For example, if only the shape of the wing is considered, it is commonly known is that a swept wing is heavier than a straight wing (Stinton D., 1966; Leland M. N. 1975). The aspect ratio and the thickness/chord ratio of the aerofoil sections used are the two most important

factors in the effect of the wing geometry upon the wing weight, performance and stability (J.Weil, 1951). The aspect ratio is a function of the span. Therefore, the greater the aspect ratio of a wing, the greater the bending moment of the lift at the root. A high aspect ratio wing compares to a wing of lower aspect ratio with the same area in that it has usually less actual thickness, and consequently a smaller depth of spar (which cause the higher end-loads in the booms). The effect of aspect ratio on the weight of the wing is very marked, as shown in Figure 1.5. A wing with a higher aspect ratio carries its lift further out from the root and the bending moments, boom sections, and weights are larger than those of a wing of smaller aspect ratio. However, the previous statement cannot really be generalized, because once the aspect ratio is calculated for a given aircraft a decrease in the value (signifying a smaller span) results in an increase in structure weight.

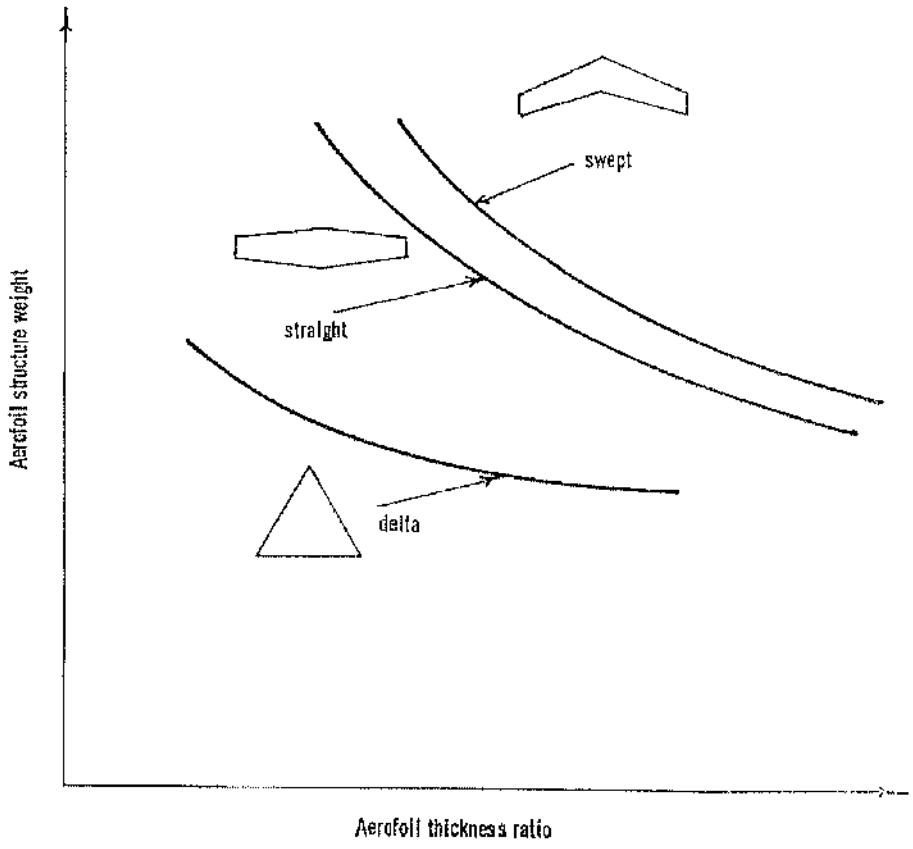

Figure 1.5 – General trend of wing weight for different planforms lifting same all-up weight (source: Stinton D., 1966)

The results of the investigation of the effect of aspect ratio on the wing gross weight can be seen in Figure 1.6. There is an optimum aspect ratio wing, and increase in structure weight at smaller aspect ratios is caused by the additional wing area needed to compensate for the decreased efficiency of the wing as a lifting member. On the other hand, the increased weight at higher aspect ratios is caused by the need to meet increased bending moments. Obviously, the optimum aspect ratio depicted in Figure 1.6 is specific for each wing and is function of the particular airplane design specification and mission requirements.

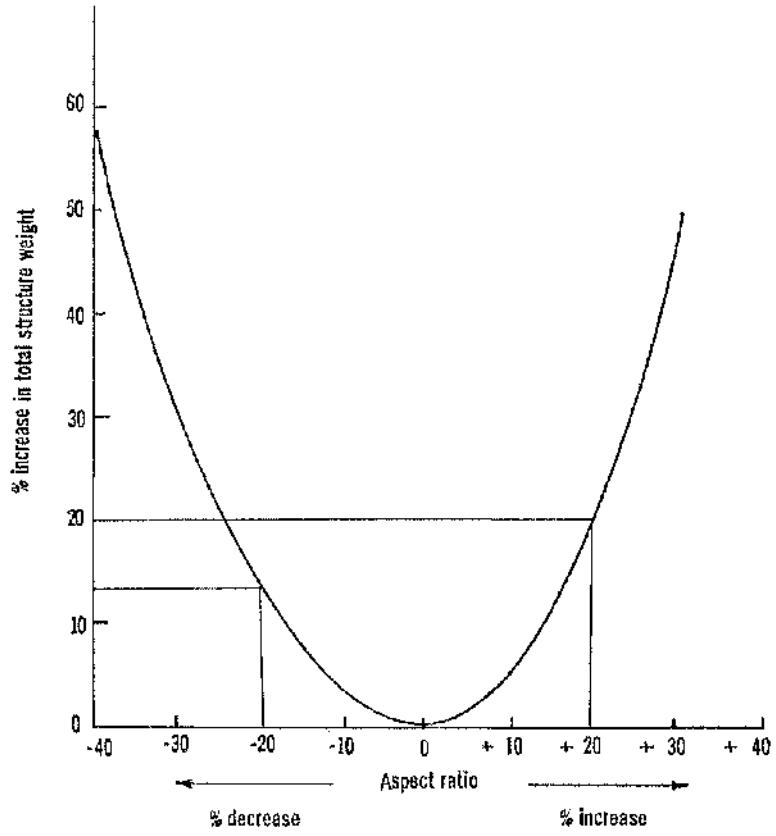

Figure 1.6 – Change of aspect ratio from the calculated "ideal" for a given aircraft upon the total structure weight (section thickness/chord ratio constant). (source: Stinton D., 1966)

The investigation of the influence of the number of ribs on the gross wing weight has to be calculated according to the aerodynamic load acting on the wing. The greatest air loads on an aircraft usually come from the generation of lift during high [g] maneuvers. Generally, these flight conditions are depicted in the [V-n] diagrams known as The Maneuvers Envelope (Figure 1.7) and The Gusts Envelope (Figure 1.8). The [V-n] diagram on Figure 1.8 is combined with Figure 1.7 to determine the most critical limit load factor at each speed.

However, this project does not analyse the wing of some particular airplane; the [V-n] diagrams are not specified. Moreover, it can be deduced that different wing load conditions result in different optimum numbers of ribs. Also, for a different wing geometry, different results from the presented calculation can be expected. Therefore, the process of the calculation developed in this thesis can not give general information about the effect of uniformly distributed ribs along the wing span for a two-spar wing. Thus, the preliminary optimum number of ribs has to be calculated separately for each new wing structure project. Consequently, this project will solve for only one particular flight condition, assumed as the worst load condition acting on the wing model investigated.

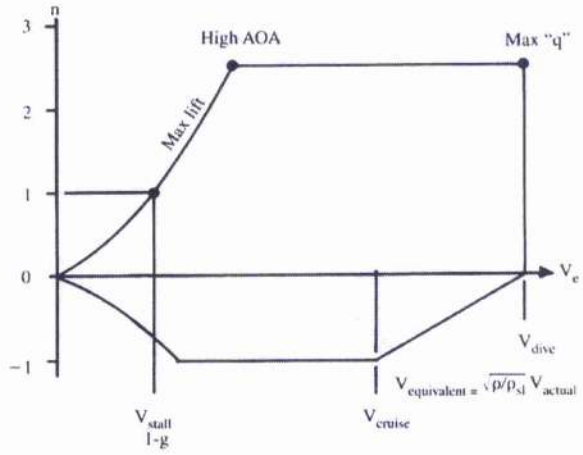

Figure 1.7 – V-n diagram (Maneuvers' Envelope) (source: Raymer D.P., 1999)

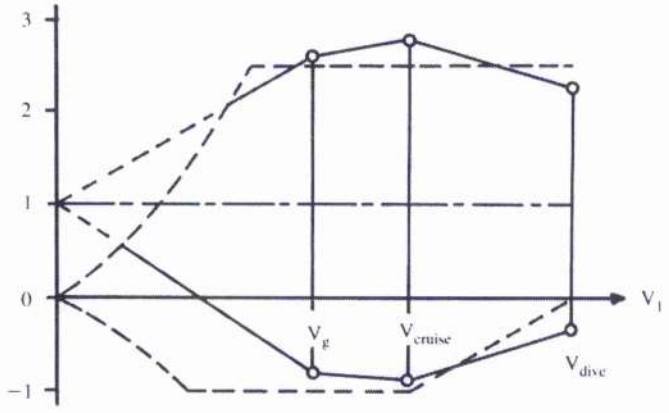

Figure 1.8 – V-n diagram (Gusts' Envelope) (source: Raymer D.P., 1999)

It is clear that the use of uniformly distributed ribs along the wing span does not correspond to real wing structures; however, the optimisation of the non-uniform spacing of the ribs on the wing span is beyond the scope of this project, though could be done as the next step or extension of the presented thesis. Attempts to optimise the ribs spacing have been made from the very beginning of avionic history (A.F.Zahm, 1920; J.A.Newlin, 1930).

The input data in this thesis are the wing model geometry and the flight conditions (assuming that the conditions cause the greatest aerodynamic load). The aerodynamic load for the particular flight conditions is calculated and consequently used in the structure calculation. In contrast with the general weight-analysis, which deals with large portions of the structure, this project tries to inherit the more detailed calculation of wing structures components, such as booms, spars web, skin. The effects of how the wing internal structure design and structure components layout distribute the aerodynamic load to the wing structure can be considered. For example in the simple spar wing structure (the spars, ribs and non- stiffened skin only), the bending moment is carried by the spars' booms, shear force is carried by the spars' webs and torque moment is carried by the cells or by the spars in the case of a wing with non-stressed skin (L.Ballenstedt, 1923, P.Kuhn, 1934).

The ribs hold the shape of the wing and carry the load from the aerodynamic pressure and the reaction shear flows from the skin and spars' webs. According to the E.E. Lundquist (1942), the main purpose of the rib in a stressed-skin wing is to stabilize the compression flange. In the performance of this function, the rib acts as a beam or a truss spanning the distance between the shear webs. The ribs are also used for the distribution of the external loads on the wing, such as engines, weapons and the loads caused by the flaps and ailerons.

Figure 1.9 shows the wing model used in the calculation. The calculation method developed in this project is based on the calculation of the minimum dimensions of spars' booms, web, skin and ribs. The consequence of minimum dimensions of wing structure components is the minimum weight of the wing for the particular number of ribs used.

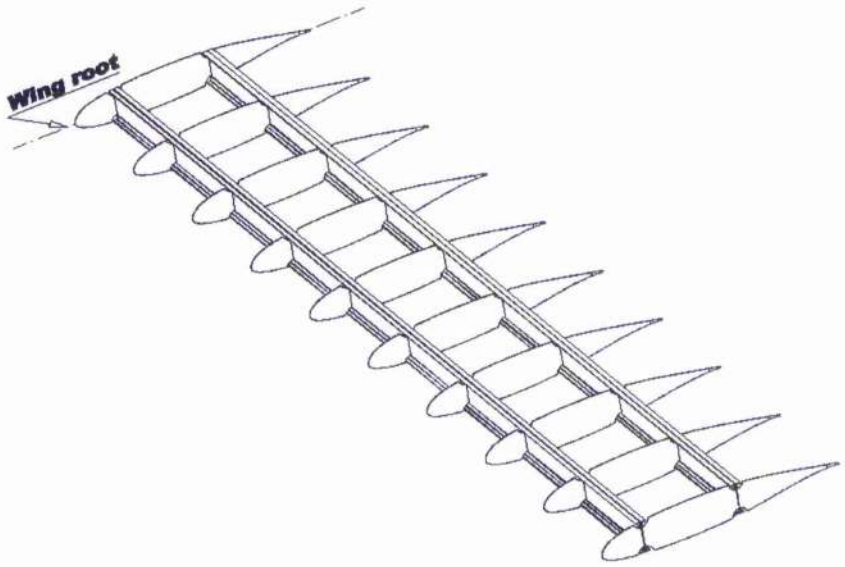

Figure 1.9 – One of the wing layout used in the calculation process

The final results are graphically expressed to show the dependence of the internal structure components weight and gross wing weight on the number of ribs used.

1.1 Current Trends in the Weight Engineering

As mentioned above, the general weight analysis usually deals with large portions of the structure such as the wing, fuselage, etc. Nowadays, most of the weight predictions are based on the Multidisciplinary Design Optimization (MDO) techniques. These techniques incorporate the influences of Aerodynamics, Structural Mechanics, Dynamics and Controls.

There are several computer programs which perform aircraft MDO e.g. ACSYNT, ASTROS or ELAPS.

- ACSYNT (Aircraft Synthesis Computer Program) is an integrated design tool used in the modeling of advanced aircraft for conceptual design studies. ACSYNT development began at NASA Ames Research Center in the 1970s and continues to this day (M.D. Ardema et.al., 1996).

- ASTROS (Automated Structural Optimization System) is a code to design the minimum weight wing subject to a large number of stresses, strain, displacement and flutter constraints. It was developed for and by the Flight Dynamics Laboratory, Air Force

Wright Aeronautical Laboratories and has been continuously upgraded (P.J. Rohl et.al., 1995).

- ELAPS (Equivalent LAminated Plate Solution) is a design-oriented structural analysis tool developed at the NASA Langley Research Center over the past 20 years. ELAPS is based upon the equivalent plate theory (M.G. Sexstone, 1998).

The MDO computer programs can be combined into one optimization process. J. Rohl et.al. (1995) decomposed the structural design of the high-speed civil transport wing into three levels. In each level they used different MDO computer program, with a purpose to gain the optimum shape of the wing given the deformation in cruise flight.

Programs such as ACSYNT traditionally use only empirical estimation methods. They can be used however, in the more analytical optimisation of the aircraft structure as the M.D. Ardema et.al. (1996) proved in their extensive research.

Despite the presence of these MDO computer programs, high fidelity aircraft system MDO remains computationally intractable (A.A. Giunta, 1997). Several of the novel modelling methods employ statistical techniques based on design of experiments theory and response surface modelling methodologies (A.A. Giunta, 1997). Together with MDO computer programs the response surface provide an effective solution of the optimising process. This combination is often used in the preliminary and conceptual design optimisation of the complex aircraft structures. G. Li et.al. (1999) used two level optimisation process during the preliminary design of the multi spar wing structure. The variable parameters were the number of ribs, spars, aspect ratio and sweep angle. The design criteria were max. displacement, flutter speed and weight. B. Liu et.al. (1999) used two-level optimisation for a composite wing design. The optimised parameter for minimum weight was ply thickness with orientation 0°, 90°, and ±45°.

The Multidisciplinary Design Optimisation (MDO) and response surface modelling are complex methods, which fit for large complex structures. They can provide the optimum layouts of the structure according to several criteria. On the other hand, the MDO methods require specific programs (ACSYNT, ASTROS, ELAPS etc.), appropriate computer performance and the optimizing calculation takes some time. Therefore, for quick estimation of structure weight, various comparisons of existing aircrafts still take place. For example, CH. Svoboda (1999) used component weight data for 61 commercial and general airplanes to develop three relationships: wing weight/reference area as a function of wing loading, empennage weight/reference area as a function of wing loading and fuselage weight/surface area as a function of wing loading.

The UL aircraft category is relatively young and usually out of interest of big aircraft companies. Therefore, their structure is a relatively simple, build from minimum components and geometry of the main parts of the plane (such as wing) vary a little among manufactured UL airplanes. Due to this, the weight prediction mostly remains on the estimation using classical methods based on actual weights of existing aircraft.

2 The Wing Model

In the last few decades Ultra Light (UL) and Very Light (VL) aircraft have become very popular, because of their simplicity and availability for general public. Nowadays, there are many small factories around the world, producing their own VL Airplanes. Those airplanes are certificated according to the ULA or VLA requirements, where one of the most important limitations is aircraft weight. In order to meet ULA and VLA requirements and produce the relatively cheap airplane, the structure of the UL and VL Airplanes is usually very simple. It is also due to technological constraints of the small factories and homebuilders.

2.1 UL and VL Aircraft

This chapter shows some real UL and VL airplanes and are used to define the dimensions of the wing model used in this project. The presented airplanes are mostly built and developed in the Czech Republic.

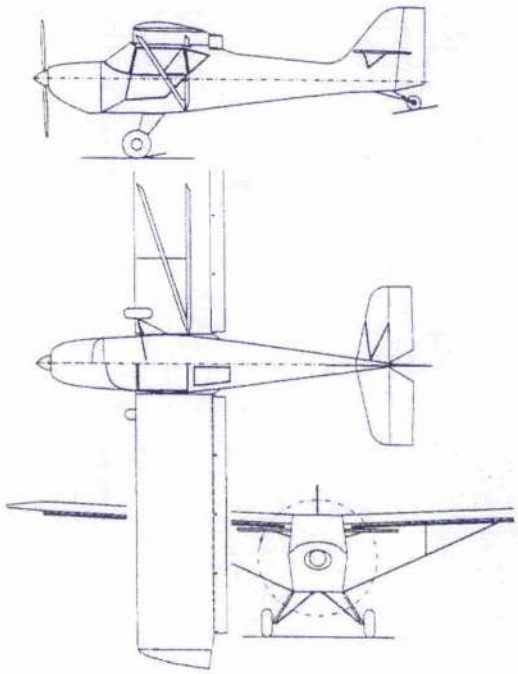

FOX 503Z/582Z/912Z

(EVECTOR a.s. Czech Republic)

Wing Span	9.2 m
Length	6.8 m
Wing Area	11.5 m^2
Empty Weight	220/235/250 kg
Maximum Weight	450 kg
Maximum Speed (allowed)	185 km/h

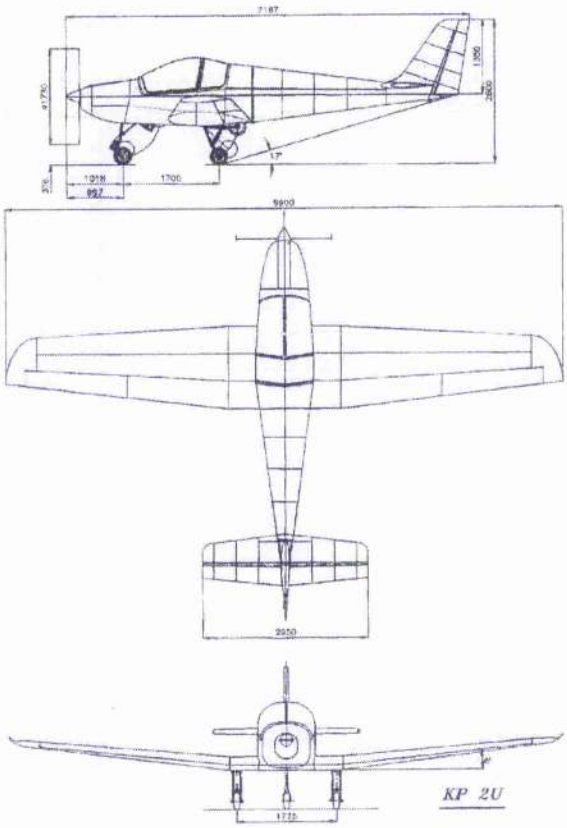

KP 2U – SOVA (OWL)

(KAPPA a.s. Czech Republic)

Wing Span	9.9 m
Length	7.2 m
Wing Area	11.85 m^2
Empty Weight	260 kg
Maximum Weight	450 kg
Maximum Speed (allowed)	260 km/h

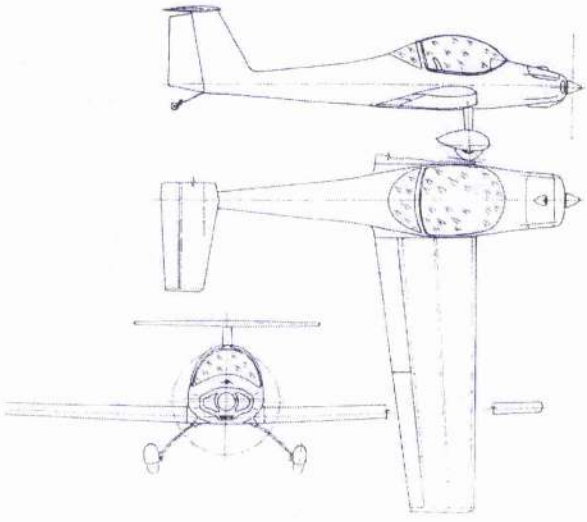

QUALT – 200 L

(BVL Czech Republic)

Wing Span	9.2 m
Length	5.9 m
Wing Area	10.5 m^2
Empty Weight	285 kg
Maximum Weight	450 kg
Maximum Speed (allowed)	250 km/h

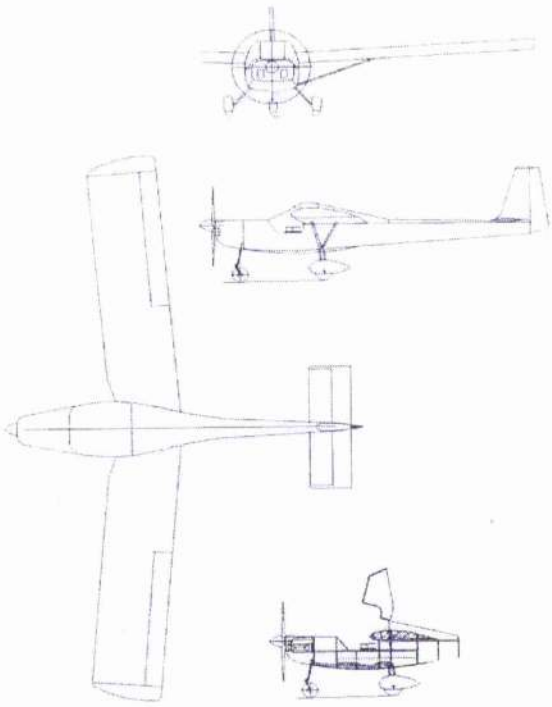

TST – 5 VARIANT

(TeST s r.o. Czech Republic)

Wing Span	10.5 m
Length	6.4 m
Wing Area	13.65 m^2
Empty Weight	260 kg
Maximum Weight	450 kg
Maximum Speed (allowed)	165 km/h

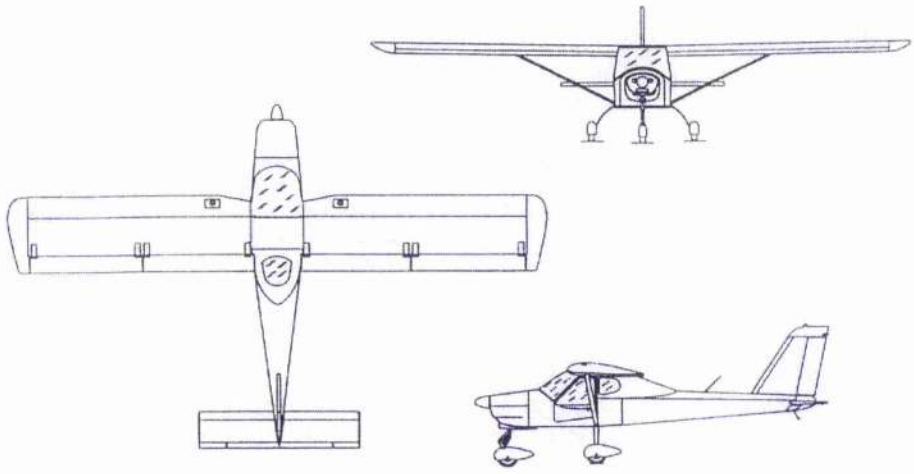

P – 92 ECHO

(TECNAM s.r.l. Italy)

Wing Span	9.6 m
Length	6.3 m
Empty Weight	280 kg
Maximum Weight	450 kg
Maximum Speed (allowed)	210 km/h

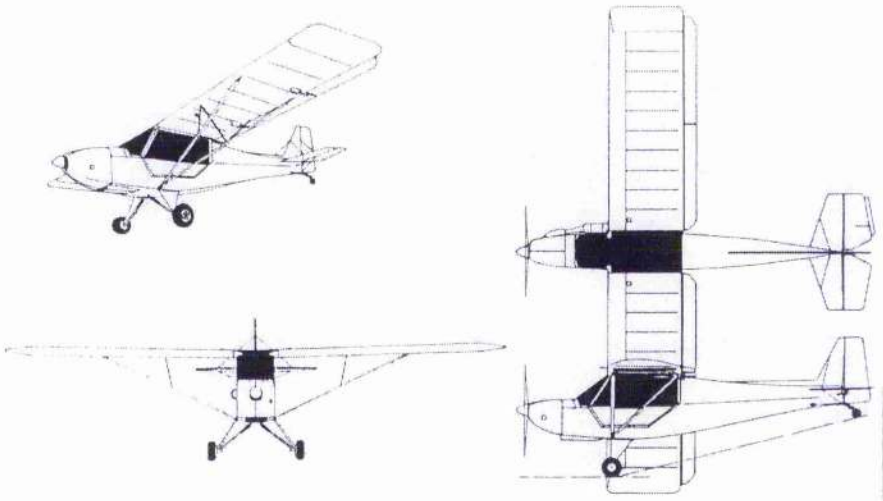

RANS S – 7 COURIER

(RANS USA, BESTAR Czech Republic)

Wing Span	8.91 m
Length	6.4 m
Wing Area	14 m^2
Maximum Weight	465 kg
Maximum Speed (allowed)	193 km/h

There are many other UL or VL airplanes; however, the purpose of this thesis is not to create the database of UL and VL airplanes. The presented samples of UL/VL airplanes give an idea of the kind of airplane this project is aimed at. Also the wing model dimensions and aerodynamic conditions used in the solution process of this project are defined according to the depicted planes.

2.2 Geometry and Internal Structure of the Wing Model Used

As explained in the Introduction, for the purpose of this project only one model of the wing will be used. According to the previous chapter where typical UL/VL airplanes were shown, the simple geometry of the wing model is used in this project. The dimensions (in mm) of the wing model used are depicted in Figure 2.1 and as can be seen, the dimensions of the model were chosen with a purpose of simplicity.

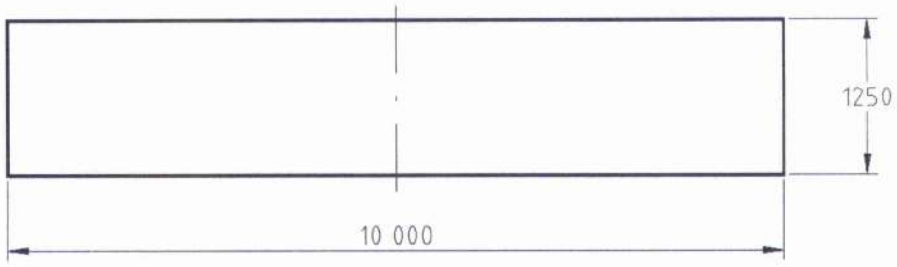

Figure 2.1 – The wing model geometry

Since it is impossible to analyse the wing weight in detail before the structural design is completed, the preliminary wing structure must be "idealised" with certain assumptions. Moreover, one of the main reasons why highly idealised situations are created as a basis for development of engineering formulas is that this process greatly simplifies the resulting equations (Shanley F.R., 1952). Thus the wing model used in this project was idealised to a wing that consists of two [I] shaped spars (Figure 2.2) with constant height over the wing span, and the spars' booms consisting of two [L] profile bars.

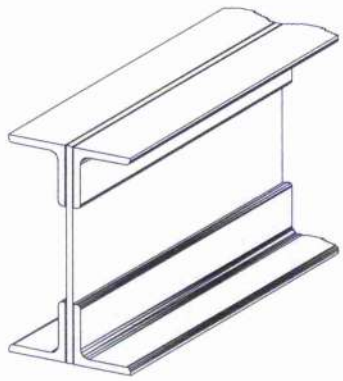

Figure 2.2 – The wing model spar

The spar web is assumed to be buckling resistant without stiffeners and lightening holes. The wing skin is assumed to be without any longitudinal stiffeners (stringers). Obviously, during the bending action the skin panels are loaded by tension (lower surface) or compression (upper surface). Also, during wing bending, the non-stiffened thin skin plate has very poor buckling resistance, and compared with spars, the amount of bending load carried by the non-stiffened skin is almost negligible. However, regarding the weight of the aerospace structures, to neglect this load carrying capacity of the skin would be too conservative. One way of significantly improving the skin participation in the bending action is to use close spaced longitudinal

stiffeners; however, the stiffened skin panel is fairly complex structure and according to A.Gomza (1948) there are particular combinations of stiffener spacing and plate thickness, dependent upon the geometrical properties of the stiffener cross section, for which the panel weight is a minimum. E.H. Schuette and J.C. McCulloch (1947) solved a similar problem in the case of multiweb wing structure used for the thin high-speed planes. The investigation of the optimum spacing and shape of the stiffener cross section could be done as future work.

As the load is increased, the skin buckles between the spars and does not carry any greater stress than the buckling stress. However, as the spars are approached, the skin (being stabilized by the spars to which it is attached) can take the higher stress and immediately over the spar the skin can take the same stress as the ultimate strength of the spar. This assumes that the skin has a continuous connection to the spar (Younger J.E., 1942; J. Špunda, 1955; E.F. Bruhn 1973; A. Píštěk 1987).

According to E.F. Bruhn (1973), various theoretical studies have been made to determine this stress distribution in the skin after buckling. These theoretical studies introduced the term "effective width of the skin" (Younger J.E., 1942; J. Špunda, 1955; E.F. Bruhn, 1973; A. Píštěk 1987), which would be considered as taking uniform stress Figure 2.3, which would give the same total sheet strength as the sheet under the true non-uniform stress distribution Figure 2.3.

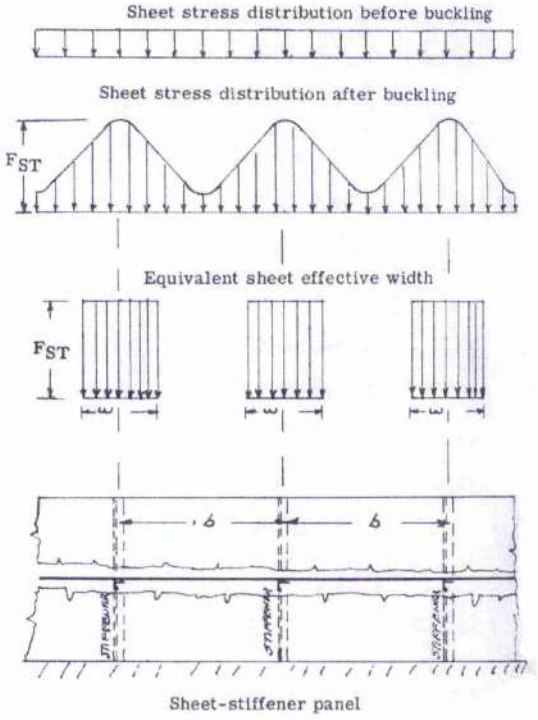

Figure 2.3 - The effective width of the skin (Sorce: E.F. Bruhn, 1973)

Many individuals have considered the question of skin effective width, e.g. Von Karman, Sechler, Timoshenko, Newell, Frankland, Margurre, Fischel, Gerard (E.F. Bruhn 1973).

The method of effective width of the skin is used in this project with the skin thickness calculated from the torque moment load. The effective width of the skin has a direct effect on the size of the necessary boom cross section area (minimum boom dimensions) and consequently saves the wing structure weight.

The next assumptions are made about the material of the wing structure components. The spars booms are assumed to be made from aluminum alloy 7075 (AlZn6Mg2Cu) and the skin and webs of the spars from aluminum alloy 2024 (AlCu4Mg1Mn). The material constants are as follows:

Booms Ultimate stress:	σ_U =	540 MPa
Booms Yield stress:	σ_Y =	440 MPa
Skin/Web Ultimate stress:	σ_U =	407 MPa
Skin/Web Yield stress:	σ_Y =	270 MPa

Aluminum material constants:		
Young's modulus:	E =	$7.2\ 10^4$ MPa
Shear modulus:	G =	$2.7\ 10^4$ Mpa
Poisson's ratio:	μ =	0.33

It can be seen that the dimensions of the internal wing structure components are not defined. It is the aim of the project to define their preliminary size with respect to minimum weight of the structure. The process of the solution will be based on the calculation of minimum dimensions of the defined wing model structure.

2.3 The Analysis of the Aerodynamic Load Distribution to the Wing Structure

As mentioned in Introduction, the aerodynamic load distribution to the wing structure depends on the wing structure type and internal lay-out of the structural components. In the case of the wing model used in this project, the bending moment is carried by the spars and partly by the skin. However, the lift force distribution on the front and rear spar is unknown. Also because of the unknown dimensions of the wing internal structure components the torque moment distribution to the two torque cells wing structure is not explicit. The purpose of this

chapter is to develop the formulas for aerodynamic load distribution to the wing structure, which will be used in the solution process.

2.3.1 The Ratio of the spars' flexural rigidity

Due to the wing model geometry (taper ratio 1, parallel spars with constant heigh) and because the spars dimensions are expected to be minimal the ratio of the spars' flexural rigidity is constant along the wing span. Consequently, the wing model's elastic axis is straight. The straight wing elastic axis the resulting aerodynamic load (Younger J.E., 1942; Špunda J., 1955) into a pure bending and pure torque load (Figure 2.4). According to the idealised wing model described above, the aerodynamic lift force is distributed on the front and rear spar in the ratio of spars flexural rigidity (Slavík S., 1997; Špunda J., 1961).

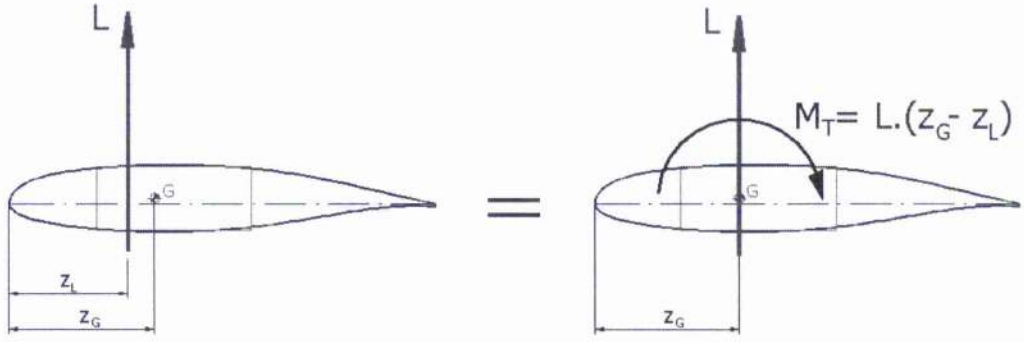

Figure 2.4 – Division of aerodynamic load on the pure torque and pure bending

The distribution of aerodynamic lift force in the ratio of spars flexural rigidities could be done only if the flexural rigidities of the spars are known. Unfortunately, the dimensions of the spars' booms, web and spars itself are unknown, which means that in this stage of the project the flexural rigidities of both spars are unknown as well. Therefore it is almost impossible to define the distribution of the aerodynamic lift on the front and rear spar with appropriate accuracy.

The solution to the presented problem of unknown flexural rigidities of the wing's spars is considered as follows. The cross-sectional area of the spars used can be basically described as in Figure 2.5. Here the characteristics of the spar's cross-sectional area can be written.

Moment of inertia: $$I_z = \frac{B.H^3 - bh^3}{12} \quad \textbf{(2-1)}$$

Section Modulus: $$Z = \frac{B.H^3 - bh^3}{6.H} \quad \textbf{(2-2)}$$

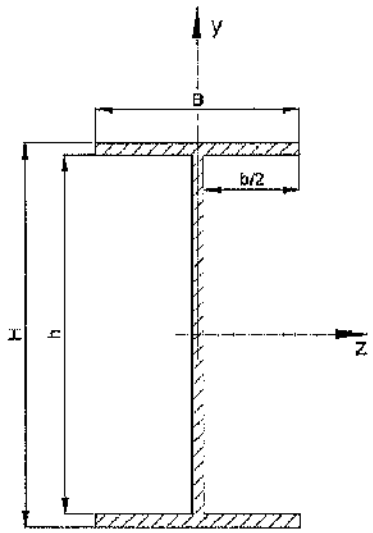

Figure 2.5 – Simplified cross-section of [I] shaped spar

Equation (2-3) represents a well-known relation between the equations (2-1) and (2-2). The parameter [H/2] in the equation (2-3) corresponds to the furthest edge from the [z] axis.

$$I_z = Z \cdot \frac{H}{2} \quad \textbf{(2-3)}$$

The minimum Section Modulus can also be obtained from the equation of stress/strength equilibrium, as equation (2-4) shows.

$$\sigma_U = \frac{M_o}{Z} \Rightarrow Z = \frac{M_o}{\sigma_U} \quad \textbf{(2-4)}$$

Now, consider two [I] shaped spars built from the same materials and used by the same technology. These spars do not have the same dimensions, yet they are geometrically similar. Each spar may be loaded by different bending moments [M_{o1}] and [M_{o2}]. M_{o1} acts on first spar, and M_{o2} on the second spar. Then, according to equation (2-4), the Section Modulus of each spar can be expressed as:

First Spar: $$Z_1 = \frac{M_{o1}}{\sigma_U} \qquad (2\text{-}5)$$

Second Spar: $$Z_2 = \frac{M_{o2}}{\sigma_U} \qquad (2\text{-}6)$$

Due to the fact that the spars are built from the same material, the ultimate stress [σ_U] in equations (2-5) and (2-6) is the same; therefore, the following equation can be written.

$$\frac{M_{o1}}{M_{o2}} = \frac{Z_1}{Z_2} \qquad (2\text{-}7)$$

The equation (2-7) says that the spar load ratio equals the ratio of spar Sections Modulus. The ratio of spars flexural rigidity could be expressed as [E_1I_{z1}/E_2I_{z2}], yet because the same materials are used $E_1 = E_2$. Thus, in this case the ratio of flexural rigidity is simply the ratio [I_{z1}/I_{z2}]. Using relation (2-3), the ratio [I_{z1}/I_{z2}] can be written in equation (2-8).

$$\frac{I_{z1}}{I_{z2}} = \frac{Z_1}{Z_2} \cdot \frac{\frac{H_1}{2}}{\frac{H_2}{2}} = \frac{Z_1}{Z_2} \cdot \frac{H_1}{H_2} = \frac{M_{o1}}{M_{o2}} \cdot \frac{H_1}{H_2} \qquad (2\text{-}8)$$

Equation (2-8) represents the unknown ratio of flexural rigidity of the two spars from this example. Generally, for the spars built from the different materials, equation (2-9) can be used.

$$\frac{E_1.I_{z1}}{E_2.I_{z2}} = \frac{E_1}{E_2} \cdot \frac{Z_1}{Z_2} \cdot \frac{H_1}{H_2} = \frac{E_1}{E_2} \cdot \frac{M_{o1}}{M_{o2}} \cdot \frac{H_1}{H_2} \qquad (2\text{-}9)$$

Equations (2-8) and (2-9) present the fact that the spars' flexural rigidities can be expressed by the spars' load ratio and ratio of spar heights. Thus, chosen spar load ratio indirectly defines the ratio of spars' flexural rigidities, which consequently allows the calculation of the position of wings' elastic axis. Moreover, if the whole structure calculation is performed for the several chosen spar load ratios, the influence of the spar load ratio on the wing gross weight can be calculated. The optimum spar load ratio may then be found. Therefore, the process of wing structure calculation was performed for three spar load ratios. First, the aerodynamic load was distributed equally [1:1] between the front and rear wing spars. Then, the calculation was done for the spar load ratio [2:1] (two thirds of the aerodynamic load was carried by the front spar and one third by the rear spar). The last spar load ratio for which the calculation of the wing structure was performed was [3:1] (three quarters of the aerodynamic load was carried by the front spar and one quarter by the rear spar). These spar load ratios define the magnitude of the bending moment carried by the particular spar.

2.3.2 Booms' Influence on the Wing Structure Components

In the case of the wing skin calculation, the skin thickness is the only unknown dimension. The other dimensions of skin sheet are defined by the distance between two adjacent ribs and by the developed length of the skin loaded by torque moment.

In the case of spar web calculation, one of the "web's sheet" dimensions used in the process of calculation is defined by the distance between two adjacent ribs. The web's sheet height and thickness are unknown. In the calculation, the web's height is assumed as the distance between the booms' centres of gravity (see Figure 2.6); therefore, the height of the web involved in the calculation is a function of a spar booms' dimensions, which are unknown. Hence, the resulting thickness of the spar's web indirectly depends on the booms dimensions as well.

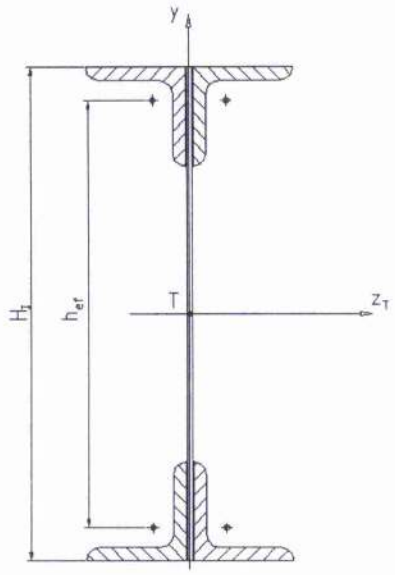

Figure 2.6 – Effective height of the wing spar.

The next complication connected with the spar's effective height relates to the bending moment distribution about the spar booms. According to Figure 2.7, the bending moment is represented by two axial forces [F_H] and [F_D] (Špunda J., 1955), which are carried by spar booms. The lever arm length of these two axial forces is equal to the spar effective height. For that reason, the axial forces [F_H] and [F_D] are functions of boom dimensions as well.

From what is written above, it can be seen that the spar boom dimensions influence the dimensions of almost all wing structure components. Moreover, the skin's and web's effective width (Younger J.E., 1942, J. Špunda, 1955, E.F. Bruhn 1973, A. Píštěk 1987) (Figure 4.4) are involved in the calculation process of bending moment distribution. The relation between the spar boom dimensions and spar effective height, the booms axial forces and effective width of the skin and web present some kind of feed-back or loop in the calculation process.

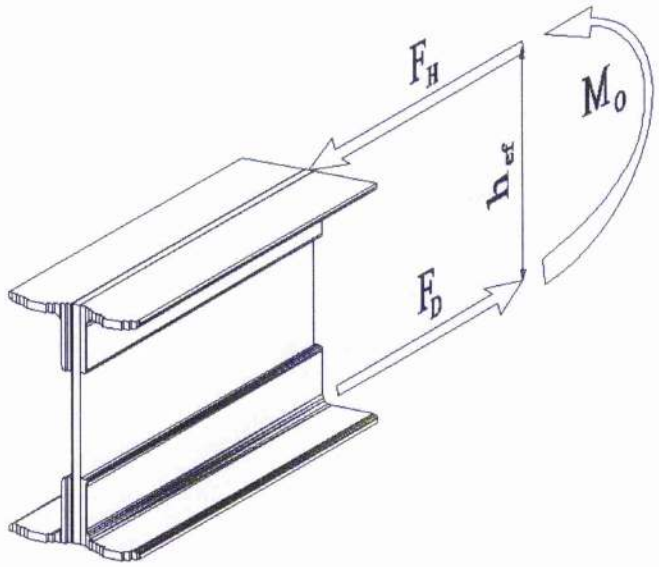

Figure 2.7 – Bending moment distribution.

The calculations of the dimensions of all wing structure components were performed in every bay of all the wing layouts (Figure 2.8) involved. As stated before, the wing layouts differ from each other in the number of ribs used, which varies from 2 to 50 along half the wing span. The whole calculation process was programmed (Marczi T., 2001) using the JAVA (Schild H., 1999) computer language.

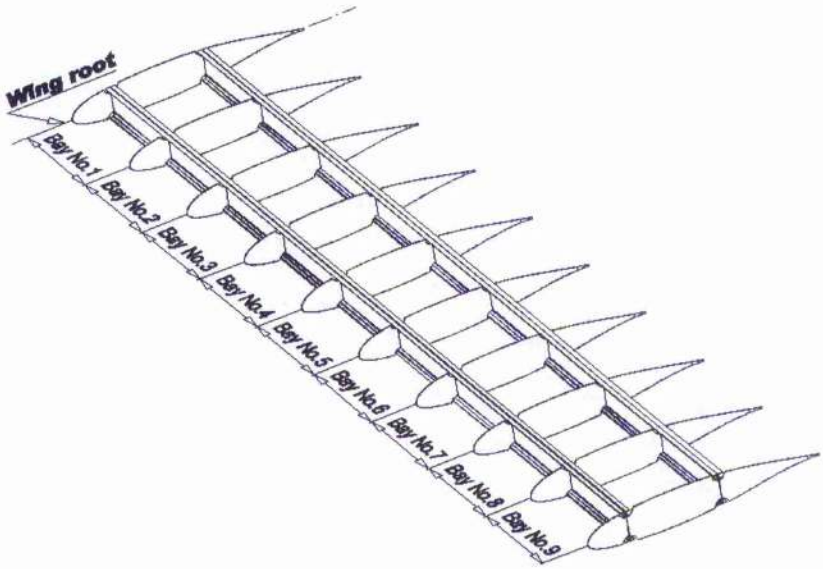

Figure 2.8 – The wing layout with ten ribs

2.3.3 Idealisation of the Torque Moment Calculation

The two torque cell wing structures are statically redundant; therefore, the simple "Bredt formula" (Kuhn P., 1956; Perry D.J., 1950) is not enough for calculation of torque moment distribution. The additional condition of the same rate of twist of both cells has to be used. The distribution of the torque moment and shear force to the section of the two cell wing is shown in Figure 2.9.

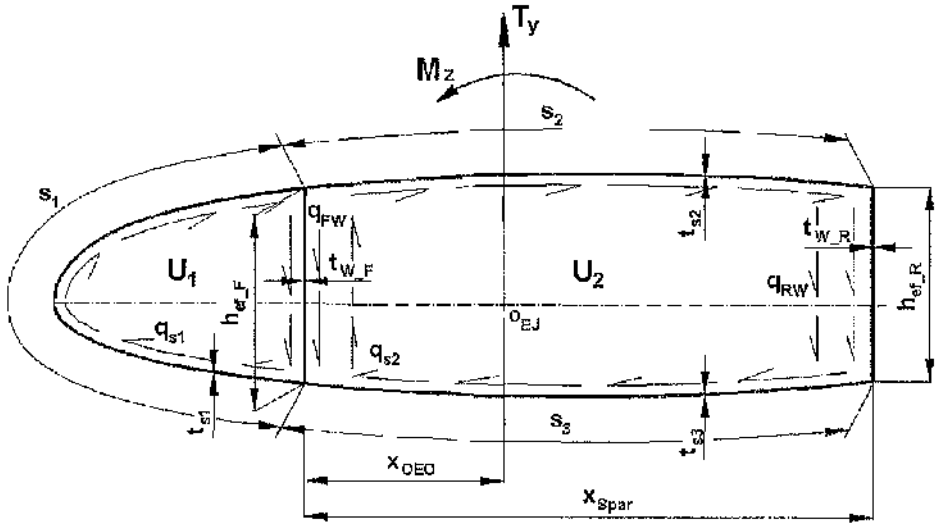

Figure 2.9 – Torque Moment and Shear Force distribution to the two cell wing structure

The ratio of the spar flexural rigidity defines the position of the wings elastic axis and the ratio in which the shear force [T_y] is distributed on the front and rear spar (Younger J.E., 1942, Špunda J., 1961). Hence Figure 2.9:

$$x_{OEO} = x_{Spar} \cdot \frac{E_R.I_R}{E_F.I_F + E_R.I_R} \qquad (2\text{-}10)$$

$$q_{FW} = \frac{T_y(x_{Spar} - x_{OEO})}{h_{ef\_F}.x_{Spar}} \qquad (2\text{-}11)$$

$$q_{RW} = \frac{T_y.x_{OEO}}{h_{ef\_R}.x_{Spar}} \qquad (2\text{-}12)$$

The torque moment distribution can be written as follows:

The Bredt Formula: $$M_z = 2.U_1.q_{s1} + 2.U_2.q_{s2} \quad \textbf{(2-13)}$$

Condition of the same rate of twist: $$\frac{1}{2.U_1}\cdot\int_1\frac{q.ds}{G.t} = \frac{1}{2.U_2}\cdot\int_2\frac{q.ds}{G.t} \quad \textbf{(2-14)}$$

Equation (2-14) can be written out as to show equation (2-15) (Příštěk A., 1988).

$$\frac{U_2}{U_1}\cdot\left[\frac{q_{s1}.s_1}{G.t_{s1}} + \frac{(q_{s1}+q_{FW}-q_{s2})h_{ef\_F}}{G.t_{WF}}\right] = \frac{q_{s2}.s_2}{G.t_{s2}} + \frac{q_{s2}.s_3}{G.t_{s3}} + \frac{(q_{s2}+q_{RW})h_{ef\_R}}{G.t_{WR}} - \frac{(q_{s2}-q_{FW}-q_{s1})h_{ef\_F}}{G.t_{WF}} \quad \textbf{(2-15)}$$

The unknown shear flows $[q_{s1}]$ and $[q_{s2}]$ can be calculated using equations (2-13) and (2-15). However, in the preliminary stage of the wing design, the dimensions of particular wing structure components such as skin, or web thickness, are unknown. Instead of unknown effective heights of the spars ($[h_{ef\_F}]$ and $[h_{ef\_R}]$ in equation (2-15)), the actual heights of the spars can be used. Nevertheless, according to the previous chapter, the effective heights of spars are crucial for both spar webs and the bending moment distribution. Therefore, it can be said that equations (2-13) and (2-14) contain nine unknown variables. The solution of this system of equations is impractical and forces the use of some idealisation method.

In preliminary design stage and preliminary skin shear flow calculation, it would not be a large error if the front torque cell is neglected and thickness of the skin is calculated from the box consisting from front spar web, rear spar web and upper and lower skin plates (Figure 2.10). For such idealised model, the shear flow in the skin can easily be calculated from the simple Bredt formula (2-16).

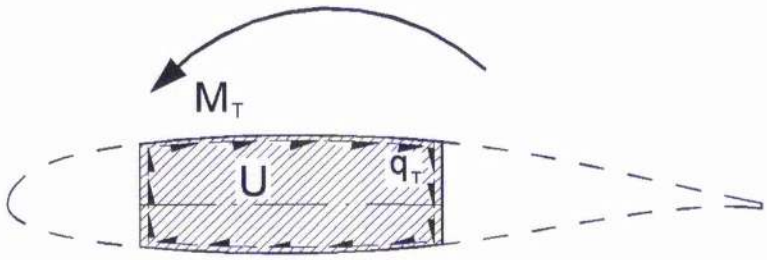

Figure 2.10 –Idealisation of torque moment distribution in the preliminary design stage

According to the presented idealisation (Figure 2.10), the shear flow in the skin can be expressed as follows:

$$q_T = \frac{M_T}{2.U} \qquad \textbf{(2-16)}$$

Equation (2-16) will be used in further calculations, yet it has to be mentioned again that such idealisation of torque moment distribution (Figure 1.1) is only relevant to the preliminary stage of the design project. More precise calculations would be done in the detailed design stage. In the detailed stage of an aircraft design all the presented idealisations are broken down and precise methods are used for all calculations of structure components.

2.4 Idealisation of the Ribs

The rib design is assumed to be similar to the spar design. Rib models have non-stiffened and buckling resistant webs without lightening holes and a simple flange around the perimeter (Figure 2.11). In the first approach, the ribs' flange dimensions [a_H] and [a_D] are assumed as constant at 25mm.

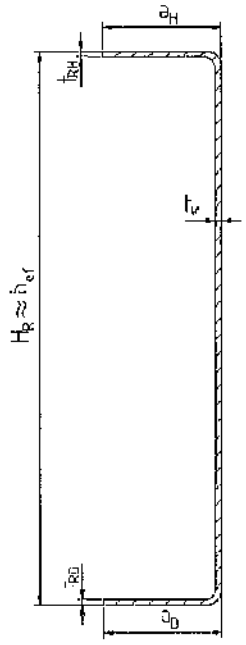

Figure 2.11 – The ribs cross-section

The idealisation of ribs flanges was done with the purpose of decreasing the number of unknown variables in the calculation process. However, in the detailed stage of the aircraft design (Figure 1.1), a more precise consideration of the rib design should be made.

3 Analysis of the Aerodynamic Load Calculation

The aerodynamic load acting over the wing defines the load of the particular wing structure components. The aerodynamic wing load depends on the flight conditions, which vary during the flight. Therefore, the usual way of calculating the wing structure is to define the worst case of the flight and subsequently calculate the aerodynamic load. The answer to the question, as to which flight condition or aerodynamic load is the worst can be found by using the flight envelope of the particular airplane. However, as explained in the Introduction neither the airplane nor the airplane's envelope is defined in this project. Thus, for the aerodynamic load calculation, a presumption of the flight conditions must be done.

3.1 The calculation input data

The aerodynamic load calculation involves the calculation of the aerodynamic lift, drag and the torque moment distribution along the wing span. For the aerodynamic load and subsequently the wing structure and wing gross weight calculations, it is necessary to define the aerodynamic condition of the flight, for which the calculation was performed. The geometry of the wing model used was already defined and is included in the input data for the aerodynamic load calculation. Thus, the input data are as follows:

- Geometry of wing: Rectangular (Untapered wing)
- Wing span: 10 m
- Aerodynamic chord 1.25 m

As already explained in the Introduction, this project is not attempting to solve for any particular wing. It tries to develop a general calculation process for the minimum dimension calculations. The flight conditions for which the project is solved are assumed according the real UL/VL airplanes (chapter 2.1) and are as follows.

- Aircraft speed: 300 km/h
- Load factor: 6
- Aircraft mass: 500 kg

The wing section also defines the aerodynamic load acting over the wing span; in this calculation the wing section MS0316 was used (Figure 3.1). Wing section MS0316 was derived in the VZLU – Czech Republic from the aerofoil MS(1) 0313 (NASA Langley). The aerodynamic and geometric characteristics of this wing section are shown in the appendix (see Figure 9.4 and Figure 9.5).

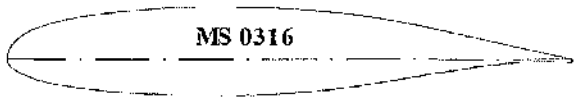

Figure 3.1 – Wing section

The chosen input data for the aerodynamic load calculation is assumed to be that which causes the maximum aerodynamic load on the wing model. The calculated aerodynamic load is subsequently used in the wing structure calculation from which the minimum dimensions of the wing structure components can be obtained.

3.2 Wing model aerodynamic calculation

The first practical theory for predicting the aerodynamic properties of a finite wing was developed during the period 1911-1918 by Ludwig Prandtl and his colleagues in Germany at Gottingen. According to equation (3-1), which represents Joukowski – Kutta theorem (J.D.Anderson, 1984), the solution of the aerodynamic lift distribution along the wing span is based on the calculation of spanwise circulation distribution (Figure 3.2).

$$L = \rho_{\infty} . v_{\infty} . \Gamma \qquad \text{(3-1)}$$

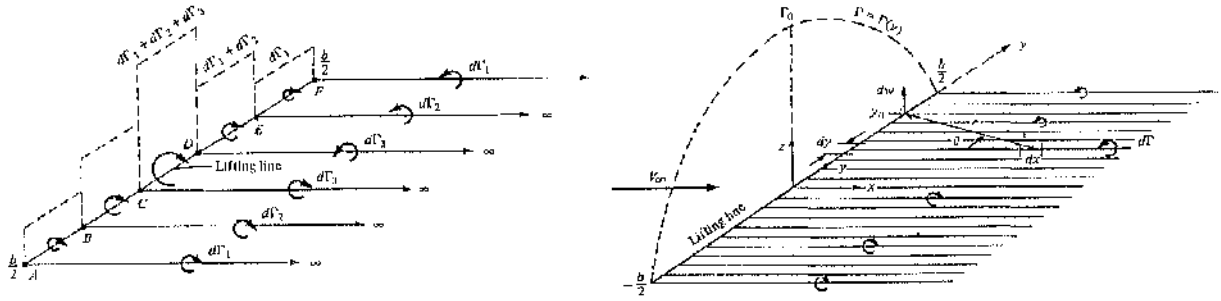

Figure 3.2 – Prandtl's lifting-line theory (Superposition of finite and infinite number of horseshoe vortices along the lifting line; figures copied from J.D. Anderson Jr., 1984)

Equation (3-2) is the fundamental equation of Prandtl's lifting-line theory (Brož, 1981), and represents the relation between the wing parameters b(z), $c^{\alpha}_{L}(z)$, $\alpha_{eff}(z)$ and the unknown distribution of the circulation.

$$\Gamma = \frac{1}{2} . v_{\infty} . b . c^{\alpha}_{L_{\infty}} . \left[\alpha_a + \frac{1}{4 . \pi . v_{\infty}} . \int_{\frac{-l}{2}}^{\frac{l}{2}} \frac{d\Gamma}{dz_1} . \frac{dz_1}{(z_1 - z)} \right] \qquad \textbf{(3-2)}$$

Further development of the Prandtl's lifting-line theory led to the solution with Fourier polynomials, quadrature method of Multhopp or extended lifting-line theory (method of Weissinger) (Schlichting H., 1979).

According to the simple lifting-line theory, the Multhopp's method is the simplest and was the most used method for the computation of the lift distribution over unswept wings. Therefore, Multhopp's method (Pope, 1951, Brož, 1981) was used for the calculation of the lift distribution along the wing model of this project.

3.2.1 Aerodynamic lift distribution calculation

Multhopp's method calculates the distribution of local nondimensional circulation [γ] (equation 3-3) at several preselected points. Figure 3.3 shows the spanwise distribution of the points in which the circulation is calculated. According to Figure 3.3, a semi-circle is placed upon the non-dimensional wing and divided into [m+1] equal angles [Θ] according to the relation (3-4).

$$\gamma_{(\Theta)} = \frac{2}{m+1} . \sum_{n=1}^{m} \gamma_{n(\Theta)} . \sum_{k=1}^{m} \sin k . \Theta_n . \sin k . \Theta \qquad \textbf{(3-3)}$$

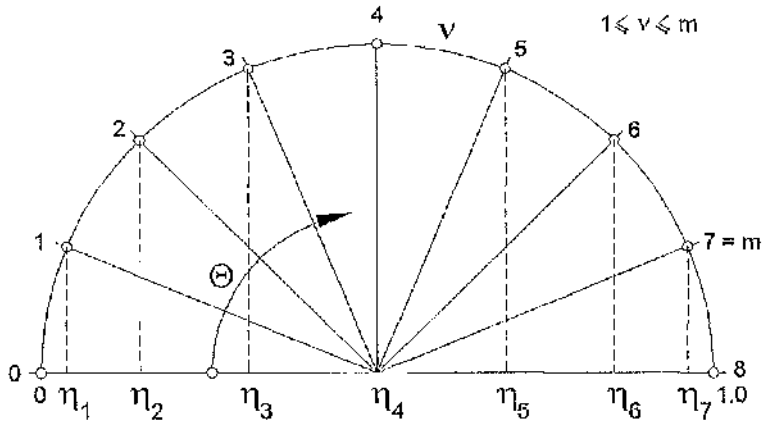

Figure 3.3 – Multhopp's spanwise point distribution in which circulation is calculated

$$\Theta_v = v.\frac{\pi}{m+1} \qquad \textbf{(3-4)}$$

From Figure 3.3 the span station is then:

$$\eta_v = \cos\Theta_v \qquad \textbf{(3-5)}$$

From Figure 3.3, and equation (3-5), it can be seen that the span stations near the tip of the wing are distributed more densely than the span stations in the middle of the wing. Consequently, it can be said that the Multhopp's simple spanwise points (stations) distribution is satisfactory enough for the most rapid changes of the lift distribution curve near the tips of the wing.

Due to the simplicity of Multhopp's method, the method was widely used for the first approach to lift distribution calculation. The method leads to the calculation of the system of [m] linear equations, yet for the symmetrical lift distribution, the system of [m] equations could be rewritten to the system of [(m+1)/2] equations. In practical use, the calculation was commonly performed for the seven Multhopp's stations, while for symmetrical lift distribution only a system of four equations were calculated.

In this project, to obtain a more precise appraisal of circulation distribution, the calculation was performed in 100 (from Figure 3.3, m = 99) span stations distributed according to the Multhopp's method (see Figure 3.3). Due to the symmetrical distribution of the aerodynamic load in this project, the calculation was carried out for the half wing's span only.

Despite this simplification, the system of 50 equations was still too complicated for manual solution. Therefore, the program "Multhopp" (Marczi T., 2001) was used. Program "Multhopp" involves the calculation of the whole aerodynamic load (aerodynamic lift, drag, aerodynamic torque moment and chordwise pressure distribution in the particular span station). Furthermore, the program allows calculations for wings of differing geometry. Due to the unsuitability of Multhopp's method for swept wings, it is not recommended to use this program for such wings. It can be used for geometrically and aerodynamically twisted wings and for flight when aileron operation results in nonsymmetrical lift distribution along the wing span.

As already stated, program "Multhopp" calculates the entire aerodynamic load acting on the wing. The Multhopp's solution of the fundamental equation of Prandtl's lifting-line theory (equation 3-2) gives the distribution of aerodynamic lift and drag along the wing span. For complete information about the aerodynamic load acting along the wing span it is necessary to calculate the spanwise distribution of the aerodynamic torque moment. As long as the chordwise position of the lift force is known at every Multhopp's stations, the torque moment distribution can be calculated. Unfortunately, the Multhopp's method does not calculate the chordwise position of the lift force. Therefore, it is necessary to use some other method for the calculation of torque moment distribution.

To obtain the spanwise torque moment distribution, the calculation of local torque moment was done at every Multhopp station. The calculation was based on the calculation of chordwise pressure distribution at each Multhopp station and the subsequent double integration of the calculated chordwise pressure distribution. The presumption that the local lift was acting at the centre of gravity of the chordwise pressure distribution area (Figure 3.4) was used in the further calculation. Next, the calculated chordwise pressure distribution at all Multhopp stations was used for enumeration of the aerodynamic load acting on the particular rib's parts (see Figure 4.7).

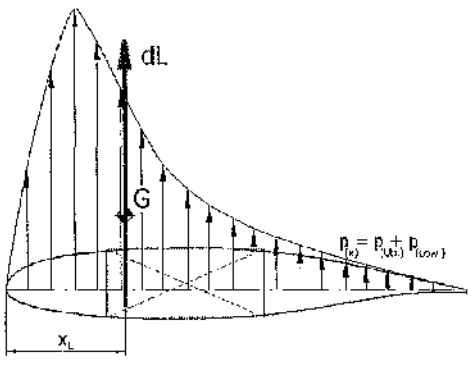

Figure 3.4 – The chordwise position of local lift force

For the calculation of the chordwise pressure distribution at Multhopp stations, the German BVF method (Špunda J., 1961) described in the Appendix was used. The resulting spanwise distribution of the aerodynamic load, which was used in further calculation, is shown on Figure 9.6 and Figure 9.7 in the Appendix.

3.2.2 The BVF Method Modification

According to the BVF method (chapter 9.1), the chordwise pressure distribution of the particular wing section is expressed as follows:

$$p = q.[c_{L\delta}.f_L(\Theta) - c_{T0}.f_T(\Theta) + \delta.f_\delta(\Theta,\phi)] \qquad \textbf{(3-6)}$$

The variables [Θ] and [ϕ] in the equation (3-6) depend only on the geometric ratio [b_k/b] and [x*/b]. Therefore, the resulting chordwise pressure distribution of the particular wing section only depends on the wing section's aerodynamic coefficients [$c_{L\delta}$], [c_{T0}] and flap deviation [δ].

Using the wing model without tilted flaps (ailerons), the lift coefficient [$c_{L\delta}$] in equation (3-6) is the same as [c_L]. The consequence of a wing model without the flaps (ailerons) is that the flap (aileron) deviation [δ] in the equation (3-6) is zero and subsequently the third part of equation (3-6) is zero. Then, the equation (3-6) could be rewritten in the form:

$$p = q.[c_L.f_L(\Theta) - c_{T0}.f_T(\Theta)] \qquad \textbf{(3-7)}$$

Since the BVF method was originally developed for the calculation of pressure distribution over the wing sections (2D), it is necessary to correct the method according to the position of the wing section along the wing span. The calculation of the chordwise pressure distribution was performed at the Multhopp stations, at which the lift coefficient [c_L] was already calculated. Then, the lift coefficient [c_L] of the particular Multhopp's station was used in the equation (3-7). Because of the constant value of torque moment coefficient for zero lift [c_{T0}] and the dependence of the function [$f_T(\Theta)$], only on the geometric ratio [x*/b], the second part of the equation (3-7), is constant for all Multhopp's stations along the wing span. Now, consider the station on the tip of the wing. It is obvious that at the tip of the wing there is zero lift, zero torque

moment, and consequently zero pressure distribution. Therefore, it was necessary to make an additional correction to the BVF method's calculation process.

The effect of function [$f_T(\Theta)$] in the equation (3-7) was corrected according to the spanwise position of the considered wing section by using the correction constant [k_T]. According to the Figure 3.5, the correction constant [k_T] is defined as the ratio (equation 3-8) of lift coefficient in the station, and the lift coefficient of the wing section at the root of the wing.

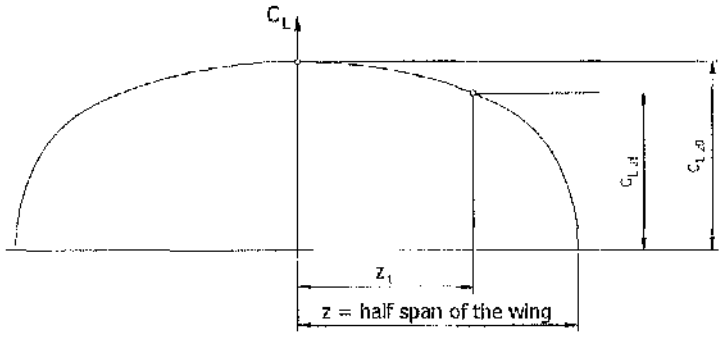

Figure 3.5 – Modification of BVF method

$$k_T = \frac{c_{Lz1}}{c_{Lz0}} \qquad \textbf{(3-8)}$$

Using the correction constant [k_T], the equation (3-7), which represents the chordwise pressure distribution of the particular wing section, can be corrected and written as follows:

$$p = q.[c_L.f_L(\Theta) - k_T.c_{T0}.f_T(\Theta)] \qquad \textbf{(3-9)}$$

From Figure 3.5 and equation (3-8) it is clear that the lift coefficient [c_L] and correction coefficient [k_T] are zero at the tip of the wing. In the wing root the value of the correction constant [k_T] is equal to one, which indicates that the equation (3-8) gives a more realistic chordwise pressure distribution along the wing span.

The process of correction and the correction constant [k_T] described above has one weak point. Theoretically, the value of the torque moment coefficient for zero lift [c_{T0}] and flap deviation [δ] is changing discontinuously at the wing station at the end of flap (Figure 3.6). The BVF method would follow this discontinuity and obviously will not give a realistic result at the

nearby stations (Figure 3.6). However, the solution of this problem is complicated enough to be solved as a separate project. Moreover, this problem is avoided by the using a wing model without flaps (ailerons).

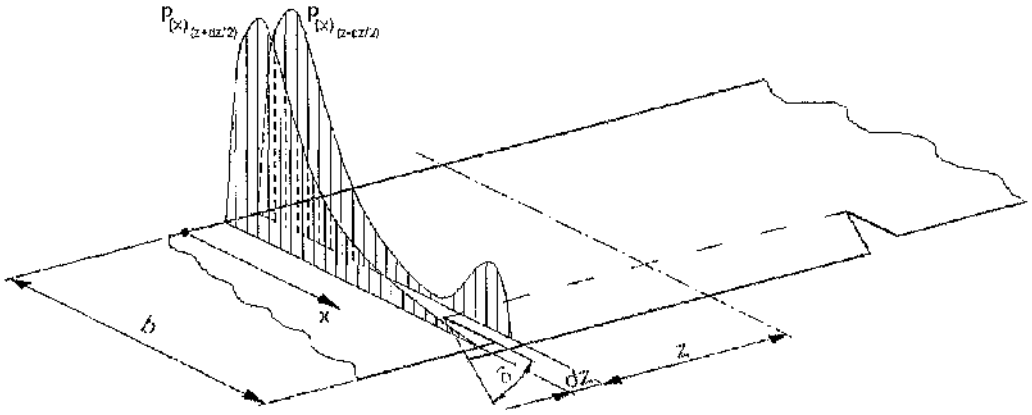

Figure 3.6 – BVF method weakness at the flap's (aileron) edge

4 Weight Optimisation Analysis

As already stated, the weight optimisation of this project is based on the calculation of minimal dimensions of the wing internal structure components. According to the wing model used, this calculation could be divided into the calculation of skin, spar webs, booms and ribs.

The aerodynamic load calculated before is used for the wing structure calculation. In the wing structure calculation process, the values of the aerodynamic loads are increased by a factor of safety [f_s]. The value of the factor of safety is assumed to be 1.5.

The basic wing structure dimensions are defined by the wing geometry and by the geometry of the wing section used. Figure 4.1 defines the spar heights and spars' positions inside of the wing model.

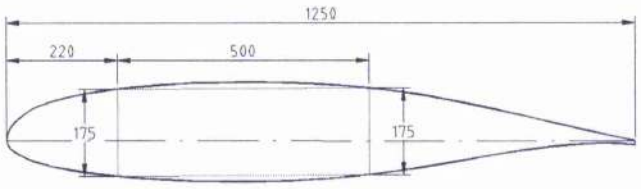

Figure 4.1 – The basic wing structure dimensions

Since the weight of a spar varies as the first power of the spar depth, the maximum spar strength-weight ratio will be gained by the use of the spar as deep as possible (W.H. Robinson, 1926). Hence the dimensions and distances of the spars are as Figure 4.1 shows. Thus, the wing structure dimensions assumed as the constants in the process of the calculation are:

- Half span of the wing: 10 000 mm
- Front spar position (measured from leading edge): 220 mm
- Rear spar position (measured from leading edge): 720 mm
- Spars height: 175 mm

4.1 Aerodynamic load distribution

According to the wing model used, the skin of the wing model is utilized for carrying the torque moment and the partly is involved in the bending (skin effective width; E.F. Bruhn, 1973). Thus, both spars are fully employed in carrying the bending moment. Regarding Figure 2.7,

which shows the bending moment distribution to the spar, the boom forces [F_H] and [F_D] can be written as:

$$F_H = F_D = \frac{M_o}{h_{ef}} \qquad (4\text{-}1)$$

Because the wing model consists of two spars, equation (4-1) contains two unknowns: [M_o] and [h_{ef}]. The unknown variable [h_{ef}] has been described above and the unknown value of the bending moment [M_o] carried by a particular spar relates to the proportion of the spar bending stiffnesses (P. Kuhn, 1956). According to two-spar structure theory (P. Kuhn, 1956), if the skin of the wing is not involved in the transmission of the bending moment, the spars share the bending load in proportion to their bending stiffnesses. Of course, except for one certain position of the load, this statement is not entirely true. The specific position of aerodynamic load mentioned above is called the shear centre.

4.2 Booms' cross section analysis

As defined in chapter 2, the booms of the wing model's spars consist of two [L] profile bars. However, there are basically two kinds of the [L] profile bars: symmetric and non-symmetric. Unfortunately, chapter 2 does not define what kind of [L] bar is used for spar booms. Figure 4.2 shows the boom, which consists of two non-symmetric [L] bars. The boom's dimensions are unknown and it will be shown that the boom in Figure 4.2 contains four unknown dimensions [B], [H], [b] and [h]. On the other hand, the cross-section of the symmetric [L] bar can be defined by only two dimensions [H] and [h]. For that reason, the booms consists of symmetric [L] bars will be used in further calculations.

As already stated, the magnitude of the booms' forces and consequently some of the structure's dimensions significantly depend on the booms' dimensions and their cross-sectional characteristics.

Due to the unknown boom dimensions, the boom cross sectional characteristics are derived analytically and the resulting equations, together with the equations of stress/strength equilibrium, are used in the further calculation.

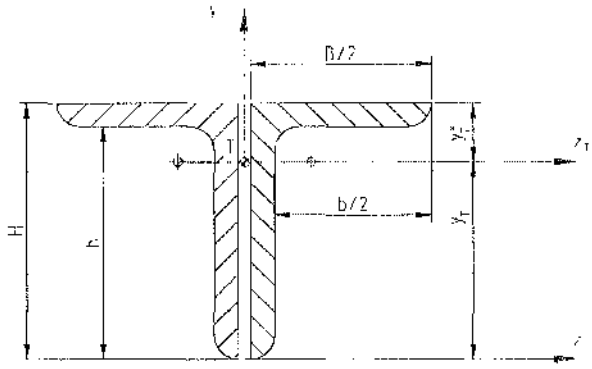

Figure 4.2 – Spar boom consists of the non-symmetrical L bars.

By using the symmetrical [L] bars for the spar booms, a number of unknowns can be eliminated. According to Figure 4.3, in contrast to the non-symmetrical [L] bar, only the two dimensions [h] and [H] define the symmetrical [**L**] bar. Figure 4.3 shows that the boom consists of two symmetrical [L] bars and the cross-sectional characteristics of such a boom can be written as follows.

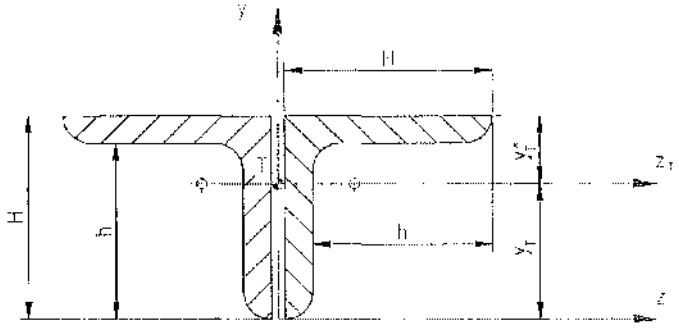

Figure 4.3 – Spar's boom consists of two symmetrical [L] bars.

Cross-sectional area:

$$A_{Boom} = 2.H.H - 2.h.h$$

$$A_{Boom} = 2.\left(H^2 - h^2\right) \qquad \textbf{(4-2)}$$

The distance of the centre of gravity used in the calculation of the effective height of the spar (see Figure 4.3):

$$y_T = \frac{2.H.H \cdot \frac{H}{2} - 2.h.h \cdot \frac{h}{2}}{2.H.H - 2.h.h} = \frac{H^3 - h^3}{2.\left(H^2 - h^2\right)}$$

$$y_T^* = \frac{2.H.H \cdot \frac{H}{2} - 2.h.h.\left(H - \frac{h}{2}\right)}{2.H.H - 2.h.h} = \frac{H^3 - 2.h^2.\left(H - \frac{h}{2}\right)}{2.\left(H^2 - h^2\right)} \qquad \textbf{(4-3)}$$

$$h_{ef} = H_I - \frac{H_H^3 - h_H^3}{2.\left(H_H^2 - h_H^2\right)} - \frac{H_D^3 - h_D^3}{2.\left(H_D^2 - h_D^2\right)} \qquad \textbf{(4-4)}$$

Although the symmetric [L] bars are used for the spar booms, each spar boom still contains two unknown variables: [H] and [h]. Consequently, the equation of the boom forces [F_H] and [F_D] (equation (4-5)) contains four unknown dimensions: H_H, H_D, h_H, and h_D. Index [H] is used for the upper spar boom and index [D] is used for the lower spar boom.

$$F_H = F_D = \frac{M_o}{H_I - \frac{H_H^3 - 2.h_H^2\left(H_H - \frac{h_H}{2}\right)}{2.\left(H_H^2 - h_H^2\right)} - \frac{H_D^3 - 2.h_D^2\left(H_D - \frac{h_D}{2}\right)}{2.\left(H_D^2 - h_D^2\right)}} \qquad \textbf{(4-5)}$$

One can note that the effective width of the skin and web are not involved in the derivation of the boom axial forces. The reason is obvious: the thickness of the skin and web are unknown and, even more, as explained in the chapter 2.3.2, the thickness of the web indirectly depends on the boom dimensions. Therefore, by involving the effective width of the skin and web in equation (4-5), it became even more complicated and will contain even more unknown variables. However, as explained later, the effective width of skin and web will be involved in the final process of calculation.

4.3 Booms' dimensions pre-solution

Each spar consists of two booms. During bending, one of the booms is loaded by compression and second by tension. Obviously, the calculation process of the compressed boom is different from the tensioned one. According the E.F. Bruhn (1973), the beam flange is stabilized in both vertical and horizontal directions by the web and skin covering respectively. Therefore, the influence of column action is negligible and the compressed flange fails by local crippling action. E.F. Bruhn (1973) presents two methods of the column's crippling strength calculation: Needham Method and Gerard Method. The compressed boom in this project was calculated according to the Gerard method, which is a more generalized and broader semi-empirical method of determining crippling stresses.

As stated in the chapter 2.2, the effective width of skin and spar's web is involved in the bending, which influences the magnitude of the boom's necessary cross-sectional area. Figure 4.4 shows the skin and web effective width of the boom used in the calculation. From Figure 4.4 it can be realized, the spar's web ends on a boom. Therefore, the calculation process of total effective width of the web differs from the skin's effective width calculation.

According to E.J. Younger (1942), the skin and web effective widths can be expressed as show equations (4-6) and (4-7).

The effective width of skin:

$$w = 1.7 t_S \sqrt{\frac{E}{\sigma_{Boom}}}$$

$$w_{Eff\_Skin} = 2.w = 3.4 t_S \sqrt{\frac{E}{\sigma_{Boom}}} \qquad (4\text{-}6)$$

The effective width of web:

$$w_1 = 0.62 t_W \sqrt{\frac{E}{\sigma_{Boom}}}$$

$$w_{Eff\_Web} = \frac{w}{2} + w_1 = \left(\frac{1.7}{2} + 0.62\right) t_W \sqrt{\frac{E}{\sigma_{Boom}}}$$

$$w_{Eff\_Web} = 1.47 t_W \sqrt{\frac{E}{\sigma_{Boom}}} \qquad (4\text{-}7)$$

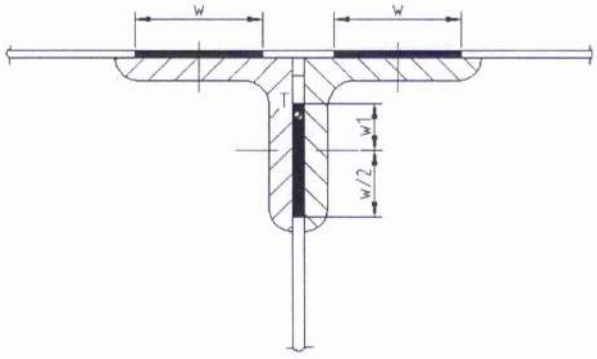

Figure 4.4 – Skin and web effective width

From equations (4-6) and (4-7) it can be realized that the effective widths of the skin and web depend on the Young's modulus of the web/skin material, the flange stress [σ_{Boom}], and web/skin thickness. Because of the dependence of the boom's crippling stress on the boom's geometry, the web's effective width of the compressed boom is a function of the boom's dimensions. Moreover, as stated before, the thickness of the web in the equation (4-16) indirectly depends on the spar boom dimensions.

If the tensioned boom is considered, the equation of stress/strength equilibrium could be written as equation (4-8):

$$\sigma_m \geq \frac{F_{D\ (h_{ef}(H_H, h_H, H_D, h_D))}}{A_{Boom\ (H_D, h_D)} + A_{Eff\_Skin} + A_{Eff\_Web\ (h_{ef}(H_H, h_H, H_D, h_D))}} \qquad (4\text{-}8)$$

Equation (4-8) shows that almost all members of the right side of the equation depend on the boom dimensions [H] and [h] (see Figure 4.3). In the case of the compressed boom, the equation of stress/strength equilibrium looks like the equation (4-9). Compared with the equation (4-8), the difference is that the effective width of the skin and web depend on the boom's crippling stress, which depends on the boom geometry and subsequently, on the boom dimensions.

$$\sigma_{Crit} \geq \frac{F_H\ (h_{ef}(H_H,h_H,H_D,h_D))}{A_{Boom}\ (H_H,h_H)+A_{Eff\_Skin}\ (\sigma_{Crit}(H_H,h_H))+A_{Eff\_Web}\ (h_{ef}(H_H,h_H,H_D,h_D),\sigma_{Crit}(H_H,h_H))} \qquad \textbf{(4-9)}$$

Substituting all variables on the right side of the equation (4-8) by equations (4-2), (4-5), (4-6) and (4-7), the complex analytical form of equation (4-8) can be written:

$$\sigma_m \geq \frac{\dfrac{M_o}{H_I - \dfrac{H_H^3 - 2.h_H^2\left(H_H - \dfrac{h_H}{2}\right)}{2.\left(H_H^2 - h_H^2\right)} - \dfrac{H_D^3 - 2.h_D^2\left(H_D - \dfrac{h_D}{2}\right)}{2.\left(H_D^2 - h_D^2\right)}}}{2.\left(H_D^2 - h_D^2\right) + 3.8t_s^2\sqrt{\dfrac{E}{\sigma_m}} + 1.57t_w^2\sqrt{\dfrac{E}{\sigma_m}}}$$

$$\sigma_m \geq \frac{\dfrac{M_o}{H_I - \dfrac{H_H^3 - 2.h_H^2\left(H_H - \dfrac{h_H}{2}\right)}{2.\left(H_H^2 - h_H^2\right)} - \dfrac{H_D^3 - 2.h_D^2\left(H_D - \dfrac{h_D}{2}\right)}{2.\left(H_D^2 - h_D^2\right)}}}{2.\left(H_D^2 - h_D^2\right) + \sqrt{\dfrac{E}{\sigma_m}}\left(3.8t_s^2 + 1.57t_w^2\right)} \qquad \textbf{(4-10)}$$

Equation (4-10) contains three known variables, or more precisely two known material constants [σ_m] and [E] and one known variable [M_o]. (At this stage, the course of the bending moment acting over the particular wing spar is known. This is due to the chosen spars load ratio.) All other variables in equation (4-10) are unknown and moreover the variable [t_w] is a function of the dimensions of the spar booms.

Undoubtedly, the calculation process of the tensioned boom is simpler than the process of the crippling stress calculation of the compressed boom. Despite using the symmetrical [L] bars in the boom construction, the number of unknown variables is still too large for a direct solution of equation (4-10). Therefore, the analytical derivation of the equation of the boom's crippling stress is not presented. As a consequence, another elimination of unknown variables is necessary.

Using identical upper and lower spar booms ($H_H = H_D$, $h_H = h_D$) would be the simplest elimination of a number of unknown variables, yet this idea was not considered, because of its low practical use. The elimination process of a number of unknown variables is based on the idea of expressing one boom's dimension as a function of the second one. For this purpose, the investigation of the boom dimensions [H] and [h] (Figure 4.3) is done.

4.3.1 The relation between the dimensions of a symmetrical [L] profile bar

As already stated, only two dimensions are necessary for full definition of symmetrical [L] bar geometry. To make the calculation more convenient, the dimensions [H] and [h] were used for the boom's geometry definition. Next, it can be said that the equation (4-2) represents the minimum necessary boom's cross-sectional area. Hence, this simple idea is considered: if the equation (4-2) represents the minimum boom's cross-sectional area, then the value of this cross-sectional area can be calculated directly from the equation of stress/strength equilibrium (see equation (4-11)).

$$\sigma_m \geq \frac{F}{A_{Boom}} \Rightarrow A_{Boom\,\min} = \frac{F}{\sigma_m} \qquad \textbf{(4-11)}$$

For the same reason as in the booms' axial forces derivation (chapter 4.2), the effective widths of skin and web are not involved in this investigation. In the further text, [A_{Boom}] will mean the boom's minimum cross-sectional area. The variable [A_{Boom}] in equation (4-11) can be substituted by equation (4-2) and equation (4-11) can be written as equation (4-12) shows.

$$2.\left(H^2 - h^2\right) = \frac{F}{\sigma_m} \qquad \textbf{(4-12)}$$

Next, it can be seen that equation (4-12) contains two unknown variables (both dimensions) [H] and [h]. The solution of equation (4-12) is obvious. By choosing the value of one unknown, the other one can be calculated directly. If the dimension [h] is assumed, and equation (4-12) is revised to the form of (4-13), the boom's dimension [H] can be calculated.

$$H = \sqrt{\frac{F}{2.\sigma_m} - + h^2} \qquad \text{(4-13)}$$

In further investigations, the boom's cross-section and the axial force [F] in the equation (4-13) are assumed as known and constant. Then, for evaluation of the boom's dimension [H], the chosen value of dimension [h] would be arbitrary and the value of the cross-sectional area will be unaffected. It is obvious that by choosing the value [h] in equation (4-12), the cross-section of the [L] profile will vary from a rectangle to the very thin and wide [L] shape. It is apparent that the optimum shape of the cross-section of [L] bar is somewhere between these two extremes. The remaining problem is, the unknown optimum – which dimensions [H] and [h] will give the "optimum" shape of [L] bar for practical use.

In the following process of calculation, the shape of the cross-section is described by the ratio of boom dimensions [h/H]. Figure 4.5 shows the typical course of the boom's dimension ratio [h/H]. Note that Figure 4.5 is plotted for the condition of constant force [F] and a constant cross-sectional area of the [L] bar (the graph in Figure 4.5 represents equation 4-12). The axial axis on Figure 4.5 represents the chosen values of dimension [h]. From Figure 4.5 it can be seen that for the constant value of cross-sectional area, the geometry of the boom's [L] bars vary according to the chosen value of the dimension [h]. The value of the boom's dimensions ratio [h/H], which gives the "optimum" shape (thickness) of the boom's [L] bar, was in the first approach, found as is indicated on Figure 4.5. From the intersection of the tangent lines (1) and (2), the line (3) was drawn under the half of the angle of the tangents (1) and (2). The intersection of line (3) with the course of the boom's dimensions ratio [h/H] relates to the value $h/H \approx 0.85$.

The boom's dimension ratio [h/H] allows us to write one [L] bar dimension as a function of the second one. The boom's dimensions ratio [h/H = 0.85] significantly simplifies all the equation, because it represents the relation between the boom's dimensions [H] and [h] (equation 4-14).

$$h = 0.85H \qquad \text{(4-14)}$$

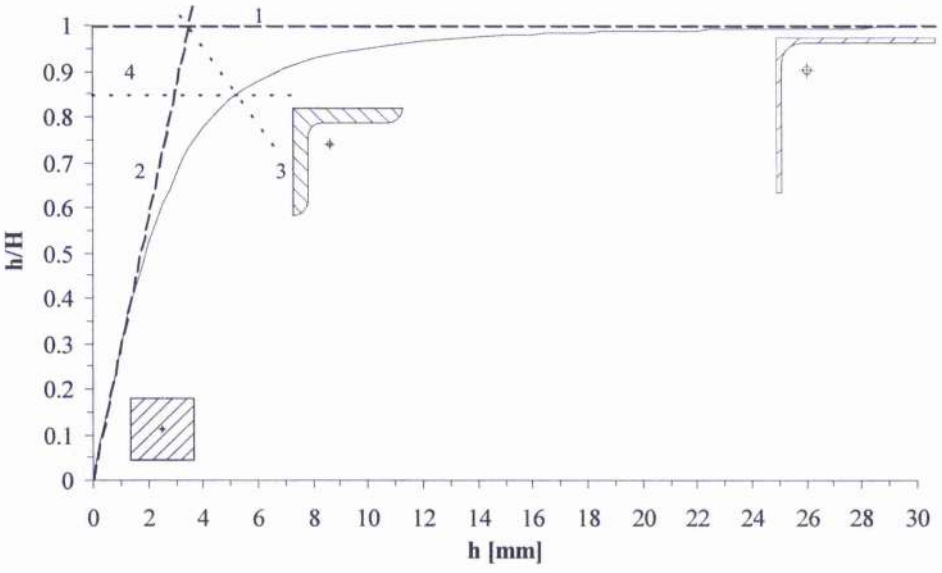

Figure 4.5 – The course of the ratio h/H

4.3.2 Booms' equations of stress/strength equilibrium

To apply and take full advantage of the already presented boom's dimension ratio [h/H = 0.85], all equations used in the process of calculation need to be rewritten.

The preceding equations of stress/strength equilibrium are equations from which the minimum boom dimensions are calculated. By using equation (4-14), the equations used in the process of minimum dimensions calculation can be written as follows:

Boom's cross-sectional area:

$$A_{Boom} = 2.\left(H^2 - (0{,}85H)^2\right) = 0{,}555.H^2 \qquad \textbf{(4-15)}$$

Boom's centre of gravity:

$$y_T = \frac{2H.H.\frac{H}{2} - 2.0{,}85H.0{,}85H.0{,}85\frac{H}{2}}{0{,}555.H^2} = \frac{H^3 - (0{,}85H)^3}{0{,}555.H^2}$$

$$y_T^* = 0{,}305.H \qquad (4\text{-}16)$$

$$y_T = 0{,}695.H \qquad (4\text{-}17)$$

It can be noticed that all equations (4-15), (4-16), (4-17) and (4-18) depend on only one variable (dimension [H] – compare with equations (4-2) and (4-5)), which indicates further simplification of the stress/strength equations of equilibrium, from which the minimum dimensions are calculated.

The spar's effective height:

$$h_{ef} = H_I - y_{T_H}^* - y_{T_D}^* = H_I - 0.305(H_H + H_D) \qquad (4\text{-}18)$$

The boom forces [F_H] and [F_D]:

$$F_H = F_D = \frac{M_o}{H_I - 0{,}305.(H_H + H_D)} \qquad (4\text{-}19)$$

The equation of stress/strength equilibrium of tensioned boom:

$$\sigma_m \geq \frac{\dfrac{M_o}{H_I - 0{,}305.(H_H + H_D)}}{0.555H_D^2 + \sqrt{\dfrac{E}{\sigma_m}} \cdot \left(3.8t_s^2 + 1.57t_w^2\right)} \qquad (4\text{-}20)$$

By application of the boom's dimensions constant [h/H], equation (4-20) proves the essential simplification of the process of the solution. Compared with equation (4-10) the equation (4-20) is obviously simpler, but still cannot be solved directly or separately because of two unknown variables [H_H] and [H_D]. Moreover, as already stated, the thickness of the spar's web [t_w] indirectly depends on the spar's boom dimensions. These relations of equation (4-20)

to the spar's boom dimensions indicate the already mentioned loop or numerical approach to the solution (chapter 2.3.2).

At this stage, when all eliminations of unknown variables have been done, analytical derivation of the boom's crippling stress may be made. As already stated, the Gerard Method (E.F. Bruhn, 1973) is used for this.

The consequence of the developed boom's dimension constant [h/H = 0.85] is probably most obvious in the solution process of the crippling stress calculation. As the next derivation of the boom's crippling stress shows, the final form of the derived crippling stress equation depends only on the boom's dimension ratio [h/H] and boom's material constants [σ_Y] and [E].

The following equations show the adjustment of the Gerard formula of crippling stress.

The Gerard formula:

$$\frac{\sigma_{Cr}}{\sigma_Y} = 0.56\left[\frac{g.t_L^2}{A_L}\cdot\sqrt{\frac{E}{\sigma_Y}}\right]^{0.85} \qquad \textbf{(4-21)}$$

According to equation (4-14) the thickness [t_L] and cross-sectional area [A_L] of the boom's [L] bar can be written as:

$$t_L = H - h = H - 0.85H = 0.15H \qquad \textbf{(4-22)}$$

$$A_L = H^2 - h^2 = H^2 - (0.85H)^2 = 0.2775H^2 \qquad \textbf{(4-23)}$$

Substituting the [L] bar thickness and cross-sectional area in equation (4-21) by equations (4-22) and (4-23) and using the Gerard constant g = 2, equation (4-21) can be revised as follows:

$$\frac{\sigma_{Cr}}{\sigma_Y} = 0.56\left[\frac{2.(0.15)^2.H^2}{(0.2775)H^2}\cdot\sqrt{\frac{E}{\sigma_Y}}\right]^{0.85}$$

$$\frac{\sigma_{Cr}}{\sigma_Y} = 0.56\left[\frac{0.045}{0.2775}\cdot\sqrt{\frac{E}{\sigma_Y}}\right]^{0.85}$$

$$\sigma_{Cr} = 0.119\sigma_Y \cdot \left[\sqrt{\frac{E}{\sigma_Y}}\right]^{0.85}$$

$$\sigma_{Cr} = 0.119\sigma_Y^{0.575} \cdot E^{0.425} \qquad \textbf{(4-24)}$$

Surprisingly enough equation (4-24) shows that using the boom's dimension constant [h/H] the crippling stress of the boom's [L] bars can be expressed only by the material constants [E] and [σ_Y]. According to this simplification of Gerard Method (E.F. Bruhn, 1973), the crippling stress of the symmetrical [L] bars can be directly calculated and written in the table; as Figure 9.3 in the appendix shows. Using this table, the value of the crippling stress of a symmetrical [L] bars could be very easily and quickly obtained, which can be presented as an extension of the Gerard Method (chapter 9.2). Next, the equation (4-9) can be rewritten in the form of equation (4-25), which demonstrates the fact that the boom's crippling stress is not the unknown variable, and according to the boom's dimension constant [h/H] the only variables are the dimensions [H] of the upper and lower spar's boom.

$$\sigma_{Cr} \geq \frac{F_{H\ (h_{ef}(H_H,H_D))}}{A_{Boom\ (H_H)} + A_{Eff\_Skin} + A_{Eff\_Web\ (h_{ef}(H_H,H_D))}} \qquad \textbf{(4-25)}$$

By substitution of equations (4-6), (4-7), (4-15) and (4-19) into equation (4-25) it can be rewritten as follows:

$$\sigma_{Cr} \geq \frac{\dfrac{M_o}{H_I - 0{,}305.(H_H + H_D)}}{0.555H_H^2 + \sqrt{\dfrac{E}{\sigma_{Cr}}} \cdot \left(3.8t_s^2 + 1.57t_w^2\right)} \qquad \textbf{(4-26)}$$

The next substitution for [σ_{Cr}] can be done and equation (4-26) can be written as shows equation (4-27).

$$0.119\sigma_Y^{0.575} \cdot E^{0.425} \geq \frac{\dfrac{M_o}{H_I - 0{,}305.(H_H + H_D)}}{0.555H_H^2 + \sqrt{\dfrac{E}{0.119\sigma_Y^{0.575} \cdot E^{0.425}}} \cdot \left(3.8t_s^2 + 1.57t_w^2\right)} \qquad \textbf{(4-27)}$$

To enumerate the minimum boom dimensions, the further calculations use equations (4-20) and (4-27). Equations (4-20) and (4-27) cannot be used separately, they will be used in the iterative process of calculation together with the equations of skin and web thickness and equations of skin and web effective widths.

4.4 Skin and spars' webs calculation

The participation of the skin in the bending is explained in chapter 2.2. The thickness of the skin is calculated from the shear flow, which results from the wing's torque moment. According to the wing model used (chapter 2.2), the dimensions of the skin plate used in the calculation process are defined by the distance of two adjacent ribs and by the distance of the wing's spars. In the next calculation, the skin and spar's web are treated as a plate or sheet with simple supported edges and buckling resistant.

Since the spar's web is assumed as buckling resistant, and according to the presumption of torque moment distribution (see Figure 2.10 or Figure 4.6), the spar webs are loaded as shown in Figure 4.6.

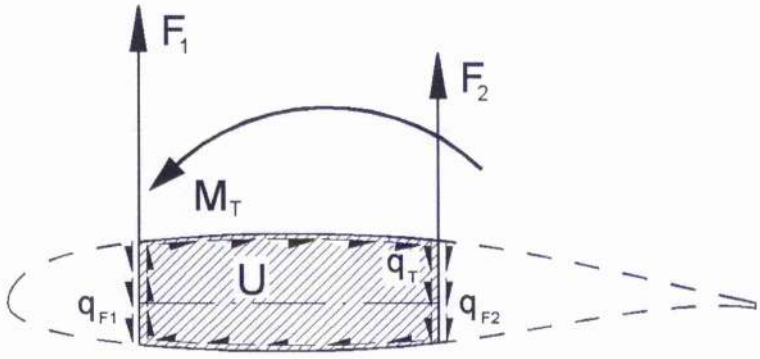

Figure 4.6 – Shear flows at the skin and spars' webs

Due to the fact that the stiffeners are not involved in the wing model used (chapter 2.2), the distance of two adjacent ribs define the length of the web plate used in the calculation process and the height of the plate is defined by the effective height of the particular spar.

The forces [F_1] and [F_2] are defined by the spar load ratios and the torque moment was re-calculated along the shear axis of the wing and subsequently used in further calculations.

4.4.1 Web and skin dimensions pre-solution.

Skin and web calculations is represented by the equation of the critical buckling shear stress [τ_{CR}], which can be written (Bruhn E.F., 1973; Timoshenko S., 1945) as:

$$\tau_{CR} = \frac{k_s \cdot \pi^2 \cdot E}{12 \cdot (1-\mu^2)} \cdot \left(\frac{t}{b_s}\right)^2 \qquad \textbf{(4-28)}$$

The diagram of the plate buckling coefficient [k_s] (ESDU 71005, 1995; Špunda J., 1961) is shown in the appendix (Figure 9.8.) Using the Poisson constant $\mu = 0.3$, the critical shear stress can be written (Špunda, 1955; Šubrt L., 1991) as:

$$\tau_{CR} = 0.91 k_s E \left(\frac{t}{b_s}\right)^2 \qquad \textbf{(4-29)}$$

Generally, the shear flow in a thin panel can be written as:

$$q_p = \tau . t \qquad \textbf{(4-30)}$$

The combination of equations (4-29) and (4-30) gives the formula from which the thickness of the calculated panel can be enumerated. Equation (4-31) represents the equation used in further calculations of skin and web thicknesses.

$$\tau_{CR} = \frac{q_p}{t} = 0.91 k_s . E \left(\frac{t}{b_s}\right)^2$$

$$q_p = 0.91 k_s . E \cdot \frac{t^3}{b_s^2} \qquad \textbf{(4-31)}$$

The shear flow [q] in equation (4-31) represents the total shear flow in the skin or web panel. Then, according to Figure 4.6, the shear flows of the skin and front and rear web can be written as the following equations show.

The skin's shear flow:

$$q_S = q_T = \frac{M_T}{2.U} \qquad (4\text{-}32)$$

The shear flow in the front spar's web:

$$q_{FW} = q_{F1} = -\frac{F_1}{h_{ef\_F}} + \frac{M_T}{2.U} \qquad (4\text{-}33)$$

The shear flow in the rear spar's web:

$$q_{RW} = q_{F2} + q_T = \frac{F_2}{h_{ef\_R}} + \frac{M_T}{2.U} \qquad (4\text{-}34)$$

By substituting equations (4-32), (4-33) and (4-34) into equation (4-31), the skin and web thicknesses can be written as:

Thickness of the skin:

$$q_S = q_T = \frac{M_T}{2.U} = 0.91 k_s.E \cdot \frac{t_S^3}{b_s^2}$$

$$t_S = \sqrt[3]{\frac{M_T.b_s^2}{1.82 k_s.E.U}} \qquad (4\text{-}35)$$

Thickness of the front spar's web:

$$q_{FW} = q_{F1} = \frac{F_1}{h_{ef\_F}} = 0.91 k_s.E \cdot \frac{t_{FW}^3}{b_s^2}$$

$$t_{FW} = \sqrt[3]{\frac{F_1 . b_s^2}{0.91 k_s . E . h_{ef\_F}}} \qquad \text{(4-36)}$$

Thickness of the rear spar's web:

$$q_{RW} = q_{F2} + q_T = \frac{F_2}{h_{ef\_R}} + \frac{M_T}{2U} = 0.91 k_s . E \cdot \frac{t_{RW}^3}{b_s^2}$$

$$t_{RW} = \sqrt[3]{\frac{\left(\frac{F_2}{h_{ef\_R}} + \frac{M_T}{2U} \right) b_s^2}{0.91 k_s . E}} \qquad \text{(4-37)}$$

The thickness can be calculated directly from equation (4-35). The value of the shorter plate dimension [b_s] depends on the rib spacing in the wing layout. If two adjacent ribs are closer than the distance between the front and rear spars, variable [b_s] in equation (4-35) equals the distance of the two adjacent ribs. Otherwise, [b_s] equals to the spar distance.

In the case of the web thickness calculation, variable [b_s] would be the distance of the two adjacent ribs, or the effective height of the particular spar [h_{ef_F} or h_{ef_R}]. Moreover, the spar's effective height occurs in the equations of shear flow caused by forces [F_1] and [F_2]. Again, because of the dependence of spar's effective height on the boom dimensions, the web thicknesses cannot be calculated directly from equations (4-36) and (4-37), yet equations (4-36) and (4-37) are used in the iterative process of calculation, together with equations (4-26) and (4-27).

4.5 Ribs load

The ribs are loaded by the shear flows from the spar webs and wing skin and by the bending moment, which results from the chordwise pressure distribution along the wing sections. Using the German BVF method (chapter 9.1), the pressure distribution along the aerodynamic chord of the wing sections is calculated. Due to the two spar wing structure, the ribs are divided into three parts. As Figure 4.7 shows, all parts of the ribs are loaded by a particular portion of the aerodynamic pressure. The forces $[T_1]$, $[T_2]$ and $[T_3]$ in Figure 4.7 represent the sum of the pressure carried by the particular rib's part. The positions of these forces are assumed as centres of gravity of the pressure distribution areas of each rib's part (Figure 4.7). The load of the particular rib part is assumed as the sum of the pressure acting on the area, which is defined by the length of the rib part and half of the distance between two adjacent ribs on the right and left side of the rib.

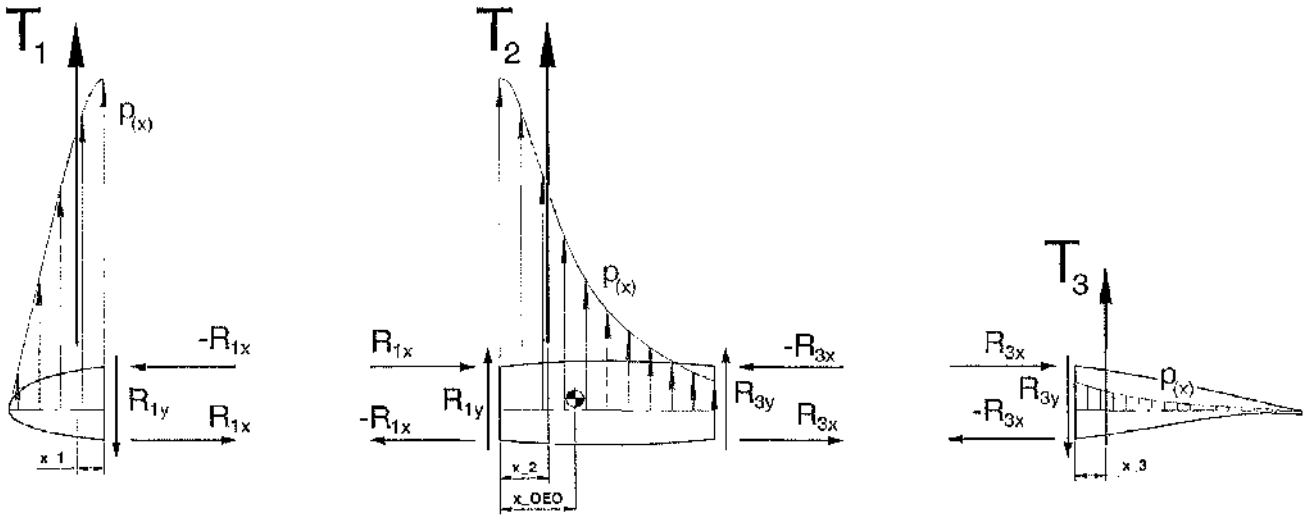

Figure 4.7 – The load of the ribs parts.

The wing section (Figure 3.1) defines the geometry of the rib parts and Figure 2.11 shows the shape of the rib cross-section. For simplicity, the presumption of the same thicknesses of all parts of the rib is used and therefore, the rib's thickness is calculated only for the middle part of the rib.

4.5.1 Ribs' dimensions calculation

The dimensions of the ribs are calculated after the dimensions of all the other structural components are known. According to the known aerodynamic load (Figure 4.7) and the rib's geometry (Figures 2.11 and 3.1), the rib's thickness is the only unknown dimension.

To calculate the thickness of the rib, the shear flows along the middle part of the rib are calculated using a common method.

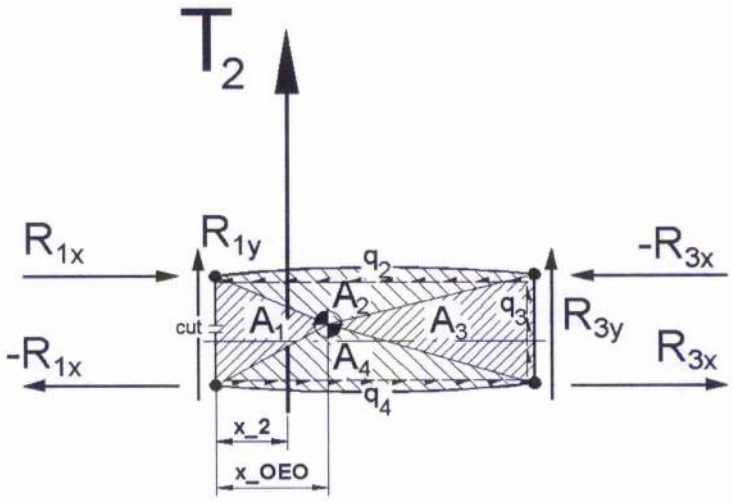

Figure 4.8 - Shear flows calculation of rib's middle part

Afterwards, when all the shear flows are known, to obtain a complete picture of the rib's middle part web and flange forces, several sections along the rib's span can be analysed as illustrated in section B-B (Figure 4.9).

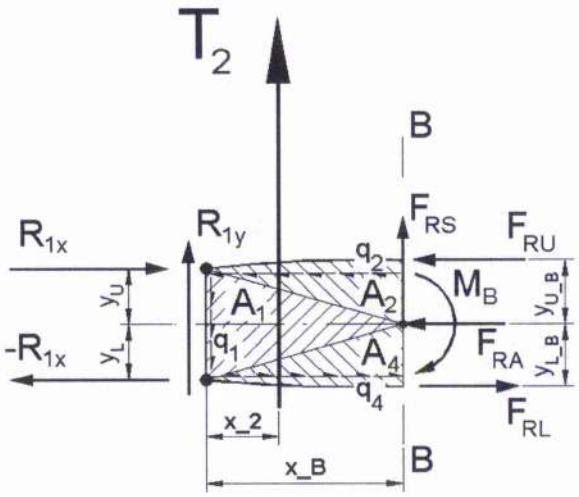

Figure 4.9 - Shear and flange forces of a rib's middle part

According to Figure 4.9, the following equations of the resultant external forces along the section [B-B] can be written as:

Moment at section [B-B]:

$$M_B = \sum M = R_{1x}.(y_U + y_L) + R_{1y}.x\_B + T_2.(x\_B - x\_2) - q_1.2.A_1 - q_2.2.A_2 - q_4.2.A_4 \qquad \textbf{(4-38)}$$

The resultant external shear force at section [B-B]:

$$F_{RS} = \sum F_y = R_{1y} + T_2 - q_1.(y_U + y_L) - q_2.(y_{U\_B} - y_U) - q_4.(y_{L\_B} - y_L) \qquad \textbf{(4-39)}$$

The resultant load normal to the section [B-B]:

$$F_{RA} = \sum F_x = (q_4 - q_2)x\_B \qquad \textbf{(4-40)}$$

After the calculation of resultant external forces at section [B-B], the flange forces at section [B-B] are calculated. From a simple static analysis, the flange forces at section [B-B] are found by taking the moments about the lower flange point at section [B-B].

$$\sum M = M_B - F_{RU}.(y_{U\_B} + y_{L\_B}) - F_{RA}.y_{L\_B} = 0 \qquad \textbf{(4-41)}$$

Hence the upper flange force at section [B-B]:

$$F_{RU} = \frac{M_B - F_{RA}.y_{L\_B}}{y_{U\_B} + y_{L\_B}} \quad \textbf{(4-42)}$$

Then, the lower flange force at section [B-B] can be easily found by using $\Sigma F_x = 0$:

$$\sum F_x = -F_{RU} - F_{RA} + F_{RL} = 0$$

$$F_{RL} = F_{RU} + F_{RA} \quad \textbf{(4-43)}$$

The described process of the load calculation is used in several sections along the middle part of the rib. Then, for further calculations, the maximum forces are used. The thickness of the rib's web is calculated in a similar way to that used on the spar's web. As for the spar webs, the equation of rib's web thickness can be derived from equation (4-29). Equation (4-44) represents the formula from which the rib's thickness is calculated.

$$t_{RibW} = \sqrt[3]{\frac{F_{RS}.b_s^2}{0.91k_s.E.H_R}} \quad \textbf{(4-44)}$$

Compared with the spar flanges, the geometry of the rib flanges is significantly simpler, and the only unknown dimension is the flange thickness.

The compressed rib's flange is calculated according to the crippling resistance theory. According to Figure 2.11, the parts of the rib are made from one piece of material. Therefore, the minimum flange thickness is equal to the rib's web thickness. The effective skin's width is involved in the rib's flange calculation (Equation (4-46)).

As mentioned above, the minimum thickness of rib's flange is the thickness of rib's web. According to known flange's force and flange's dimensions, the stress in the flange is calculated (Equation (4-45)). Then, the limiting crippling stress of a compressed flange with a thickness of the rib's web is calculated (Equation (4-46)). If the flange's stress is lower than the crippling stress, the thickness of the rib's web is used as the thickness of the compressed flange in further calculations. If the flange's stress is higher than the crippling stress, the thickness of

compressed rib's flange is calculated from equation (4-47), in which the effective width of the skin (Equation (4-49)) is involved.

The development of equation (4-47) leads to the quadratic equation (4-50), from which the minimum thickness of the rib's compressed flange is calculated.

$$\sigma_{FRC} = \frac{F_{RU}}{A_{RU}} = \frac{F_{RU}}{a_H . t_{RibW}} \qquad (4\text{-}45)$$

$$\sigma_{CR} = 0.56\sigma_Y . \left[\frac{g . t_{RibW}^2}{A_{RU}} . \sqrt{\frac{E}{\sigma_Y}} \right]^{0.85} \qquad (4\text{-}46)$$

$$\sigma_{CR} = 0.56\sigma_Y . \left[\frac{g . t_{RH}^2}{A_{RU} + A_{ef\_RUSK}} . \sqrt{\frac{E}{\sigma_Y}} \right]^{0.85} \qquad (4\text{-}47)$$

$$\sigma_{CR} = 0.56\sigma_Y . \left[\frac{g . t_{RH}^2}{a_H . t_{RH} + w_{RS} . t_S} . \sqrt{\frac{E}{\sigma_Y}} \right]^{0.85} \qquad (4\text{-}48)$$

$$w_{RS} = 1.9 t_S . \sqrt{\frac{E}{\sigma_{CR}}} \qquad (4\text{-}49)$$

Hence

$$\sigma_{CR}^{\frac{1}{0.85}} = (0.56\sigma_Y)^{\frac{1}{0.85}} . \frac{g . t_{RH}^2}{a_H . t_{RH} + w_{RS} . t_S} . \sqrt{\frac{E}{\sigma_Y}}$$

$$g . (0.56\sigma_Y)^{\frac{1}{0.85}} . \sqrt{\frac{E}{\sigma_Y}} . t_{RH}^2 - \sigma_{CR}^{\frac{1}{0.85}} . a_H . t_{RH} - \sigma_{CR}^{\frac{1}{0.85}} . w_{RS} . t_S = 0 \qquad (4\text{-}50)$$

The following simplification can be used:

$$a = g . (0.56\sigma_Y)^{\frac{1}{0.85}} . \sqrt{\frac{E}{\sigma_Y}} ; \qquad b = -\sigma_{CR}^{\frac{1}{0.85}} . a_H ; \qquad c = -\sigma_{CR}^{\frac{1}{0.85}} . w_{RS} . t_S ;$$

Then, the solution of equation (4-50) can be written as follows:

$$D = b^2 - 4.a.c$$

$$x_{1,2} = \frac{-b \pm \sqrt{D}}{2.a} \qquad (4\text{-}51)$$

From equation 4-50 can be seen, that the discriminant [D] is always positive, the (-b) gives the positive value as well and the square root from discriminant [D] is always bigger than (-b). Therefore, the equation of minimum thickness of rib's compressed flange takes the form of equation (4-52).

$$t_{RH} = \frac{-b + \sqrt{D}}{2.a} \qquad (4\text{-}52)$$

The thickness of the tensioned flange is calculated directly from the equation of stress/strength equilibrium. The equations of the tensioned rib's flange are as follows:

$$\sigma_m \geq \frac{F_{RL}}{A_{RL} + A_{ef\_RI.Sk}} = \frac{F_{RL}}{a_D.t_{RD} + 1.9t_{RD}.\sqrt{\frac{E}{\sigma_{CR}}}}$$

$$t_{RD\_min} = \frac{F_{RL}}{\sigma_m \left(a_D + 1.9\sqrt{\frac{E}{\sigma_m}} \right)} \qquad (4\text{-}53)$$

If the resulting thickness [t_{RD_min}] is lower than the thickness of the rib's web [t_{RibW}], the rib's web thickness is used in further calculations.

The calculation of the compressed rib's flange has only one more condition. If the crippling stress was higher than the ultimate stress of the rib's material, the thickness of the compressed rib's flange is calculated in a similar way to the tensioned flange (equation (4-53)).

The calculation of the rib dimensions is the last step in the calculation process of the minimum dimensions of the wing structure components. According to the known dimensions of the wing structure components, the weights of the particular components and whole wing are calculated.

4.6 Calculation Process – the Iterative Loop

In the previous chapters, the equations used in the calculation process were derived. Most of these equations cannot be solved directly and have to be used together with others equations in some kind of iterative calculation.

According to the wing model used, and what has already been written, there are only a few structure dimensions, which have to be calculated. They are: the booms dimensions [H] and [h], effective height [h_{ef}] of the front and rear spar, thickness of the front and rear spar's web ([t_{FW}] and [t_{RW}]), skin thickness [t_S], and rib web and flange thicknesses ([t_{Rib_W}], [t_{RH}] and [t_{RD}]). Due to the presumptions which are used, only the skin thickness can be directly calculated. The other wing structure component dimensions are mostly depend on the effective height of the particular spar, which is unknown. The iterative loop in the process of calculation is due to the dependence of the effective height of the spar on the spar's boom dimensions. The calculation process expressed by flowchart shows Figure 9.9 in the appendix.

In the first step of the calculation, the skin's thickness was calculated, and the effective height of both spars was assumed to be the spar's height. Then, using equations (4-20), (4-27), (4-36) and (4-37) the spar's dimensions were calculated and subsequently, according to the spar's height and the already calculated boom dimensions [H] and [h], the new value of the spar's effective height was calculated (equation (4-4)). In the next loop of the calculation, this new value of the spar's effective height [h_{ef}] is used and the new values of the spar's dimensions are calculated. By using equation (4-4), the spar's effective height was calculated again and subsequently the spar's dimensions are calculated as well. This iterative process or calculation loop is terminated when the calculated value of the spar's effective height is the same as in the previous step. Then, the spar's dimensions are at a minimum.

The spar and skin dimensions are calculated in all bays of the particular wing layout (Figure 1.9). (Wing layouts differ in the number of ribs used.) Afterwards, when all the spar and skin dimensions along the span of the wing model are known, the dimensions of the ribs are calculated. In this stage of the calculation, all wing structure dimensions of a particular wing layout are known. Thus, the gross weight of the wing structure components and the whole wing can be calculated.

The next chapter brings a discussion and comparison of the results obtained from the calculation of this project.

5 Analysis of Calculated Wing Gross Weight

This chapter presents the results obtained from the calculation process described above. The whole calculation was done for three different spar load ratios and 49 wing layouts, which differ in the number of ribs used. Moreover, as will be explained later in this chapter, the entire calculation was performed for the three different boom dimension ratios [h/H]. The aim of this chapter is to analyse the results and optimise the spar load ratio, the boom dimension ratio and the number of ribs for the minimum gross weight of the wing model used. Note that the presented results are valid only for the wing model used in this project, and only for the flight conditions defined in the chapter 3.1. However, by changing the input data to the calculation process of this project (wing external dimensions and flight conditions), the developed calculation process can be easily used for the other two spars wings. It also must be remembered that the project is based on the idea of a preliminary design, when the results from the preliminary structure calculations are used to help designers in the following stage of the design process (Figure 1.1).

As stated earlier, the calculation was done for three distributions of aerodynamic load on the wing's spars. The results from the calculation of these three distributions of load are plotted together to show the optimum load distribution. It should be noted that the wing model used always has one rib in the middle span section, and therefore, the total sum of the ribs along the wing span is an odd number.

To check the calculated structure dimensions the small program (Marczi T., 2001), which is on the attached CD-ROM can be used (use file "Results Wing Components Dimensions.bat").

The source data of the diagrams presented in this chapter can be inspected in the program (Marczi T., 2001) "Results Wing Weight.bat" also on the attached CD-ROM.

5.1 Wing Gross Weight as a Function of Number of Ribs

After the calculation of the minimum dimension, the weight of the complete structure was calculated for the wing model used. As for the wing structure dimension calculation, the weight calculation was performed for all wing structural layouts used. The horizontal axis of the presented diagrams in this chapter represents the wing model with different numbers of ribs used. On the vertical axes of the diagrams, the particular wing layout weight is drawn. Due to the symmetrical aerodynamic load distribution along the wing span, all the diagrams are plotted for half the wing span only.

Figure 5.1 shows the dependence of the wing model structure components' weight on the number of ribs used and Figure 5.2 represents the dependence of the gross wing weight on the number of ribs used. Figures 5.1 and 5.2 relate to the [1:1] aerodynamic load distribution.

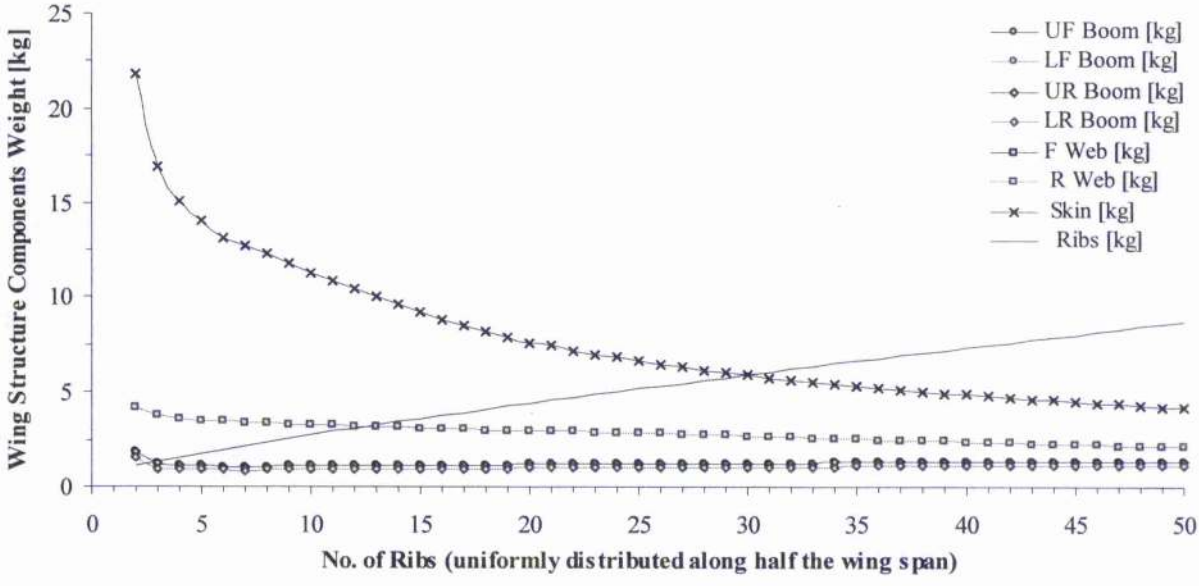

Figure 5.1 - Influence of Number of Ribs on the weight of the wing model structure components. (Graph is ploted for the spars' load ratio 1:1)

It can be seen from Figure 5.1 that the plots of the front and rear web weights overlay each other, as do the plots of the upper booms of the front and rear spars and the lower spar booms. It is due to the ratio of aerodynamic load distribution on the front and rear spar [1:1]; for which the dimensions of front and rear spars are the same. Next, it is evident that the skin and ribs contain the greater part of the wing model gross weight. Compared with other wing structure components, the weight of the skin is mostly influenced by the number of ribs used. This is due to the idealisation used for the skin panel calculation (Chapter 2), where the non-stiffened skin is used and therefore the side dimensions of the skin panel have a great influence on the panels' limiting shear flow. The downward trend of skin weight according to the number of ribs used is apparent from Figure 5.1. Due to the relatively small side dimension [h_{ef}] of the spar web panel used in the calculation, the downward trend of the spar web weight is not as steep as the trend of the skin weight.

The plot of the boom weights has a very gradual rise. The almost constant value of spar boom weight can be explained by the fact that the booms are loaded by the axial forces [F_H] and [F_D] (Figure 2.7), which are calculated from the spanwise bending moment distribution, which is constant for all calculated wing layouts.

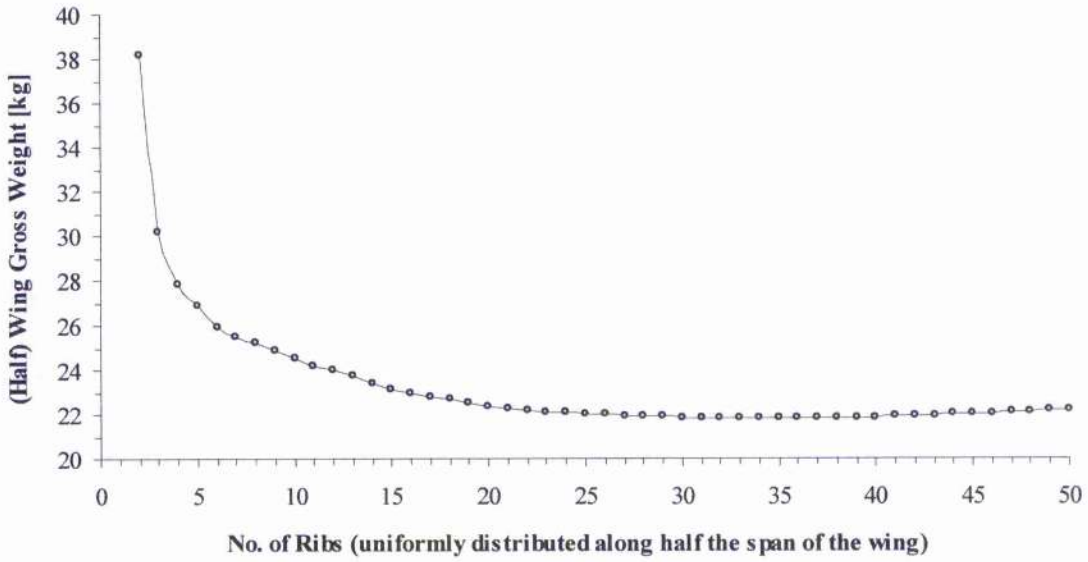

Figure 5.2 - Influence of Number of Ribs on the gross weight of the wing model used. (Graph is ploted for the spars' load ratio 1:1)

From Figure 5.1 it is clear that for the spars' load ratio 1:1 and the boom dimension ratio [h/H = 0.85], the number of ribs uniformly distributed along the wing span have no significant influence on the weight of the wing structure components. The exception is the skin, because in the wing model used the spacing of the ribs defines one of the skin panel dimensions, which in real structures, does not have to occur if stiffeners are used.

The left part of the plot on Figure 5.2 is mostly affected by the dramatic drop of the skin weight course (Figure 5.1), meanwhile the gradual rise of the right part of the graph on Figure 5.2 is due to the steady increase of the rib weights course displayed on Figure 5.1.

Similar diagrams can be plotted for the spar load distributions [2:1] and [3:1] (Figure 9.15, Figure 9.16, Figure 9.21 and Figure 9.22 in the appendix). However, the presented graphs of the wing model gross weight are very "flat" in the area of minimum weight and do not define the optimum number of ribs very clearly. Moreover, the presented results are clearly theoretical, because the calculated thicknesses and dimensions are not adjusted according to the manufactured material thicknesses. The resulting adjustment on the practical values is done in the next chapter.

5.2 Practical Structure Dimensions Constrains

The previous calculation was done theoretically, without regard to manufacturing or technological constraints. The calculated thicknesses of wing structure components were not adjusted to the thicknesses of manufactured materials. Additionally, the calculated boom widths are too narrow for practical use; therefore it is necessary to adjust them according to actual technological reality. The appendix contains an example of the calculated dimensions of the wing structure components (Figure 9.10, Figure 9.27 and Figure 9.28).

The solution of this problem follows two different ideas. The first is based on the fact that according to the resulting dimensions of the spar booms, the booms are relatively thick. This is due to the boom dimension ratio [h/H]. The thinner boom [L] bars with the same cross-sectional area as the current booms would be wider and therefore, as shown in the following chapter, the re-investigation of the boom dimension ratio [h/H] is done. The second approach to obtain the practical results implements the additional condition into the process of dimensions calculation.

This additional condition is based on the direct dimension adjustment on the minimum practical value, which in the case of boom widths is assumed as 25mm. The material thicknesses (catalog Aircraft Spruce, 1997-1998) used in the calculation process are (in [mm]): 0.4, 0.5, 0.6, 0.8, 1.0, 1.2, 1.5, 2.0, 2.5, 3.0, 4.0, 5.0, 6.0 and 8.0.

5.2.1 Re-investigation of Booms' Dimensions Ratio [h/H]

As stated above, the re-investigation of the boom dimensions ratio [h/H] was the first step in the attempt to obtain a more practical result. According to the small resulting values of the boom dimensions [H] and [h] (Figure 4.3), it is determined that the value [0.85] of boom dimensions ratio [h/H] relates to the relatively thick and too narrow [L] bars. By decreasing the thickness of boom [L] bars an increase in boom dimensions [H] and [h] can be achieved. Therefore, the values [0.9] and [0.95] of the boom dimensions ratio [h/H] are used in the following calculation. According to what has already been stated about the relation between the spar boom dimensions and aerodynamic load distribution to the wing structure, any change of the resulting boom dimensions results in the redistribution of the aerodynamic load to the wing structure. Subsequently, this change in the aerodynamic load distribution modifies the necessary minimum values of the structure's component dimensions. Therefore, the adjustment of the structure's component dimensions has been implemented to the structure calculation process and the calculation of all wing layouts was performed again.

The calculation with the adjustment of the calculated values of the dimensions is performed for the already defined three spars' load ratios [1:1], [2:1] and [3:1] and all three

boom dimensions ratios [h/H = 0.85; 0.9 and 0.95]. The following graphs represent the dependence of the resulting gross weight of the wing model used on the number of uniformly distributed ribs along the wing span. The graphs of the wing structure component's weights vs. number of ribs are shown in the appendix (Figure 9.11 till Figure 9.26). All these graphs relate to the wing structures with minimal practical dimensions. As already stated, the minimum boom dimension [H] is assumed as 25mm and "practical" values of thicknesses of the skin, ribs and spar webs are defined in the chapter 5.2.

All calculated dimensions have therefore been rounded up or down to the "practical" values defined above. For example, according to the calculation, the "theoretical" and "practical" thickness distribution of the skin in the wing model with five ribs along half the wing span and with the spar load ratio of [2:1] and boom dimension ratio of [0.9] is as follows:

	Theoretical	Practical
1. Bay (root):	t_s = 0.33 mm	0.4 mm
2. Bay:	t_s = 0.57 mm	0.6 mm
3. Bay:	t_s = 0.78 mm	0.8 mm
4. Bay:	t_s = 1.0 mm	1.0 mm

It can be seen that the theoretical thickness of the skin in the wing model described above is very close to the practical values. However, if it is considered the skin's thickness distribution of the same wing model but with nine ribs along the wing span, a large difference between the theoretical and practical results can be seen.

The "theoretical" thickness distribution of the skin in the wing model with nine ribs along half the wing span and with the spar load ratio of [2:1] and boom dimension ratio of [0.9] is as follows:

	Theoretical	Practical
1. Bay (root):	t_s = 0.17 mm	0.4 mm
2. Bay:	t_s = 0.3 mm	0.4 mm
3. Bay:	t_s = 0.41 mm	0.6 mm
4. Bay:	t_s = 0.52 mm	0.6 mm
5. Bay:	t_s = 0.62 mm	0.8 mm
6. Bay:	t_s = 0.72 mm	0.8 mm
7. Bay:	t_s = 0.82 mm	1.0 mm
8. Bay:	t_s = 0.92 mm	1.0 mm

Next, it is clear that in the wing model with nine ribs uniformly distributed along half the wing span, the distance between the two adjacent ribs is half of the distance of two adjacent ribs of the wing model with five ribs along half the wing span. Thus, according to the "practical" thicknesses of the skin shown above, it is evident that the weight of the skin of these two wings is the same. The presented example explained why the course of the resulting gross weight of the wing models with the practical dimensions is not smooth as one would expect. However, because this project deals with the preliminary design stage, and according to all the simplifications used, the results are calculated only with "some" accuracy. Therefore, it could not be a very large error; if we draw the smooth curve to represent the gross weights of the wing models.

The following diagrams (Figure 5.3, Figure 5.4 and Figure 5.5) represent the plots of the gross weight of the wing models using the "practical" dimensions. The diagrams are plotted for the all three spars' load ratios [1:1], [2:1] and [3:1] and each diagram contains three curves, which represent the wing models with three different booms' dimension ratios [0.85], [0.9] and [0.95].

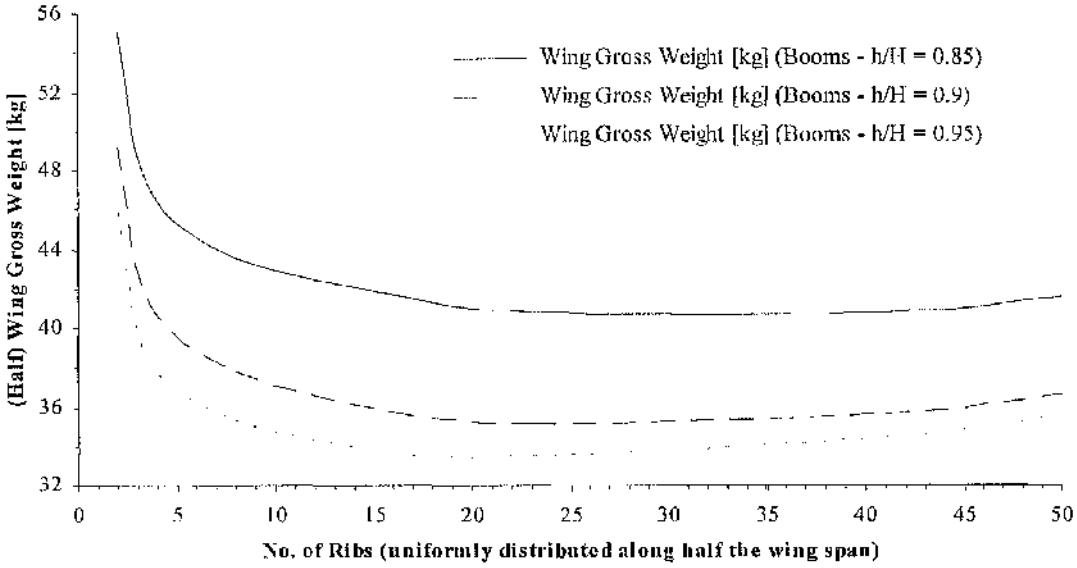

Figure 5.3 - Wing model's gross weight vs. Number of ribs
(Wing models with "practical" dimensions and spar load ratio [1:1])

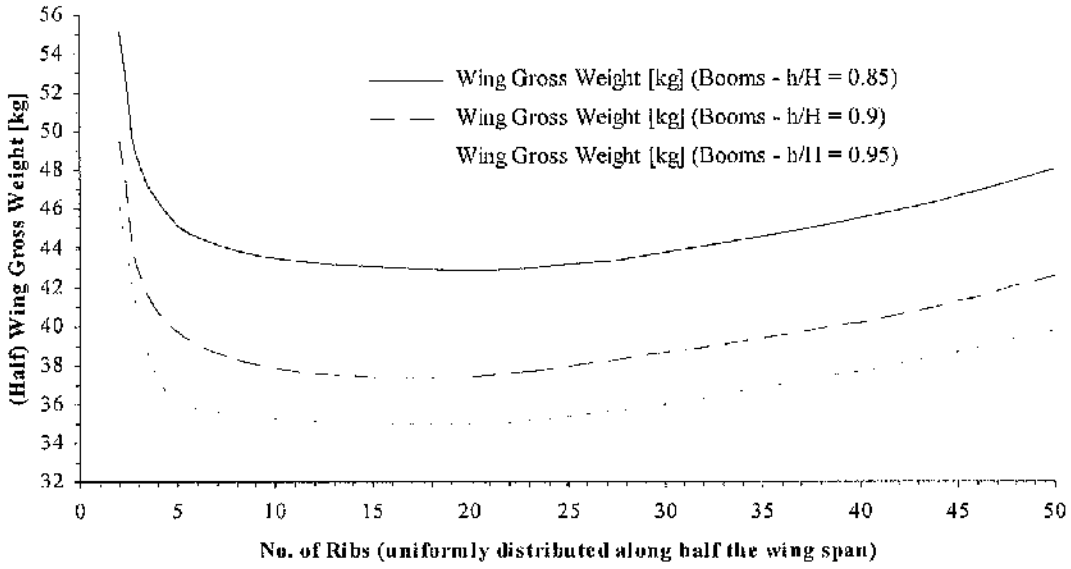

Figure 5.4 - Wing model's gross weight vs. Number of ribs
(Wing models with "practical" dimensions and spar load ratio [2:1])

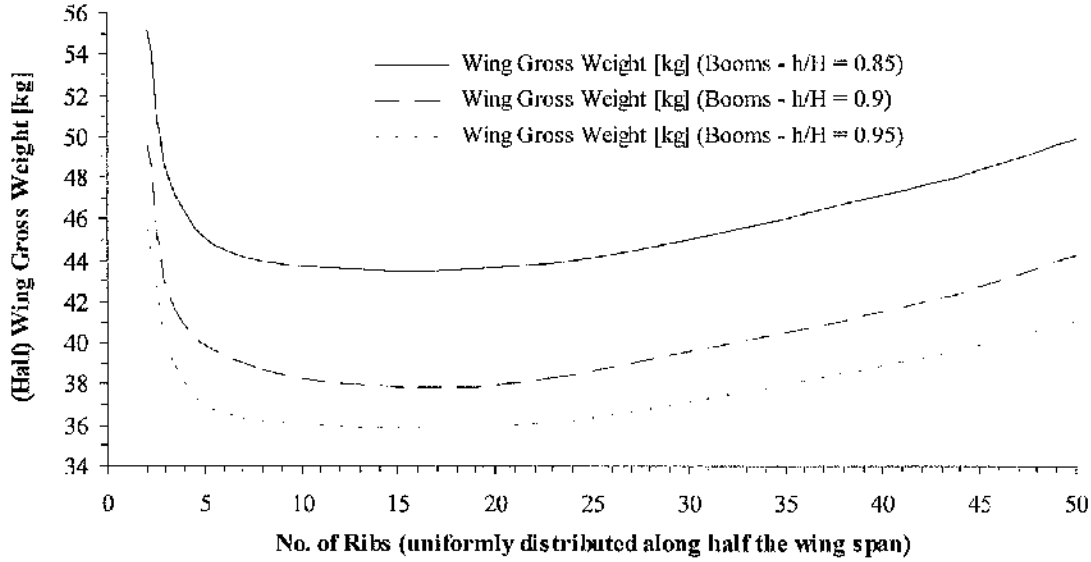

Figure 5.5 - Wing model's gross weight vs. Number of ribs
(Wing models with "practical" dimensions and spar load ratio [3:1])

The graphical representations of the results of all wing models with different combination of spar load ratio and boom dimension ratio are presented in the appendix (Figure 9.11 till Figure 9.26).

From Figures 5.3 to 5.5 it is clear that for the particular load conditions the boom dimension ratio [h/H = 0.95] produces the lightest wing structure, and the heaviest wing structure relates to the boom dimensions ratio [h/H = 0.85]. However, if we compare the wing models that have a spar boom dimension ratio of [0.95] according to the spars load ratio, it will be realised that the lightest structure is obtained from a spar load ratio of [1:1] (Figure 5.6).

As already stated, the boom dimension ratio [0.85] produces relatively narrow and thick [L] bars. According to Figure 5.6, to obtain the lightest wing structure related to this boom dimension ratio, a large number of ribs must be used. In contrast with the curve of the wing gross weight related to the spars load ratio [1:1], the curves of wing model gross weight with spars load ratio [2:1] and [3:1] are flat at the interval of 5 to 20 ribs.

From Figure 5.6, the conclusion can be made that for a particular wing model used, the minimum number of ribs which relates to the minimum weight of the wing structure lies in the interval five to twenty ribs (distributed uniformly on half the wing span) and the "optimum" spar load ratio is [2:1]. However, the results of the wing model gross weight with the ratio of the spar load [3:1] differs from those of wing model gross weight with the spar load ratio [2:1] by only about 3%. Also, the constant weight value in the interval of 5 to 20 ribs along half the wing span (the spar load ratios of 2:1 and 3:1), shows that the number of ribs in this interval has no significant influence on the gross weight of the wing model used. Note that the previous statement is valid only for the wing models with the "practical" dimensions of the structure components and only for the wing models and load conditions used in this project.

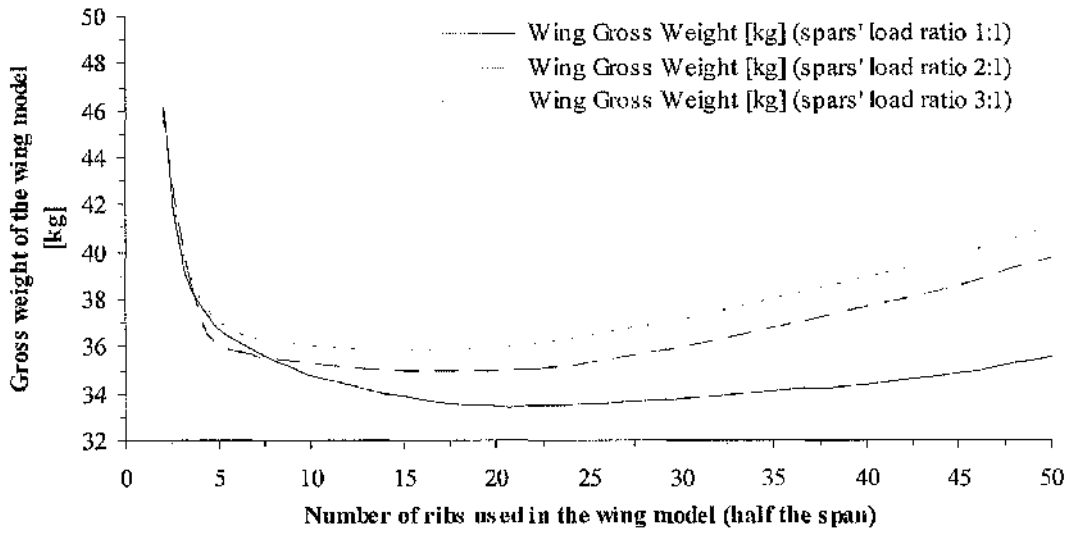

Figure 5.6 - Comparison of wing models' gross weight according to the spar load ratios. (The comparison is done for the wing structures with the boom dimension ratio h/H = 0.95)

As stated above, the boom dimension ratio [h/H = 0.95] produces the lightest "practical" wing structure. Therefore, the value [0.95] could be assumed as the optimum value of the boom dimension ratio [h/H]. The spar load ratio [1:1] is assumed as unsuitable for the wing model used; the spars load ratios [2:1] and [3:1] produce a more acceptable structure.

The presented results analysis is valid only for the loads conditions and wing model used in this project. However, the calculation process developed in this thesis can be used for other wing geometry and flight conditions and results from such calculations can be analysed in similar way. As an example, in the next chapter, the whole calculation process is performed for the same wing model, but for a different airplane weight. Airplane weight is one of the input data for the aerodynamic calculation. Aircraft weight directly affects the magnitude of the resulting aerodynamic load; therefore, different results should be expected.

5.2.2 Influence of Aircraft Weight

In this chapter, both aerodynamic and structure calculation are performed for the same wing geometry and aircraft speed as defined in the chapter 2.2, though with a different value for the aircraft weight. Therefore, different results from the aerodynamic calculation are obtained with a consequence on the results from the structure calculation.

The previous calculation was done for the aircraft weight 500 kg, which relate to the weight of UL and VL aircraft. For the purpose to check the influence of aircraft weight on the resulting dimensions of the wing model used, the following weights of the aircraft were considered: 800 kg, 1000 kg and 1200 kg. Obviously, these values of aircraft weight do not correspond to the UL or VL category of the airplanes and were used only to prove the applicability of the developed method of minimum dimension calculation on different input conditions. The chosen values of the aircraft weight represent average values of the small Czechoslovak sport planes depicted in table on Figure 5.7. One can notice, the wing span 10m of wing model used in this project correspond to the average value of the wing span of the airplanes depicted in Figure 5.7.

Type of the Aircraft	*Wing Span [m]*	*Empty Weight [kg]*	*max. Weight [kg]*	*max. Speed [km.h^{-1}]*
Zlin - 226 MS Trener	10.28	570	820	250
L - 40 Metasokol	10.05	534	935	240
L - 60 Brigadyr	13.96	912	1560	160
L - 200 Morava	12.33	1325	1950	305
Zlin - 42 MV	9.11	645	970	226
Zlin - 142	9.16	730	1090	234
Zlin - 43	9.76	730	1350	235

Figure 5.7 – Small Czechoslovak sport airplanes

The results from the aerodynamic calculation of these three wings are depicted in the Figures 9.29 to 9.34 in the appendix. The resulting diagrams of the wing gross weight dependence on the number of uniformly distributed ribs along the wing span are analysed in this chapter.

The process of calculation was performed for the spar load ratio [2:1] and all three boom dimension ratios [0.85, 0.9, 0.95] involved in the previous calculation. The results from the calculation of these three wings are shown in the following diagrams (Figure 5.8, Figure 5.9 and Figure 5.10). All diagrams in Figure 5.8, Figure 5.9 and Figure 5.10 are plotted for the wing structures with "practical" dimensions.

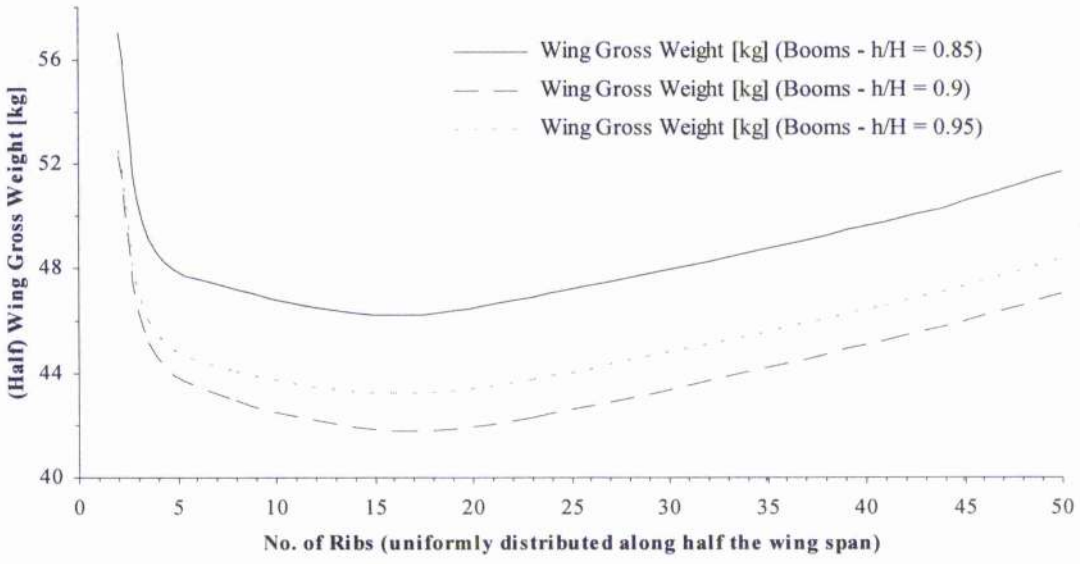

Figure 5.8 - Wing gross Weight vs. Number of uniformly distributed ribs along the wing span (Aircraft Weight = 800 kg)

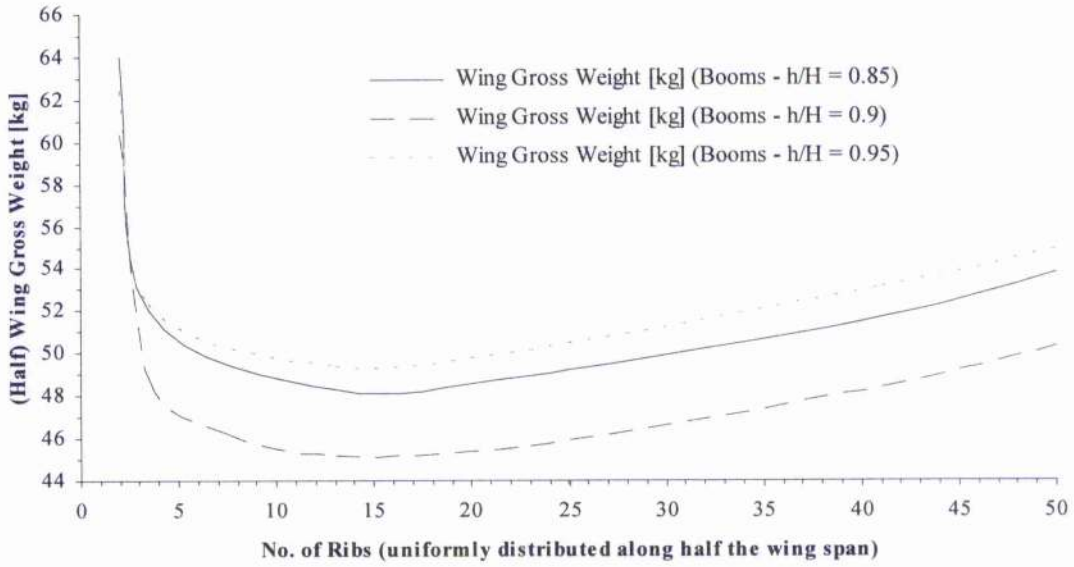

Figure 5.9 - Wing gross Weight vs. Number of uniformly distributed ribs along the wing span (Aircraft Weight = 1000 kg)

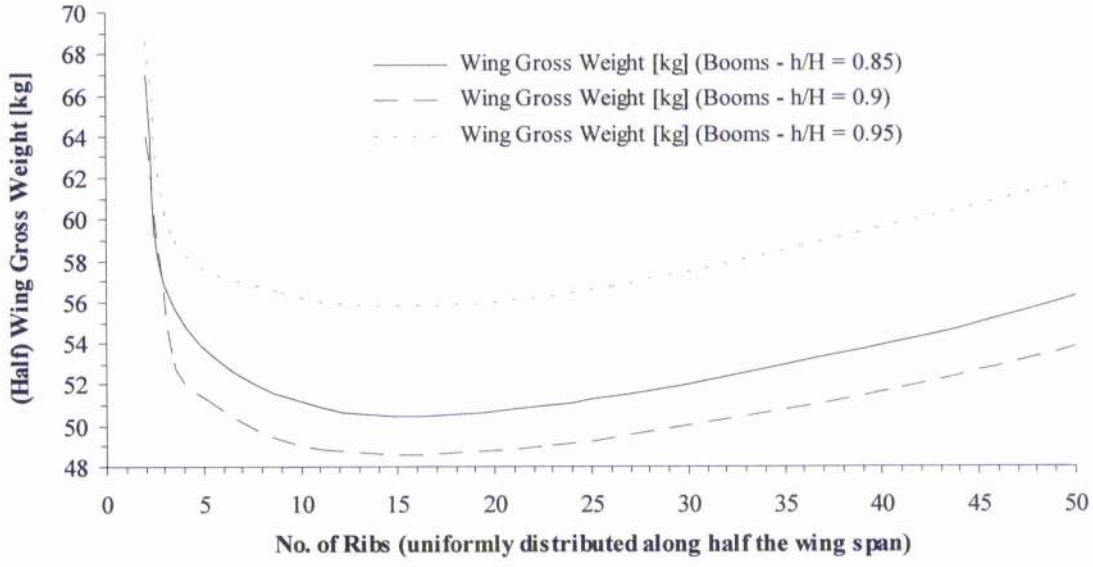

Figure 5.10 - Wing gross Weight vs. Number of uniformly distributed ribs along the wing span (Aircraft Weight = 1200 kg)

It can be seen that the graphs shown in Figures 5.8 to 5.10 are similar to those, shown in Figure 5.4. From Figures 5.8 to 5.10, the optimum number of ribs can be assumed as fifteen ribs uniformly distributed along half the wing span.

Using to the previous three diagrams, another important conclusion can be drawn. By increasing the aircraft weight (aerodynamic load on the wing), the boom dimension ratio [h/H = 0.95] becomes unsuitable for the practical use. In particular, the booms loaded by the compression become very wide. Figures 5.8 to 5.10 show an "upward" movement of the gross weight of the wing with boom dimension ratio [h/H = 0.95]. Thus, the boom dimension ratio [h/H = 0.9] became the optimum for these three wing models. However, it is clear, that a further increase airplane weight (aerodynamic load on the wing) will cause another change in the optimum boom dimension ratio [h/H]. In Figure 5.10 it can be seen that the gross weight data of the wing with the boom dimension ratio [h/H = 0.85] are close to that of the wing with the boom dimension ratio [h/H = 0.9]. Therefore, it can be concluded that with the further increasing aircraft weight, the boom dimension ratio [h/H = 0.85] becomes the optimum.

The results of this chapter confirmed what was already written above. All the results from the presented calculations are valid only for the particular wing model and used load conditions. However, according to the Figure 5.4, Figure 5.8, Figure 5.9 and Figure 5.10 one can conclude, that the aircraft weight has no significant influence on the optimum number of ribs in the case of wing model used. The applicability of the developed method of minimum dimension calculation in the preliminary stage of the aircraft design has also been proven.

5.3 Results Comparison

The aim of this chapter is to compare the results obtained from the analytical solution of the aerodynamic and structure calculation of the wing model used with the results obtained from the CFD and FEM calculation of the same wing model.

The analytical solution of the wing model is based on the idea to calculate the minimum dimension of the wing structure components in the preliminary stage of the wing structure design. For the aerodynamic calculation, the simple "Multhopp method" (Pope, 1951) was used and during the structure calculation process, lots of simplification was necessary to use. The results from the analytical solution are the "minimum" dimensions of the structure components.

These resulting dimensions are used for drawing one CAD model of the wing with six ribs on half the wing span and subsequently this CAD model is calculated by using the CFD and FEM method. Finally, the results from the analytical and computer calculation can be compared.

5.3.1 CFD/FEM Calculation

For CFD and FEM calculation, the program "*FEM-M*' developed at the department of Aerospace Engineering at the University of Colorado at Boulder was used. This program includes aeroelastic simulation of the computed wing model.

For the CFD and FEM calculations it was necessary to produce the CAD model of the wing used. For this purpose, CAD program "IDEAS" was used and resulting CAD model of the wing is shown in the Figure 5.11 (note, that this represents half the span of the wing model used).

Figure 5.11 – CAD model of half the wing (program "IDEAS")

In the next step, the CAD-model of the wing was meshed. For meshing, triangular shell elements were used with bar elements for the booms of the spars and ribs. The meshed CAD-model of the wing is shown in Figure 5.12. The boundary conditions at the nodes on the perimeter of the root wing section were modelled as clamped.

Figure 5.12 – The CFD/FEM mesh of the wing model

First, for the required flight conditions (chapter 3.1) the aerodynamic pressure along the wing span was calculated and consequently, the resulting pressure distribution was used as the load in the FEM calculation. One of the output from the FEM calculation is displacement in the nodes of meshed model and according to known displacements, which cause the change of the input data to the CFD calculation, the aeroelastic behaviour of the wing model was simulated.

The Figure 5.13 and Figure 5.14 represents the overall view on the top and bottom surface of the deformed wing model after calculation. The magnitude of the stress can be realized from the scale (units are [Pa]) shown in the Figure 5.13 and Figure 5.14.

Figure 5.13 - Stress distribution on the top surface of the wing model

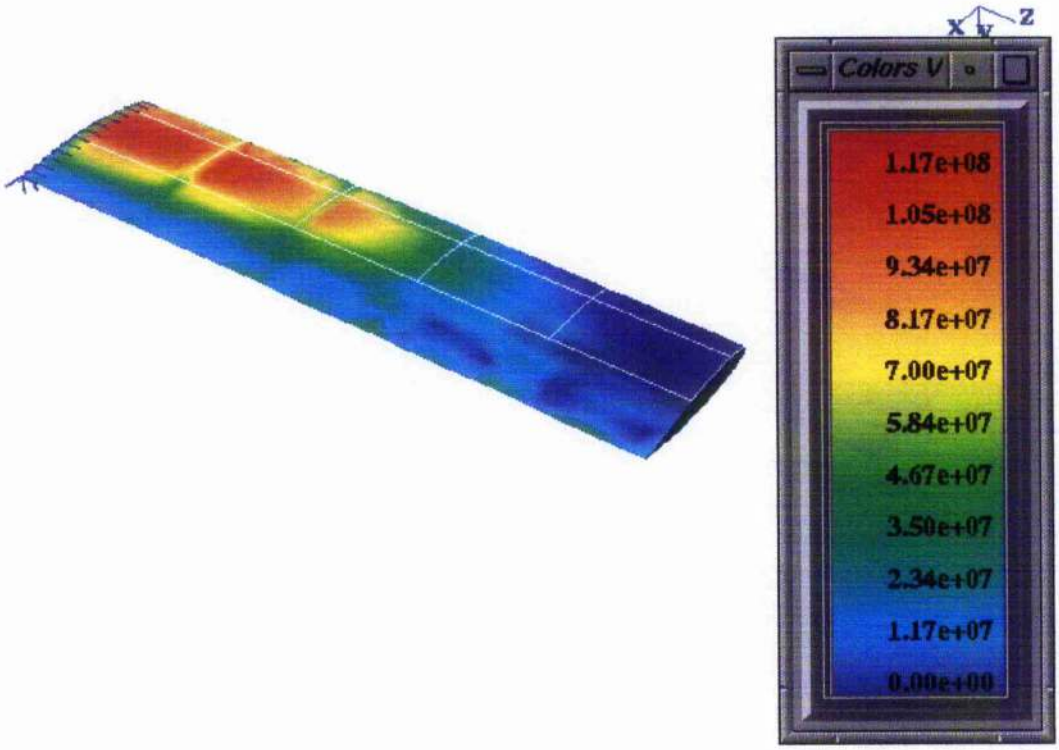

Figure 5.14 - Stress distribution on the bottom surface of the wing model

5.3.2 Comparison of Analytical and CFD/FEM Results

During the analytical aerodynamic calculation, one of the unknown values was wing angle of attack. For the particular wing model and flight condition used (chapter 3.1), the resulting value of the angle of attack is 3.877°. This value was used as input data in the CFD calculation. For this value of angle of attack the resulting lift is expected to be 29430 N, which is also the result from the analytical calculation. For the angle of attack 3.877°, the resulting lift from the CFD calculation is 28445.71 N. A difference of about 3.5%. Also as mentioned above, the computational process involved the effect of aeroelasticity; therefore, the conclusion of the effect of wing deformation on the resulting wing lift can be done. The results from the aerodynamic calculations are depicted in the file "lift.data" on the attached CD-ROM. The first row of the results in this file relates to the straight (undeformed) wing, meanwhile the last row relates to the final deformation of the wing. This shows that that for this particular wing, the deformation has little influence upon the resulting aerodynamic forces. According to the file "wing.strdisp", where nodal displacements are depicted, the greatest displacement caused by bending (on the tip of the wing) is about 120 mm. For the wing with a half span of 5m a displacement of 120 mm on the tip of the wing is not much, indicating the rigidity of the wing model.

The Multhopp method is one of the first methods used for the solution of equation 4-2. In contrast to the Multhopp method, the CFD methods provides more accurate results and moreover, together with the FEM calculation are capable include the effects of structural deformation (aeroelasticity). However, the small difference of 3.5% in the resulting lift force from the analytical (Multhopp) and CFD calculation indicates that for the preliminary design calculation, the simple Multhopp method is satisfactory.

In the presented thesis the minimum dimensions of wing structure are calculated from the equations of stress/strength equilibrium. Hence, the stress in the structure components is maximum (ultimate). The FEM model was created according to the resulting dimensions from the analytical calculations. With the "correct" FEM model, the stresses in the FEM model components would be expected "the same" as in the analytical model (ultimate stress). However, modelling of the wing for the FEM analysis from the stress/strength point of view is a far more complex task, requiring a thorough understanding of FEM analysis theory and a deep insight into wing design. Unfortunately the presented CAD model of the wing was created as a perfect shell with additional bar elements, without any discontinuities in the skin as riveting produces, or imperfect connections of spars and skin or web and booms. The presumption of the clamped root section of the wing is also not necessarily correct.

According to analytical results, the thickness of the skin panel in the root bay is 1mm. Panel side dimensions are 500mm x 1000mm. From Figure 9.8 the Buckling coefficient [k_s] of this plate has value 5.9. The critical buckling stress of the skin is calculated from the equation (4-29) and is equal to 1.336 MPa. According to Figure 5.13, the average stress in the root panel of the upper skin is around 85 MPa. It is clear, that such value is not acceptable. It seems, that the bending moment is distributed to the whole cross-section of this rigid shell structure, meanwhile in the analytical calculation was carried out mainly by the spar booms and partly by the effective width of the skin (Younger J.E, 1942; J. Špunda, 1955; E.F. Bruhn, 1973; A. Píštěk, 1987). There is also a great difference in the axial force of the spar booms if the analytical and FEM calculation is compared. From Figure 9.7, the average bending moment in the root bay of the wing is about 35 900 Nm. The effective height of the front spar is 153.69 mm. Using equation (4-1), the axial force of the booms is 234 KN. In FEM model, the spar booms are modeled by bar elements. The results from the FEM calculation are the displacements in the nodes; therefore, the axial force [$\mathbf{f}^*$] of the boom has to be calculated using the Member Stiffness Matrix [$\mathbf{k}^*$] and member joint displacement [$\mathbf{u}^*$]:

$$\mathbf{k}^*.\mathbf{u}^* = \mathbf{f}^* \qquad (5\text{-}1)$$

An example of this calculation is given in the appendix Figure 9.35. In Figure 9.35 the boom axial force was calculated according to the resulting displacement obtained from the FEM analysis. From this calculation, the axial force of the boom has a value of 5517.69 N, which is very small in comparison to the analytical calculation. The results of the FEM analysis indicate that the model used in the FEM calculation is not exact. Therefore, in this case, the obtained results from the FEM calculation cannot provide satisfactory information about the stress distribution in the wing structure used and because of this, the comparison with analytical results has relatively little meaning.

The creation of a "correct" model of such a complex structure as a wing requires great experience in the application of Finite Element modelling. On the other hand, this valuable experience showed the weak and strong points of the FEM calculation and it is a possible area for future work in this field.

6 Conclusion

The aim of the project was to develop a method for the preliminary estimation of the optimal number of uniformly distributed ribs for a two spar wing structure with a focus on minimum wing weight. In order to compare the wings according to their gross weight, the project was based on the calculation of minimal dimensions of wing structure components. Basically the whole project has been divided into four main parts: Model definition, Aerodynamic load calculation, Minimal structure dimensions calculation and Results analysis.

In the first part of the project, the necessary idealisations of the wing structure were defined. Then, due to unknown wing internal structure dimensions and consequently the unknown ratio of spar flexural rigidity, the relationship between the spar load ratio and ratio of spar flexural rigidity was investigated. The result from this investigation (equations 2-8 and 2-9) allowed the calculation of the position of the wing elastic axis to be made. This consequently divides the aerodynamic load acting on the wing model into a bending load and a torque load. The equation (2-8) expressed the ratio of the spar's flexural rigidity by the ratio of the spar load and ratio of the spar heights. However, equation (2-8) is valid only for spars with geometrically similar cross-sections and made from the same material. In the case of the spars with similar cross-sections, but different materials used, equation (2-9) has to be used.

Nevertheless, the ratio of the spar loads were not defined in this project, which led to the question, "which spar load ratio gives the minimum weight?". Therefore, the three load ratios of the wing spars [1:1], [2:1] and [3:1] were considered in the project.

The second part of the project focused on the calculation of the aerodynamic load distribution along the span of the wing model. Nowadays, there are several complex and precise methods for the aerodynamic calculation of the wing. The Multhopp method used in this project is less precise, but much simpler and its accuracy for this project's purpose is satisfying. Furthermore, the simplicity of this method was found reasonable for writing an independent program for aerodynamic load distribution along the wing span. The output files from program "Multhopp" (Marczi T., 2001) were directly used in the further process of calculation. The "Multhopp" program itself is more sophisticated than is necessary for this project, and can be used for other wing aerodynamic load investigations both practical and theoretical.

The next controversial aspect of aerodynamic load calculation could be the German BVF method used for calculation of chordwise aerodynamic pressure distribution of wing sections. As for the calculation of lift distribution along the wing span, there exists several precise methods or computer programs for the calculation of chordwise pressure distribution of wing section. However, the German BVF method has been widely used in the past, and its accuracy for

classical subsonic wing sections is reasonable (Špunda J., 1961). Moreover, the process of the calculation of the BVF's method is simple enough for the direct implementation to the process of aerodynamic load calculation along the wing span (program "Multhopp"). The necessary extension and disadvantage of this extension of BVF method were discussed in chapter 3.2.2 and the method itself is presented in chapter 9.1.

Once the wing's aerodynamic load was defined, the wing structure calculation could begin. As stated above, final results were obtained by comparison of one wing model with different numbers of ribs uniformly distributed along the wing span. Due to the same flight conditions and shape of all the wing models used, the calculated spanwise aerodynamic load distribution was constant for all wing layouts involved in the calculation. The condition of minimal weight leads to the calculation of minimal wing structure component dimensions.

During the analysis of wing structure components calculation, the high influence of spars boom geometry on the structure components dimensions was found out and consequently, the investigation of the boom geometry was done. The investigation of the boom geometry contains probably the most original approach to the final solution. The result of this investigation, boom dimension ratio [h/H] (dimensions [h] and [H] see Figure 4.3), simplified the process of calculation. Moreover, according to the final equation (4-36), from which the crippling stress of booms was calculated, the important conclusion or extension of Gerard's Method (E.F. Bruhn, 1973) of crippling stress calculation was done and follows: by using the dimensions ratio [h/H], crippling stress of the symmetrical [L] bar could be expressed directly as a function of material constants [σ_Y] and [E] (equation (4-36)).

Due to the fact that the dimensions of the wing structure components were unknown in this project, it is understandable that a detailed calculation of the wing structure components was unworkable. Therefore, the idealisation of the calculation process was necessary. Probably the most controversial idealisation of the calculation process is the exclusion of the leading part of the skin from the carrying of a torque moment. However, reasons for such strong idealisation are explained in chapter 2.3.3. Next, due to the simple wing model with stressed skin but without the stiffeners, the skin is treated as a flat panel loaded by shear from only the torque moment and the skin contribution to the bending resistance of the entire wing is expressed by the effective width of the skin (Figure 4.4) (Younger J.E., 1942, J. Špunda, 1955, E.F. Bruhn 1973, A. Píštěk 1987). The non-stiffened sheet has very poor buckling resistance and the method of "effective width" of the skin was commonly used in the past with an appropriate accuracy. In the detailed design stage, the precise calculation take its place, yet as Figure 1.1 shows, the airplane design is a continual process and the detailed design is based on the information from the previous stages.

The results obtained from the calculation are analysed in the last part of this paper. The presented results show large differences between the wing structures with theoretical minimal components dimensions and structures with component dimensions adjusted to the minimal practical values. However, resulting courses of wing model gross weights curves have expected [U] shape running, yet this is without the clear definition of one particular case of a number of ribs, which relate to the minimum wing model weight. The minimum weight of the wing model used (500 kg) occurs in the interval of 5 to 20 ribs, uniformly distributed along half the wing span (with a spar load ratio of [2:1] and [3:1] and the ratio of boom dimensions of [h/H = 0.95]). The spar load ratio [1:1] was found unsuitable for the wing model used in this project, because the minimum weight of the wing model with this spar load ratio relates to the wing with a large number of ribs. Next, according to the boom shape analysis of this project, it was found, that the boom dimension ratio [h/H = 0.95] produces the most practical symmetric [L] bars. However, the extension of the calculation presented in chapter 5.2.2 proved, that the optimum boom dimension ratio [h/H] significantly depends on the airplane weight, respectively on the load carried by the wing. Next, according to the results obtained from the calculations of four different aircraft weights (Figures 5.4, 5.8, 5.9 and 5.10), the optimum number of ribs of the wing model used can be assumed as twenty-nine (fifteen along half the wing span).

The comparison of the CFD calculation with the "old" Multhopp method showed the difference 3.5% in the resulting lift force, which indicates that for the preliminary design calculation, the simple Multhopp method is satisfactory enough. Also it was shown that the resulting deformation of the particular wing model has very little effect on the resulting aerodynamic lift.

Due to the unrealistic wing model used in the FEM calculation, the results from the FEM calculation cannot be assumed as true and therefore the comparison of results obtained from the analytical approach and FEM calculation was not presented in this thesis. However, as already mentioned, performed FEM analysis can be credited as a great experience and will be evaluated in the future work.

This project highlights the problem of the preliminary calculation of wing structure with a focus on the minimal weight and brings a huge amount of possibilities to extend the presented work. As examples of the uses to which this project can be extended, calculations could involve a wing model consisting of one spar, cases of non-uniformly distributed ribs along the wing span, or the uses of different wing geometries and geometry of internal wing structures. The expected difficulties of such projects could be to find and express the relations between the structure dimensions and load distribution, put them together, and calculate the minimum (preliminary) dimensions. Obviously, for a more complicated model of the wing structure, more

complex processes of the solution could be expected. However, the idealisation of the structure and the solution process will also be necessary.

7 References:

Anderson J. D., Fundamentals of Aerodynamics, McGraw-Hill Book Company, 1976, ISBN 0-07-001656-9

Ardema M.D., Chambers M.C., Patron P.A., Hahn A.S., Miura H., Moore M.D., Analytical Fuselage and Wing Weight Estimation of Transport Aircraft, Ames Research Center, NASA Technical Memorandum 110392, May 1996

Ballenstedt L., Influence of Ribs on Strength of Spars, NACA TN. No. 139, 1923

Bromley S., Robinson W.H., The Lateral Failure of Spars, NACA TN. No. 232, 1926

Brož V., Aerodynamika nízkých rychlostí, Ediční středisko ČVUT-Praha, 1981, č. publikace 3780, Czech Republic

Bruhn E.F., Analysis and Design of Flight Vehicle Structures, Jacobs Publishing, INC., 1973, ISBN 01892522700

Caddell W.E., On the Use of Aircraft Density in Preliminary Design, SAWE Paper No. 813, May 1969

Everling E., The Increase in Dimensions of Airplanes – Weight, Area and Loading of Wings, NACA TN. No. 132, 1923

Fieldman J.P., Introduction to Aircraft Design, Cambridge University Press, 1999, ISBN 0 521 44319 9

Gomza A., Seide P., Minimum-Weight Design of Simply Supported Transversely Stiffened Plates Under Compression, NACA TN. No.1710, 1948

Giunta A.A., Aircraft Multidisciplinary Design Optimization Using Design of Experiments Theory and Response Surface Modeling Methods, Virginia Polytechnic Institute & State University, Blacksburg, VA, May 1997

Hall CH.W., Structural Weight of Aircraft as Affected by the System of Design, NACA TN. No.206, 1924

Iglesias S., Mason W.H., Optimum Spanloads Incorporating Wing Structural Weight, AIAA-2001-5234, 2001

Kuhn P., Analysis of 2-Spar Cantilever Wings With Special Reference to Torsion and Load Transference, NACA TN. No. 508, 1934

Kuhn P., Stresses in Aircraft and Shell Structures, McGraw-Hill Book Company, 1956, Library of Congress Catalog Card Number 55-11174

Leland M.N., Fundamentals of Aircraft Design, METS, Inc., 6520 Kingsland Court, San Jose, California 95120

Li G., Wang H., Aryasomayajula S.R., Grandhi R.V., Two-Level Optimization of Airframe Structures Using Response Surface Approximation, Structural and Multidisciplinary Optimization, Volume 20, Issue 2, pp. 116-124, ISSN: 1615-147X (printed Version), ISSN: 1615-1488 (electronic Version)

Liu B., Haftka R.T., Akgun M.A., Two-Level Composite Wing Structural Optimization Using Response Surfaces, Structural and Multidisciplinary Optimization, Volume 20, Issue 2, pp. 87-96, ISSN: 1615-147X (printed Version), ISSN: 1615-1488 (electronic Version)

Lundquist E.E., Schwartz E.B., A Study of General Instability of Box Beams With Truss-Type Ribs, NACA TN. No. 866, 1942

Megson T.H.G., Aircraft Structures for Engineering Students, Edward Arnold (Publishers), 1972, ISBN 0713132760

Marczi T., Effect of the number of uniformly distributed ribs along the wing span on the wing gross weight, presented on the conference "Advance Engineering Design", Glasgow, 2001

Marczi T., Program "Weight Optimisation", 2001, see Attached CD-ROM

Marczi T., Program "Multhopp", 2001, see Attached CD-ROM

Marczi T., "Results Wing Components Dimensions", 2001, see Attached CD-ROM

Marczi T., "Results Wing Weight", 2001, see Attached CD-ROM

Newlin J.A., Trayer G.W., The Design of Airplane Wing Ribs, NACA TN. No. 345, 1930

Perry D. J., Aircraft Structures, McGraw-Hill Book Company, INC., 1950

Píštěk A., Grégr O., Kahánek V., Bohm R., Pružnost a životnost letadel I, VUT-Brno, 1988, č. publikace 1511, Czech Republic

Pope A., Basic Wing and Airfoil Theory, McGraw-Hill Book Company, 1951

Raymer D.P., Aircraft Design: A Conceptual Approach, American Institute of Aeronautics and Astronautics, Inc., 1999, ISBN 1-56347-281-0

Rohl P.J., Mavris D.N., Schrage D.P., Combined Aerodynamic and Structural Optimization of a High-Speed Civil Transport Wing, Persented at the 36th AIAA Structures, Dynamic and Materials Conference, New Orleans, LA, April 1995

Schlichting H., Truckenbrodt E., Ramm H.J., Aerodynamics of the Airplane, McGraw-Hill International Book Company, 1979, ISBN 0-07-055341-6

Schuette E.H., McCulloch J.C., Charts for the Minimum-Weight Design of Multiweb Wings in Bending, NACA TN. No. 1323, 1947

Sexstone M.G., Aircraft Structural Mass Property Prediction Using Conceptual-Level Structural Analysis, 57th Annual International Conference of the Society of Allied Weight Engineers, Wichita, Kansas, May 18-20, 1998 pp.15

Svoboda Ch., Aluminum Structural Member Component Weight as a Function of Wing Loading, Aircraft Design, Volume 2, Issue 4, 1999, © 2000 Elsevier Science Ltd, PII: S1369-8869(99)00019-1

Shanley F.R., Weight-Strength Analysis of Aircraft Structures, 1952, The RAND Corporation, Library of Congress Catalog Card Number 52-5339

Shild H., The Complete Reference JAVA 2, 1999, Osborne Mc Graw-Hill, ISBN 0072130849

Slavík S., Stavba Letadel, ČVUT-Praha, 1997, PLU 1812, Czech Republic

Stinton D., The Anatomy of the Aeroplane, American Elsevier Publishing Company, Inc. 1966, Library of Congress Catalog Card No. 66-27666

Spearman L.M., A Review of 50 Years of Aerodynamic Reaserch With NACA/NASA, ICAS-94-3.1.3, 1994

Špunda J., Pevnost leteckých konstrukcí – Konstrukce a pevnost letounu, VTA AZ, 1955, č. zakázky 1156/55, Czech Republic

Špunda J., Stavebná mechanika a pevnost letounu, VUT-Brno, 1961, Tisk 2010, Czech Republic

Špunda J., Stavebná mechanika a pevnost letounu – Sborník tabulek, VUT-Brno, 1961, č. tisku 2010-T, Czech Republic

Šubrt L., Teorie desek a skořepin, ČVUT-Praha, 1991, č. publikace 7308, Czech Republic

Timoshenko S., Strength of Materials – Advance Theoty and Problems, D. Van Nostrand Company, Inc. New York, November 1945

Torrenbeek E., Prediction of Wing Group Weight for Preliminary Design, Aircraft Eng., July 1971 pp.16-21

Weil J., Polhamus E.C., Aerodynamic Characteristics of Wings Designed for Structural Improvement, NACA RM. L51E10a, 1951

Younger J.E., Mechanics of Aicraft Structures, McGraw-Hill Book Company, 1942

Zahm A.F., Relation of Rib Spacing to Stress in Wing, NACA TN. No.5, 1920

Zink P.S., Mavris D.N., Flick P.M., Love M.H., Development of Wing Structural Weight Equation for Active Aeroelastic Wing Technology, SAE International and American Institute of Aeronautics and Astronautics, AIAA1999-01-5640

Catalog Aircraft Spruce & Specialty Company, Worldwide Distributor of Certificated and Homebuilt Aircraft Supplies, 1997-1998

Catalog ESDU 71005, 1995

8 Bibliography

Čtverák J., Mertl V., Píštěk A., Soubor podkladů pro pevnostní výpočty leteckých konstrukcí, Letecký ústav VUT Brno, 1997, Czech Republic

Bartsch H.J., Matematické vzorce, SNTL-Nakladatelství technické literatury, Praha, 1983, 04-020-83

Benscoter S.U. MacNeal R.H., Equivalent Plate Theory for a Straight Multicell Wing, NACA TN. No. 2786, 1952

Bubeník F., Pultar M., Pultarová I., Matematické vzorce a metody, Vydavatelství ČVUT, Praha, 1997, ISBN 80-01-01643-9, Czech Republic

Kreyszig E., Advanced Engineering Mathematics, John Wiley & Sons, New York, 1999, ISBN 0-471-15496-2

Kuhn P., The Strength and Stiffness of Shear Webs With Round Lightening Holes Having 45 Flanges, NACA ARR. L-323, 1942

Levy S., Fienup K.L., Woolley R. M., Analysis of Square Shear Web Above Buckling Load, NACA, TN. No. 962, 1945

Šuľženko M.N., Konstrukce Letadel, SNTL Praha, 1953, DT 629.13, Czech Republic

Ratzersdorfer J., Calculation of Wing Spars, NACA TN. No. 34, 1920

9 Appendix

9.1 The chordwise pressure distribution calculation – The BVF Method

The German BVF method (Špunda, 1961) calculates the chordwise pressure distribution of the common subsonic wing sections. The pressure in this method is expressed as the sum of the aerodynamic pressure acting on the upper and lower side of the particular wing section. The calculation process of the BVF method is based on the superposition of three functions (see Figure 9.1). Then, equation (9-1) expresses the resulting chordwise pressure distribution of considered wing section.

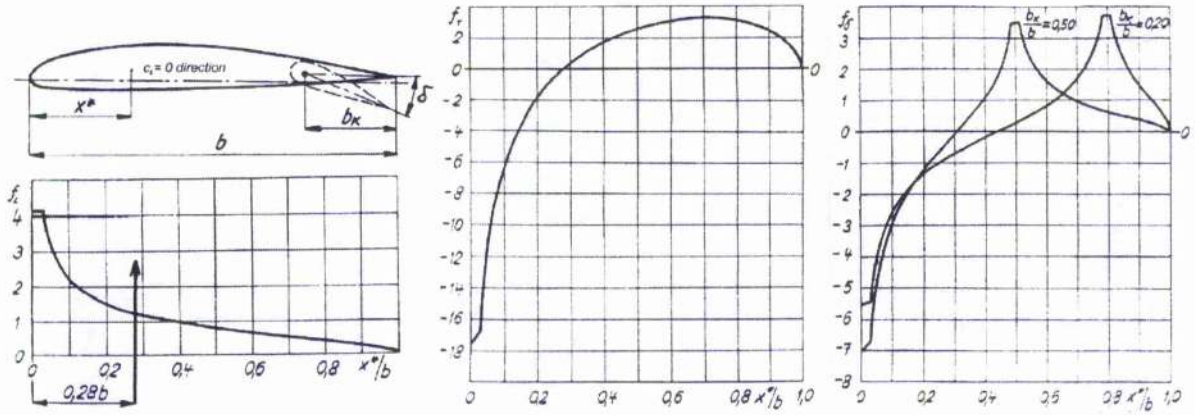

Figure 9.1 – The functions used in the German BVF method

$$p = q.[c_{L\delta}.f_L(\Theta) - c_{T0}.f_T(\Theta) + \delta.f_\delta(\Theta,\phi)] \qquad \textbf{(9-1)}$$

The variable [Θ] in the equation (9-1) is defined as:

$$\Theta = \arccos\left(1 - 2\cdot\frac{x^*}{b}\right) \qquad \textbf{(9-2)}$$

From equation 12-2 can be realized, the variable [Θ] is just function of chordwise position, in which the aerodynamic pressure is calculated.

The functions [$f_L(\Theta)$], [$f_T(\Theta)$] and [$f_\delta(\Theta)$] are defined as follow:

$$f_L(\Theta) = 0.716 \cdot \operatorname{cotg}\frac{1}{2}\Theta \qquad (9\text{-}3)$$

$$f_T(\Theta) = 5.80 \cdot \sin\Theta - 3.26 \cdot \operatorname{cotg}\frac{1}{2}\Theta \qquad (9\text{-}4)$$

$$f_\delta(\Theta,\phi) = 1.30 \cdot \log\frac{1-\cos(\Theta+\phi)}{1-\cos(\Theta-\phi)} + (0.024 - 1.273 \cdot \sin\phi) \cdot \operatorname{cotg}\frac{1}{2}\Theta \qquad (9\text{-}5)$$

The constant [ϕ] used in the equation (9-5) is defined as follow:

$$\phi = \arccos\left(2 \cdot \frac{b_k}{b} - 1\right) \qquad (9\text{-}6)$$

The lift coefficient of wing section with tilted flap (aileron) [$c_{L\delta}$], could be expressed as the equation (9-7) shows.

$$c_{L\delta} = c_{L(\delta=0)} + \frac{\partial c_L}{\partial \delta} \cdot \delta \qquad (9\text{-}7)$$

The ratio [$\partial c_L/\partial\delta$] could be written as follow:

$$\frac{\partial c_L}{\partial \delta} = \frac{\partial c_L}{\partial \alpha} \cdot \frac{d\alpha}{d\delta} \qquad (9\text{-}8)$$

According the German BVF method, the ratio [$d\alpha/d\delta$] could be expressed by equation (9-9):

$$\frac{d\alpha}{d\delta} = \frac{\pi - \phi + \sin\phi}{\pi} \qquad (9\text{-}9)$$

Substituting the [ϕ] in the equation (9-9) by the equation (9-6), the ratio [$d\alpha/d\delta$] could be written as follow:

$$\frac{d\alpha}{d\delta} = \frac{4}{\pi} \cdot \left(1 - \frac{1}{6} \cdot \frac{b_k}{b}\right) \cdot \sqrt{\frac{b_k}{b}} \qquad \textbf{(9-10)}$$

The results from experimental work proved, that the ratio [$\partial c_L/\partial\delta$] for greater values of flap (aileron) deviation [δ] has the downward trend. The change of value of ratio [$\partial c_L/\partial\delta$] is expressed by the efficiency [η_δ] (Figure 9.2). Then, the resulting lift coefficient of the wing section with tilted flap (aileron) previously expressed by equation (9-7) could be corrected by the efficiency [η_δ] and written as equation (9-11) shows.

$$c_{L\delta} = c_{L(\delta=0)} + \frac{\partial c_L}{\partial \delta} \cdot \delta \cdot \eta_\delta \qquad \textbf{(9-11)}$$

The BVF method allows recalculation of the torque moment characteristic of wing section without the flap on the instant of tilted flap as well. According to BVF method, for torque moment recalculation, the equation (9-12) can be used.

$$c_{T\delta} = c_{T(\delta=0)} + \delta \cdot \left(\frac{\partial c_T^*}{\partial \delta} - 0.28 \cdot \frac{\partial c_L}{\partial \delta}\right) \qquad \textbf{(9-12)}$$

where:

$$\frac{\partial c_T^*}{\partial \delta} = -0.39 \cdot \sin\phi + 0.222 \cdot \sin 2\phi - 0.017 \cdot \cos\phi + 0.0075 \qquad \textbf{(9-13)}$$

The ratios [$d\alpha/d\delta$] and [$\partial c_T/\partial\delta$] depends only on the ratio [b_k/b] and their are graphically expressed on Figure 9.2.

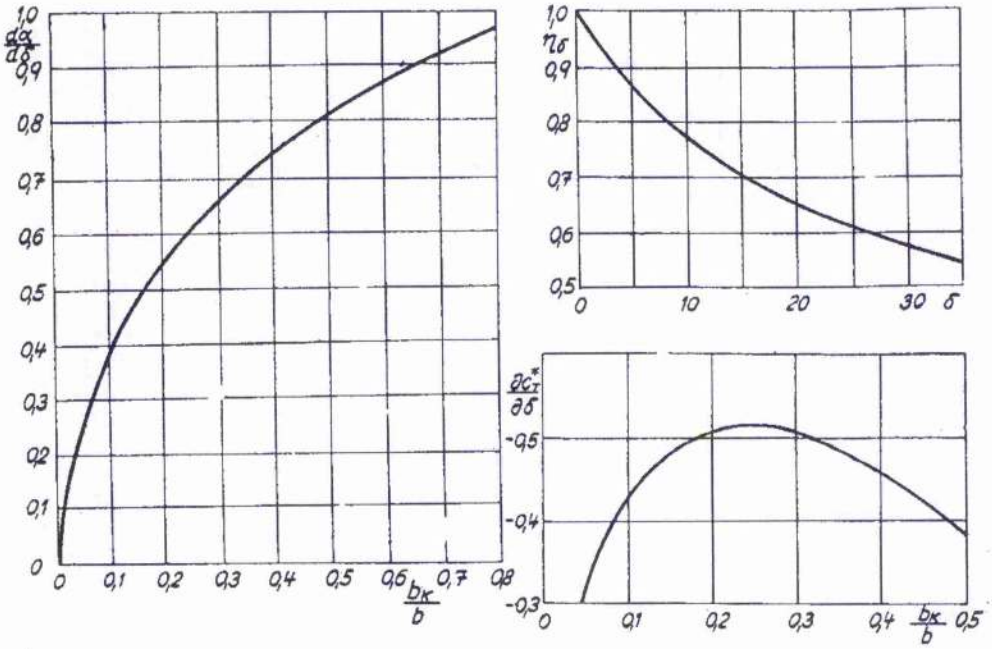

Figure 9.2 – The courses of the ratios [dα/dδ], [$\partial c_T/\partial\delta$] and efficiency [$\eta_\delta$] used in the BVF method

9.2 Extension of Gerard Method for symmetrical [L] bars

The Gerard Method (E.F. Bruhn, 1973) calculate the crippling stress according to equation (9-14):

$$\frac{\sigma_{Cr}}{\sigma_Y} = 0.56\left[\frac{g.t_L^2}{A_L}.\sqrt{\frac{E}{\sigma_Y}}\right]^{0.85} \qquad \textbf{(9-14)}$$

If the boom dimension ratio [h/H] is used, the thickness [t] can be expressed as equation (9-15) shows and cross-sectional area [A] of [L] bar can be written as equation (9-16) shows. Then, according to the chapter 4.3.2, the symmetrical [L] bar's crippling stress can be written as equation (9-17) presents.

$$\frac{h}{H} = const$$

$$t_L = H - H.const = H.(1-const) \qquad \textbf{(9-15)}$$

$$A_L = H^2 - H^2.const^2 = H^2.(1-const^2) \qquad \textbf{(9-16)}$$

$$\frac{\sigma_{Cr}}{\sigma_Y} = 0.56\left[\frac{g.(1-const)^2.H^2}{(1-const^2)H^2}.\sqrt{\frac{E}{\sigma_Y}}\right]^{0.85}$$

$$\sigma_{Cr} = 0.56\sigma_Y.\left[\frac{g.(1-const)^2}{(1-const^2)}.\sqrt{\frac{E}{\sigma_Y}}\right]^{0.85}$$

$$\sigma_{Cr} = 0.56\left(\frac{g.(1-const)^2}{(1-const^2)}\right)^{0.85}.\sigma_Y.\left[\sqrt{\frac{E}{\sigma_Y}}\right]^{0.85}$$

If substitution: $C = 0.56\left(\frac{g.(1-const)^2}{(1-const^2)}\right)^{0.85}$ is use, then:

$$\sigma_{Cr} = C.\sigma_Y^{0.575}.E^{0.425} \qquad \textbf{(9-17)}$$

For symmetrical [L] bars the Gerard's constant [g] has value [g = 2]. Thus, the following table (Figure 9.3) with crippling stresses calculated according the [L] bars dimensions (Figure

4.3) ratio [h/H] could be written. Table on Figure 9.3 is written for [L] bars' materials: Aluminum and Steel. The crippling stresses are calculated only for the dimensions ratios [h/H], which relate to the [L] bars with lower value of crippling stress than ultimate stress.

According to Gerard Method (E.F. Bruhn, 1973): g = 2

		Material ASM USA											
		Aluminum						Steel					
E [MPa]		7.20E+04						2.10E+05					
		2014	2024	7075	2024	6003	3003	1025	1045	5135	5135	4130	4130
	σ_m [MPa]	390	460	540	407	290	150	490	640	780	930	640	880
	σ_Y [MPa]	255	325	440	270	235	100	295	390	640	785	440	690
h/H	C	σ_{CR} [Mpa]											
0.8	0.156	-----	-----	-----	-----	-----	-----	-----	-----	-----	-----	-----	-----
0.81	0.149	-----	-----	-----	-----	-----	-----	-----	-----	-----	-----	-----	-----
0.82	0.141	-----	455.70	-----	-----	-----	-----	-----	-----	-----	-----	-----	-----
0.83	0.134	375.83	432.08	514.30	388.38	-----	-----	-----	-----	-----	-----	-----	-----
0.84	0.127	355.30	408.48	486.21	367.17	-----	-----	-----	-----	-----	-----	-----	-----
0.85	0.119	334.79	384.90	458.14	345.98	-----	-----	-----	-----	-----	-----	-----	-----
0.86	0.112	314.28	361.31	430.07	324.78	-----	-----	-----	632.40	-----	-----	-----	877.95
0.87	0.105	293.75	337.71	401.98	303.56	280.27	-----	-----	591.09	-----	883.78	633.55	820.60
0.88	0.097	273.19	314.07	373.84	282.31	260.65	-----	468.19	549.72	730.85	821.91	589.20	763.16
0.89	0.090	252.57	290.37	345.63	261.01	240.98	147.44	432.86	508.23	675.70	759.89	544.73	705.56
0.9	0.083	231.87	266.58	317.30	239.62	221.23	135.36	397.39	466.58	620.33	697.62	500.09	647.75
0.91	0.075	211.07	242.66	288.83	218.12	201.38	123.21	361.73	424.71	564.66	635.02	455.22	589.62
0.92	0.068	190.11	218.57	260.16	196.46	181.39	110.98	325.82	382.55	508.61	571.98	410.03	531.09
0.93	0.060	168.97	194.26	231.22	174.61	161.21	98.64	289.58	340.00	452.03	508.35	364.42	472.01
0.94	0.053	147.57	169.65	201.94	152.50	140.80	86.14	252.90	296.94	394.78	443.97	318.27	412.23
0.95	0.045	125.83	144.66	172.19	130.03	120.06	73.46	215.65	253.20	336.63	378.57	271.39	351.51
0.96	0.037	103.64	119.15	141.82	107.10	98.88	60.50	177.62	208.55	277.26	311.81	223.52	289.52
0.97	0.029	80.81	92.90	110.58	83.51	77.10	47.17	138.49	162.60	216.18	243.12	174.28	225.74
0.98	0.020	57.00	65.53	78.01	58.91	54.39	33.28	97.69	114.70	152.50	171.50	122.94	159.24
0.99	0.011	31.49	36.20	43.09	32.54	30.04	18.38	53.97	63.36	84.24	94.74	67.92	87.97

Figure 9.3 – Symmetrical [L] bars' crippling stress

9.3 Attached CD-ROM

Attached CD – ROM contains programs, which were used during the solution process of this project. All programs were written in the computer language JAVA. Basically, there are three independent programs in the folder "MSc – Programs". In the next, the programs will be called according to the folder in which they are situated. Thus, these three programs are: "Multhopp", "MSc - Project – Not Adjusted Results" and "MSc - Project - Adjusted Results".

All three programs contain graphical environment; therefore it is very easy work with them. Next, all three programs contain several sub-programs, which can be run by using the ".bat" files pasted to the main folder of particular program. Names of these ".bat" files correspond to the names of particular sub-programs and indicates, what the programs do. (In the case of the folder "MSc - Project - Adjusted Results", there are four other folders: "500 kg", 800 kg", "1000 kg" and 1200 kg", which corresponds to the calculation of the wing model with different load conditions – chapter 5.2.2.)

As already stated, program "Multhopp" was written to calculate the aerodynamic load distribution along the wing span. The program allows the calculation of the wings with common geometry, wing with tilted ailerons and geometrically or aerodynamically twisted wings.

The remaining two programs use the results from the program „Multhopp" and as their titles indicate, program "MSc - Project – Not Adjusted Results" calculates minimal theoretical weight of the wing and dimensions of the wing structure components and program "MSc - Project - Adjusted Results" calculates the minimal practical weight of the wing and dimensions of wing structure components.

The required operating system is Windows 9x or Windows NT. The simplest way to run the attached programs is to copy whole folder "Tomas MARCZI – MSc CD-ROM" directly on "C" drive (*c:\Tomas MARCZI – MSc CD-ROM*). Then, by using the ".bat" files from the main folders of particular programs all the sub-programs could be run.

Programs are written with respect to the simplicity of operating. Thus, they guide the user itself; therefore, it is not necessary to write the manuals of these three programs.

For completeness' sake, there is folder "CFD & FEM Files" pasted to the folder "Tomas MARCZI – MSc CD-ROM", in which the graphical results from the FEM analysis are located.

Folder "Jre 1.1.8" contains JAVA Run-time Environment, which is necessary for running programs written in JAVA language.

a	c_D	c_L	m_T
-16	0.0352	-1.2	0.23
-14	0.023	-1.08	0.2
-12	0.0164	-0.9	0.155
-10	0.0126	-0.73	0.1125
-8	0.0104	-0.54	0.065
-6	0.0082	-0.3	0.005
-4	0.007	-0.08	-0.05
-2	0.0068	0.16	-0.11
0	0.0068	0.38	-0.165
2	0.0074	0.58	-0.215
4	0.0086	0.8	-0.27
6	0.0096	0.99	-0.3175
8	0.0108	1.18	-0.365
10	0.0122	1.35	-0.4073
12	0.0144	1.53	-0.4525
14	0.0194	1.7	-0.495
16	0.0344	1.85	-0.5325
18	0.06	1.9	-0.545
20	0.12	1.5	-0.445

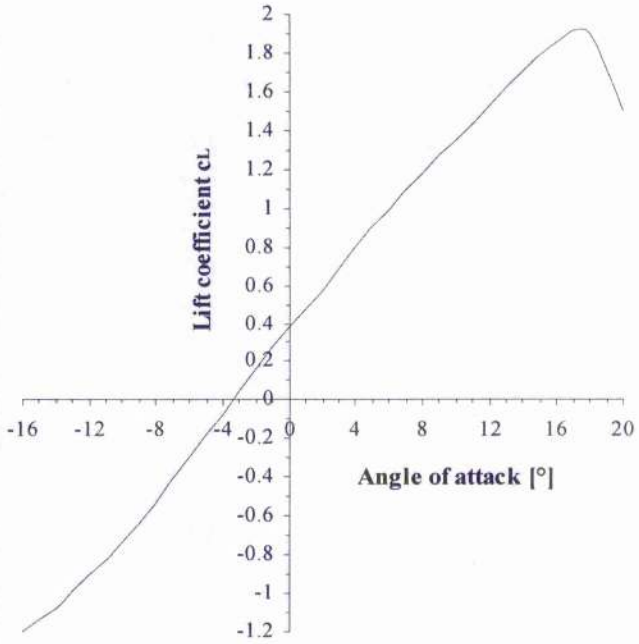

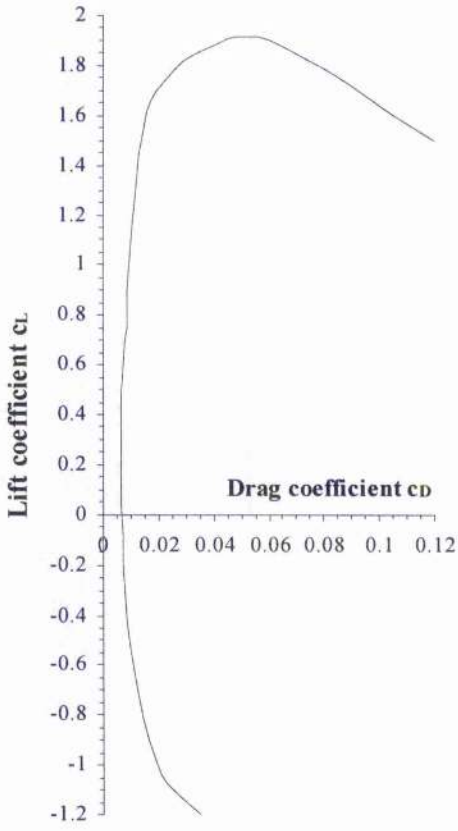

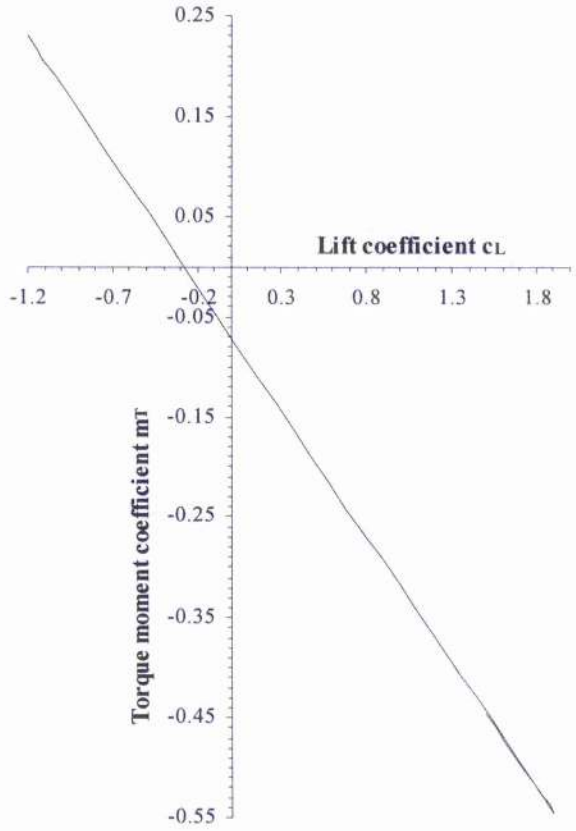

Figure 9.4 – The aerodynamic characteristics of the MS 0316 wing section

x [mm]	y_H [mm]	y_D [mm]
0	0.0986	0.0986
0.2	1.3735	-0.6663
0.5	2.0241	-1.1116
1.25	3.0536	-1.7827
2.5	4.1932	-2.4996
3.75	5.0118	-3.028
5	5.6203	-3.4625
7.5	6.4925	-4.1508
10	7.1238	-4.6498
12.5	7.6188	-5.0472
15	8.0208	-5.376
17.5	8.3511	-5.6493
20	8.6264	-5.8755
22.5	8.8554	-6.0605
25	9.0428	-6.21
27.5	9.192	-6.3281
30	9.3058	-6.4188
32.5	9.3872	-6.4836
35	9.4395	-6.5235
37.5	9.4632	-6.5368
40	9.4582	-6.521
42.5	9.4251	-6.4729
45	9.3598	-6.3903
47.5	9.265	-6.2713
50	9.1386	-6.1163
52.5	8.978	-5.9258
55	8.7803	-5.6986
57.5	8.5418	-5.4322
60	8.2594	-5.1256
62.5	7.932	-4.78
65	7.5602	-4.4008
67.5	7.1467	-3.9956
70	6.6956	-3.5725
72.5	6.2111	-3.1393
75	5.6981	-2.703
77.5	5.1607	-2.2726
80	4.6026	-1.8592
82.5	4.0283	-1.4745
85	3.4418	-1.1303
87.5	2.8543	-0.8371
90	2.2705	-0.6052
92.5	1.6906	-0.4476
95	1.1194	-0.3839
97.5	0.5616	-0.4419
100	0.0145	-0.6653

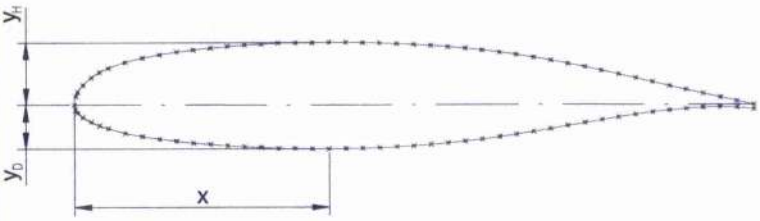

Figure 9.5 – The geometric characteristic of the MS 0316 wing section

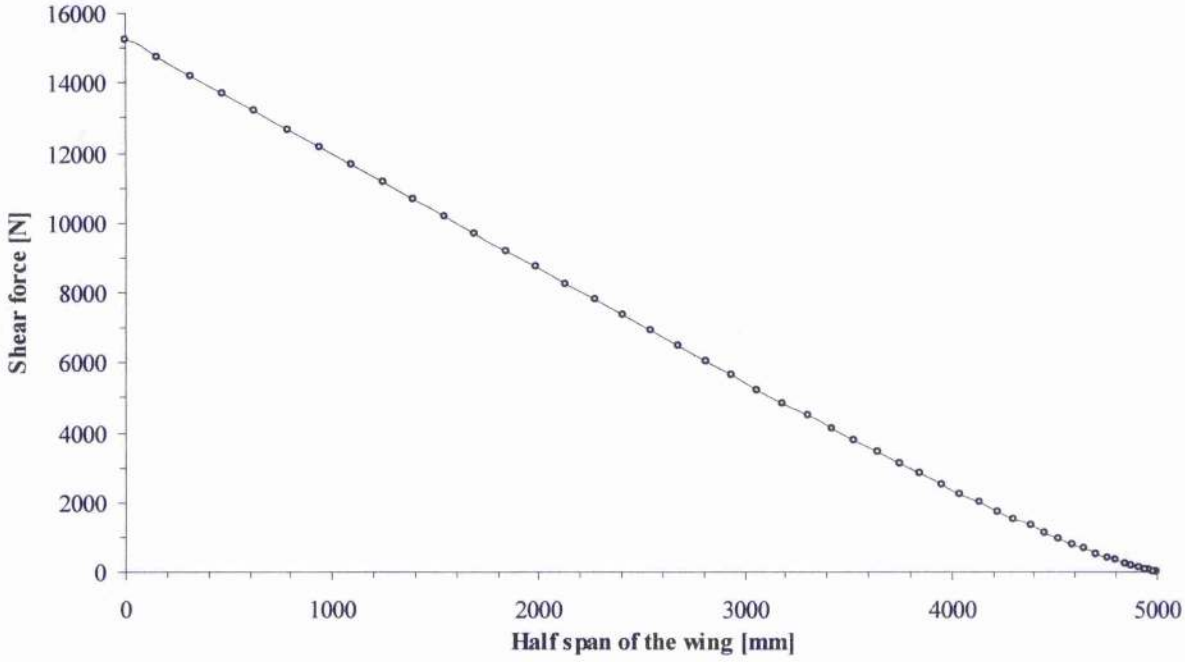

Figure 9.6 – The shear force distribution along half the span of the wing

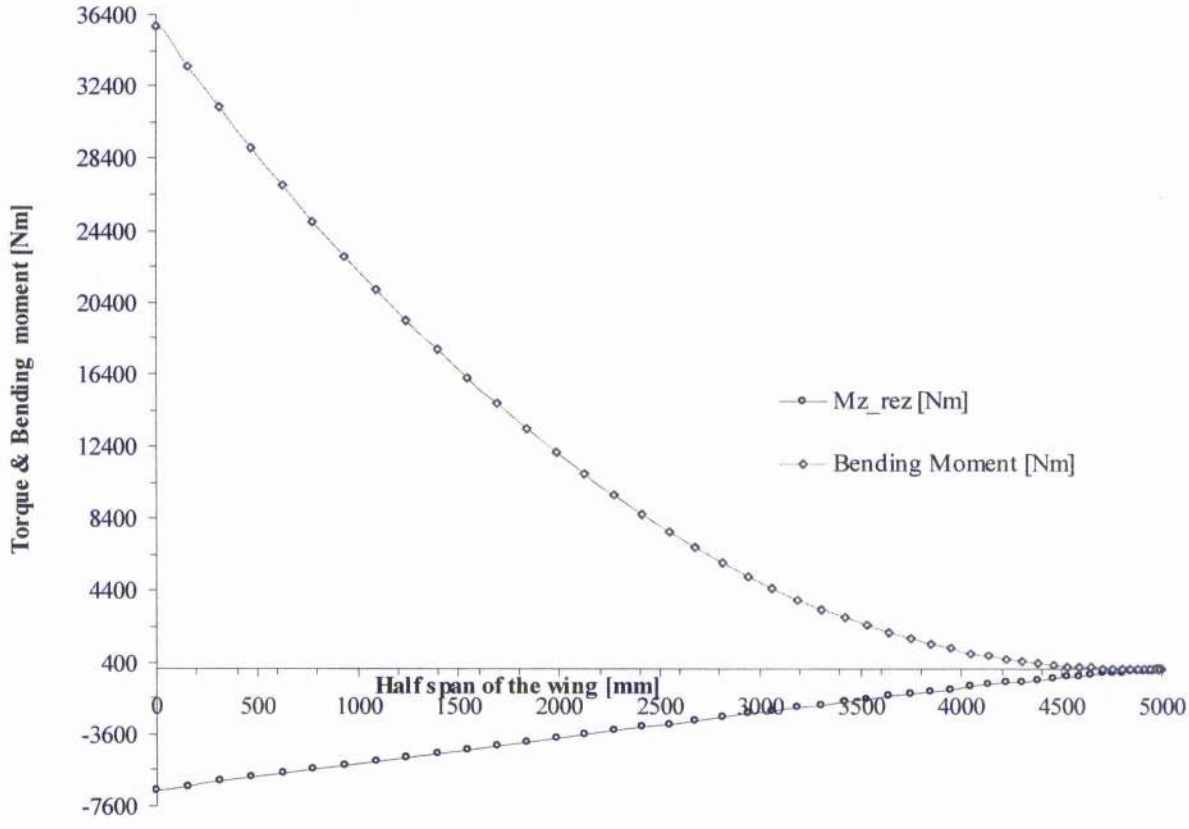

Figure 9.7 – The bending moment distribution and torque along half the span of the wing

b/a	ks
0	4.86
0.05	4.875
0.1	4.9
0.15	4.94
0.2	5
0.25	5.1
0.3	5.24
0.35	5.325
0.4	5.49
0.45	5.7
0.49	5.9
0.55	6.02
0.6	6.17
0.65	6.32
0.7	6.53
0.75	6.77
0.8	7.02
0.85	7.32
0.9	7.645
0.95	8
1	8.41

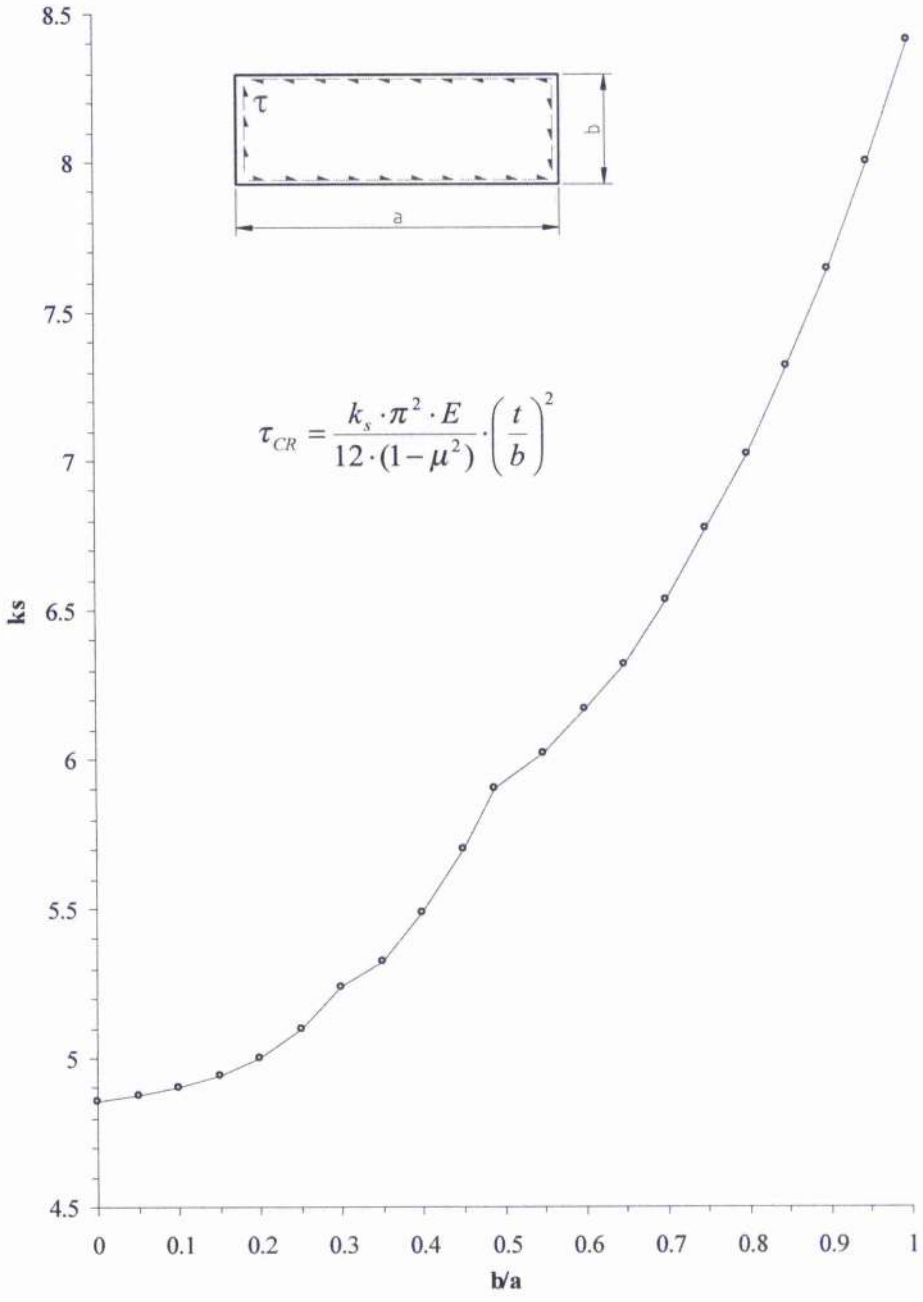

Figure 9.8 - The buckling coefficient [k_s] of flat plate in shear (simply supported edges)

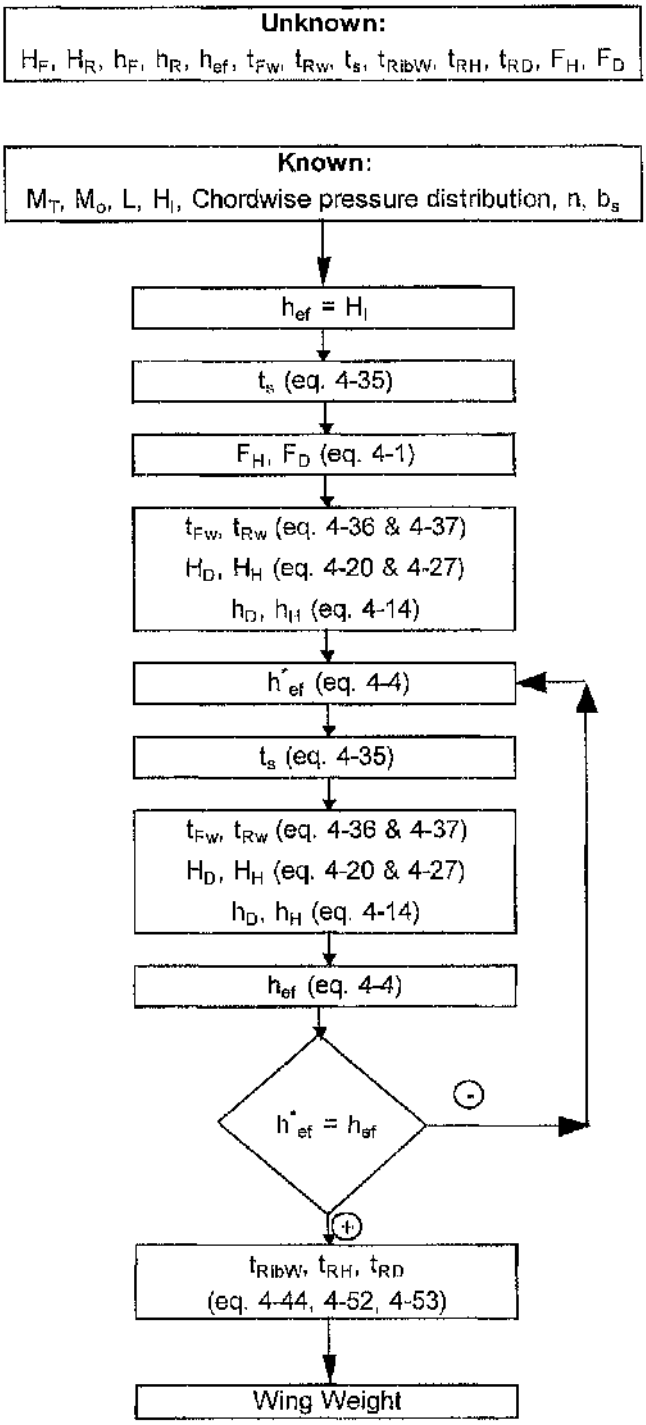

Figure 9.9 - Calculation Process (iterative loop)

Notation:

ts	- Skin Thickness [mm]
h_ef_F	- Effective Hight of the Front Spar [mm]
twF	- Thickness of the Front Web [mm]
HHF	- Dimension [H] of Front Spar Upper Boom [mm]
hHF	- Dimension [h] of Front Spar Upper Boom [mm]
HDF	- Dimension [H] of Front Spar Lower Boom [mm]
hDF	- Dimension [h] of Front Spar Lower Boom [mm]
h_ef_R	- Effective Hight of the Rear Spar [mm]
twR	- Thickness of the Rear Web [mm]
HHR	- Dimension [H] of Rear Spar Upper Boom [mm]
hHR	- Dimension [h] of Rear Spar Upper Boom [mm]
HDR	- Dimension [H] of Rear Spar Lower Boom [mm]
hDR	- Dimension [h] of Rear Spar Lower Boom [mm]
trw	- Rib's Web Thickness [mm]
trFU	- Rib's Upper Flange Thickness [mm]
trFL	- Rib's Lower Flange Thickness [mm]

Spar load ratio 3:1; boom dimension ratio h/H = 0.85

Bay	ts	h_ef_F	twF	HHF	hHF	HDF	hDF	h_ef_R	twR	HHR	hHR	HDR	hDR	trw	trFU	trFL
1	0.09	174.05	0.69	1.61	1.37	1.49	1.26	174.44	0.48	0.95	0.81	0.87	0.74	0.49	0.49	0.88
2	0.16	172.92	0.92	3.55	3.02	3.27	2.78	173.77	0.64	2.1	1.79	1.93	1.64	0.53	0.53	0.98
3	0.22	171.71	1.09	5.62	4.78	5.18	4.4	173.06	0.76	3.31	2.81	3.04	2.59	0.56	0.56	1.06
4	0.27	172.5	1.23	4.44	3.77	3.76	3.2	172.25	0.85	4.7	4	4.33	3.68	0.84	0.84	1.58
5	0.32	171.02	1.34	6.93	5.89	6.12	5.2	173.23	0.93	3.17	2.69	2.63	2.23	0.34	0.34	0.75
6	0.37	169.59	1.43	9.37	7.97	8.38	7.12	172.42	1	4.53	3.85	3.92	3.33	0.41	0.41	0.91
7	0.43	168.2	1.52	11.74	9.98	10.57	8.99	171.74	1.06	5.7	4.85	5	4.25	0.41	0.41	0.96
8	0.47	166.77	1.6	14.18	12.05	12.83	10.91	170.73	1.12	7.42	6.3	6.6	5.61	0.53	0.53	1.2
9	0.52	165.34	1.67	16.61	14.12	15.08	12.82	170.12	1.17	8.45	7.18	7.55	6.42	0.5	0.5	1.2
10	0.56	163.89	1.73	19.1	16.23	17.37	14.77	169.18	1.22	10.06	8.55	9.04	7.69	0.57	0.57	1.36
11	0.62	162.46	1.79	21.54	18.31	19.62	16.68	168.65	1.26	10.96	9.32	9.86	8.39	0.54	0.54	1.37
12	0.66	160.99	1.85	24.04	20.44	21.94	18.65	167.73	1.3	12.54	10.66	11.32	9.62	0.6	0.6	1.51
13	0.7	159.5	1.9	26.59	22.6	24.28	20.64	166.82	1.34	14.09	11.98	12.75	10.84	0.65	0.65	1.64
14	0.75	158.01	1.95	29.12	24.76	26.62	22.63	166.32	1.38	14.95	12.7	13.53	11.5	0.64	0.64	1.67

Figure 9.10 - Structure component dimensions of wing with fifteen ribs

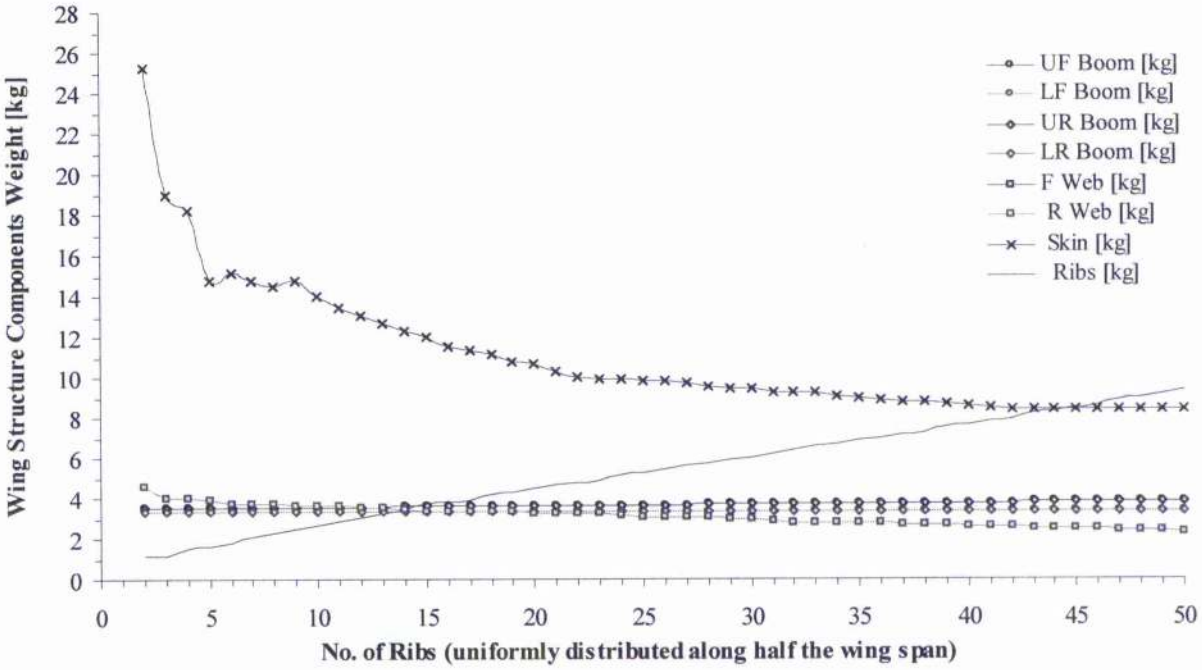

Figure 9.11 - Effect of number of uniformly distributed ribs on the weight of the wing model's components. (Spar load ratio 1:1; Boom dimensions ratio h/H = 0.9; practical dimensions)

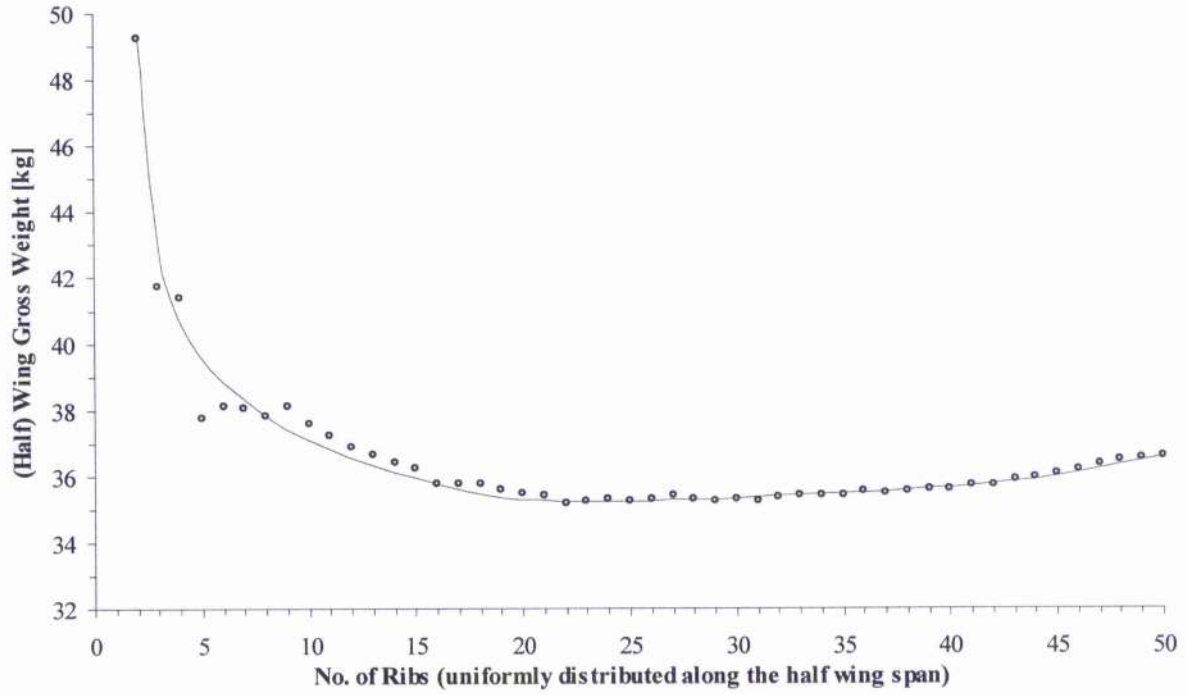

Figure 9.12 - Effect of number of uniformly distributed ribs on the gross weight of the wing model. (Spar load ratio 1:1; Boom dimensions ratio h/H = 0.9; practical dimensions)

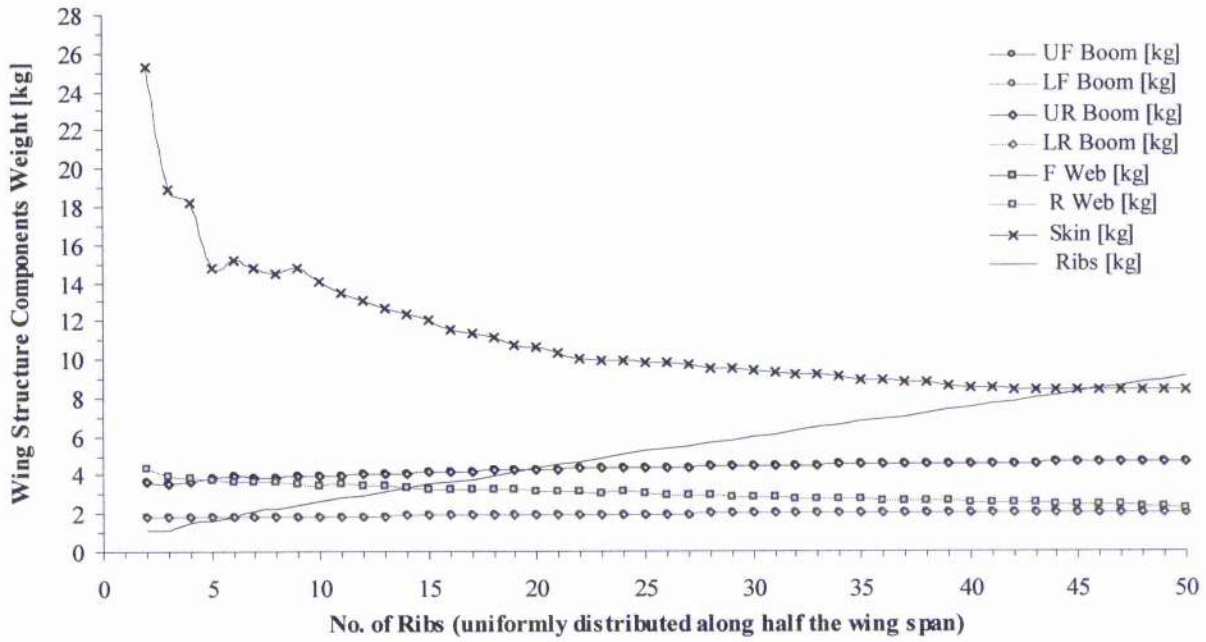

Figure 9.13 - Effect of number of uniformly distributed ribs on the weight of the wing model's components. (Spar load ratio 1:1; Boom dimensions ratio h/H = 0.95; practical dimensions)

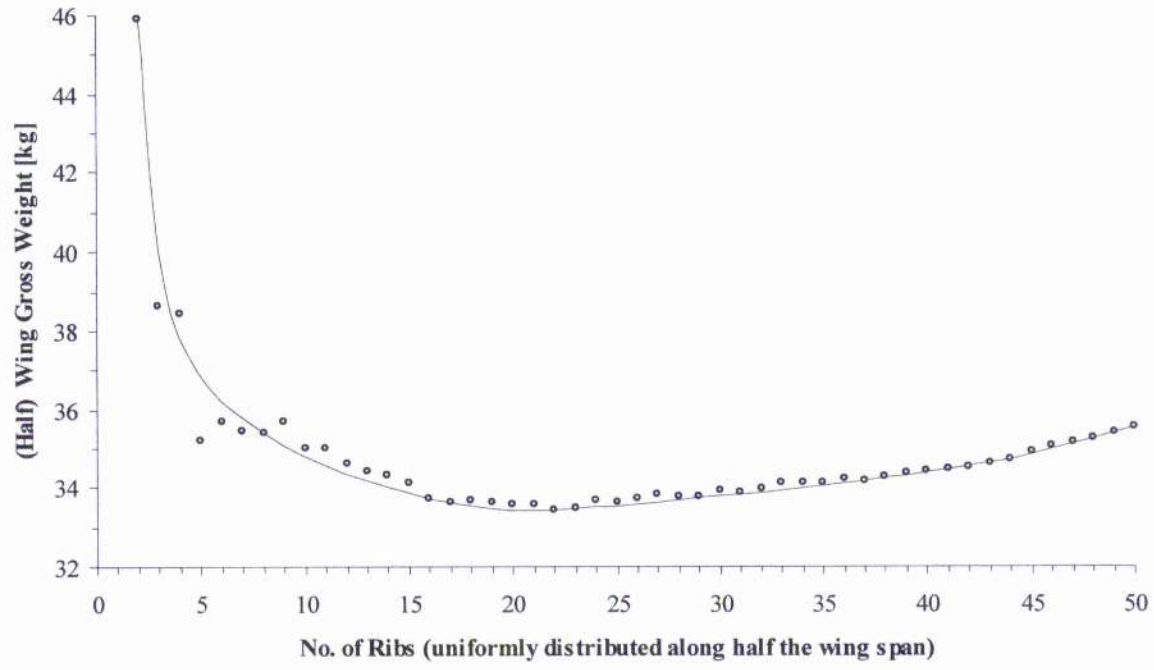

Figure 9.14 - Effect of number of uniformly distributed ribs on the gross weight of the wing model. (Spar load ratio 1:1; Boom dimensions ratio h/H = 0.95; practical dimensions)

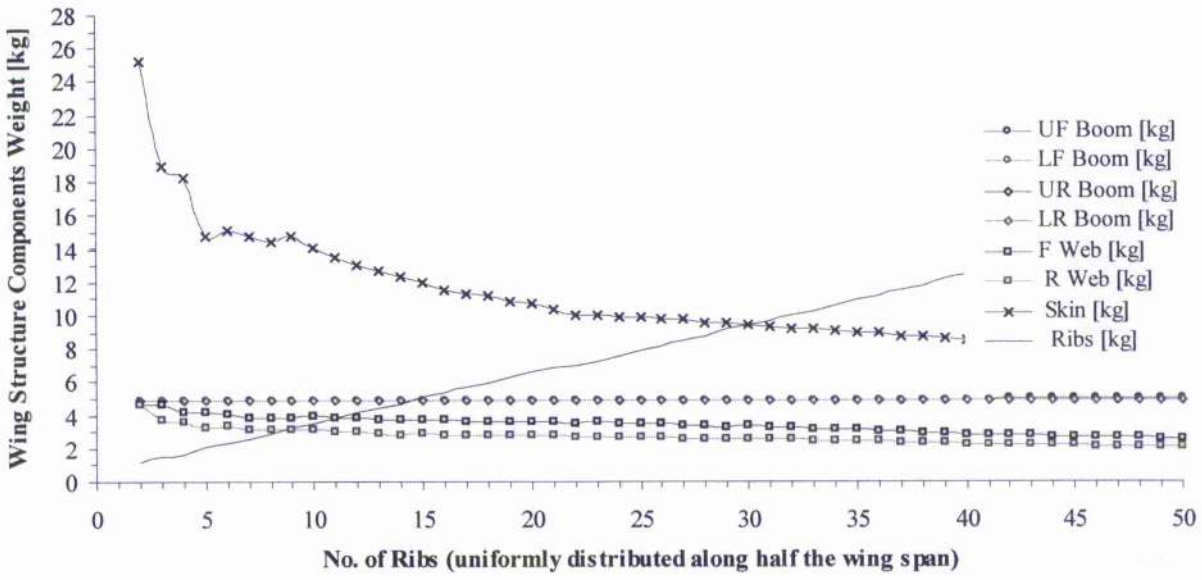

Figure 9.15 - Effect of number of uniformly distributed ribs on the weight of the wing model's components. (Spar load ratio 2:1; Boom dimensions ratio h/H = 0.85; practical dimensions)

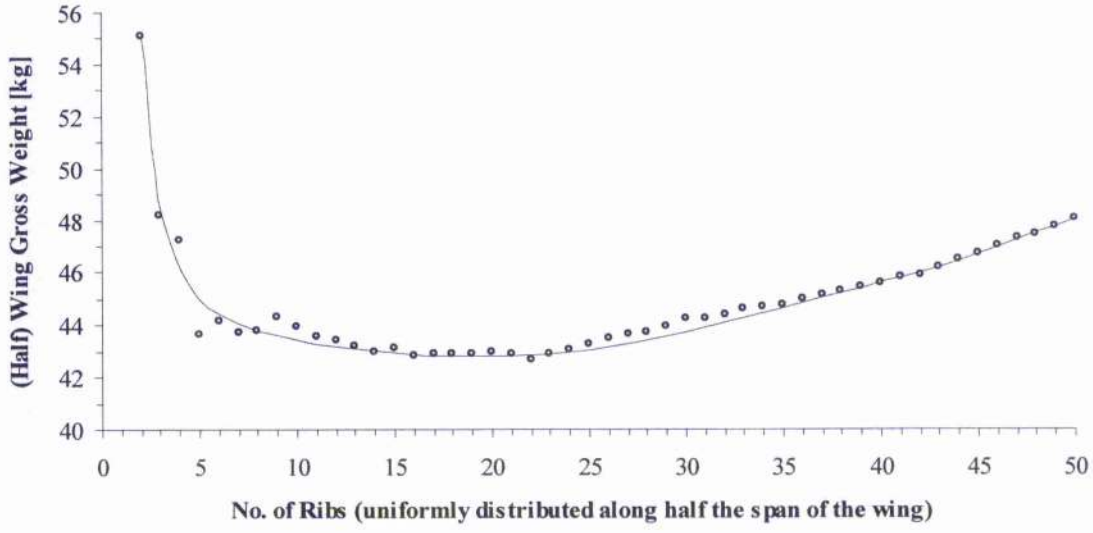

Figure 9.16 - Effect of number of uniformly distributed ribs on the gross weight of the wing model. (Spar load ratio 2:1; Boom dimensions ratio h/H = 0.85; practical dimensions)

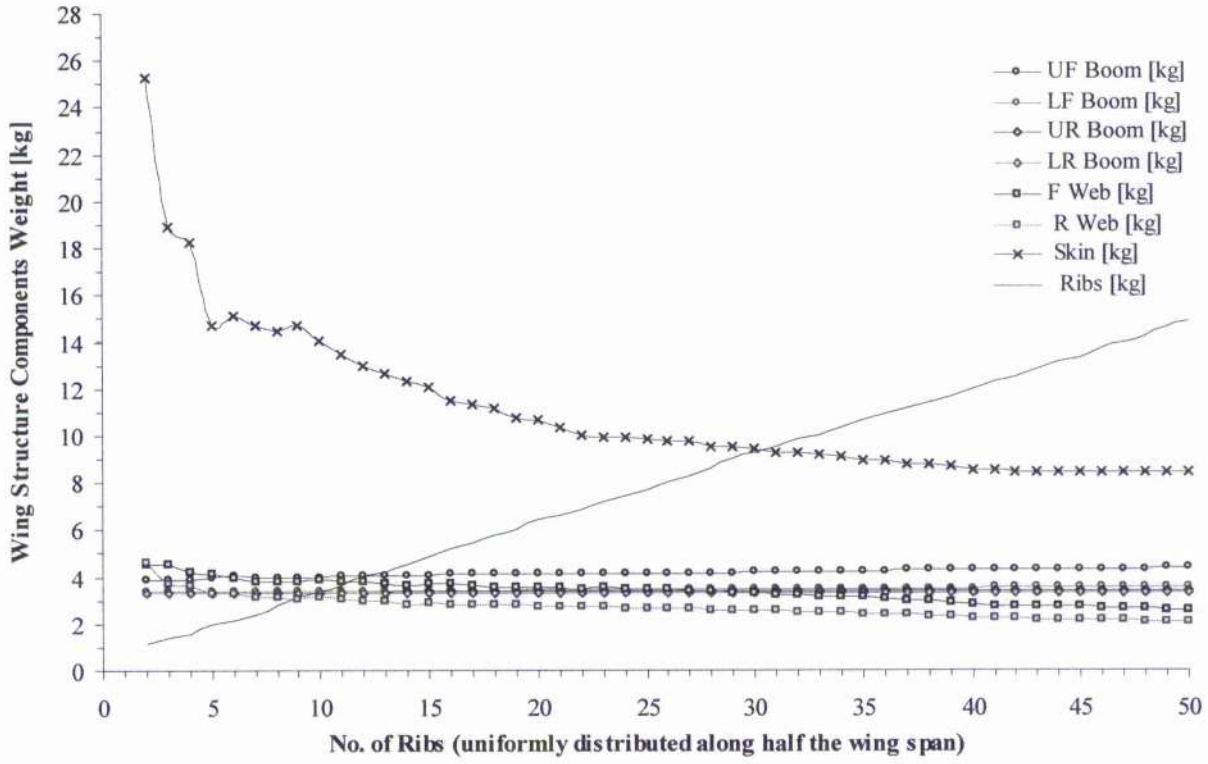

Figure 9.17 - Effect of number of uniformly distributed ribs on the weight of the wing model's components. (Spar load ratio 2:1; Boom dimensions ratio h/H = 0.9; practical dimensions)

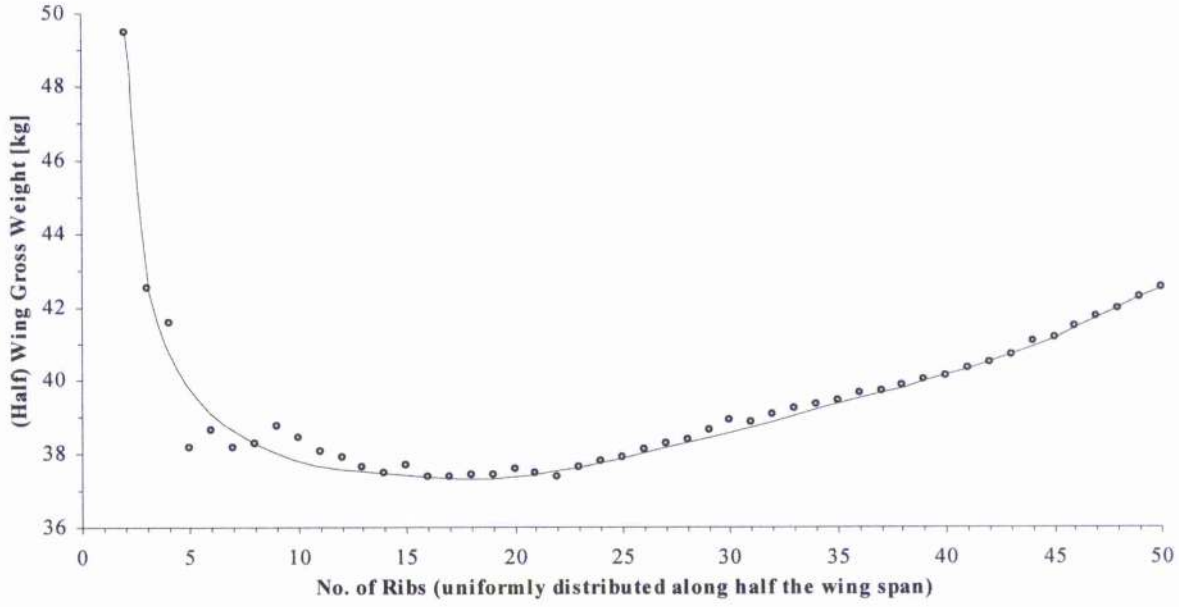

Figure 9.18 - Effect of number of uniformly distributed ribs on the gross weight of the wing model. (Spar load ratio 2:1; Boom dimensions ratio h/H = 0.9; practical dimensions)

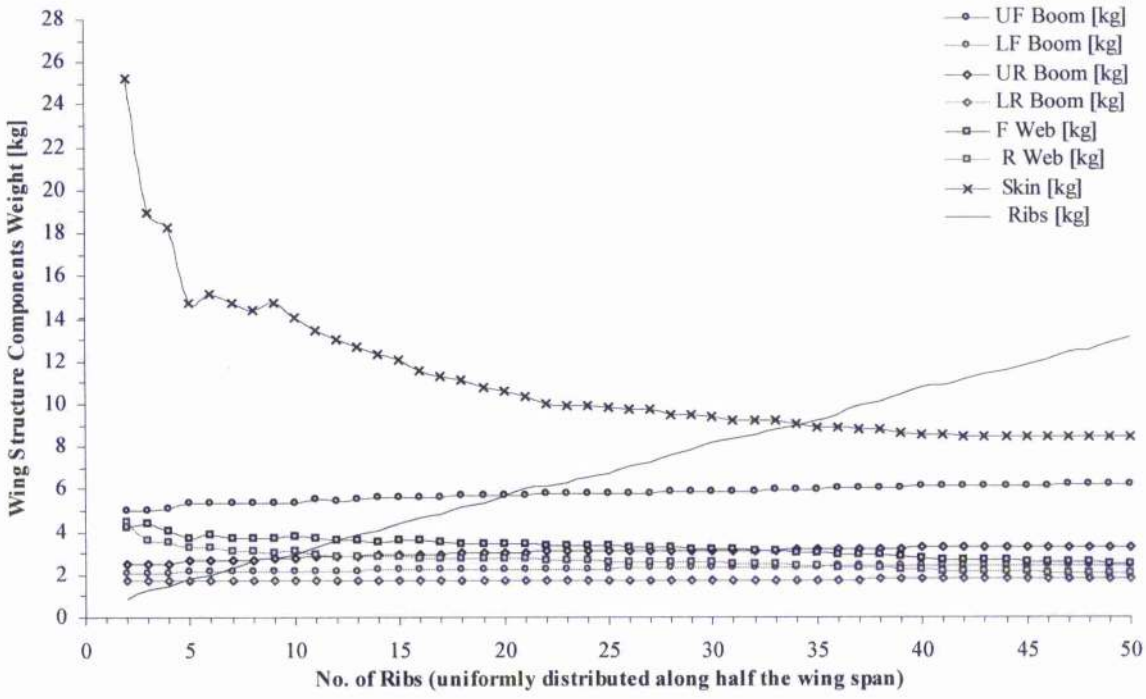

Figure 9.19 - Effect of number of uniformly distributed ribs on the weight of the wing model's components. (Spar load ratio 2:1; Boom dimensions ratio h/H = 0.95; practical dimensions)

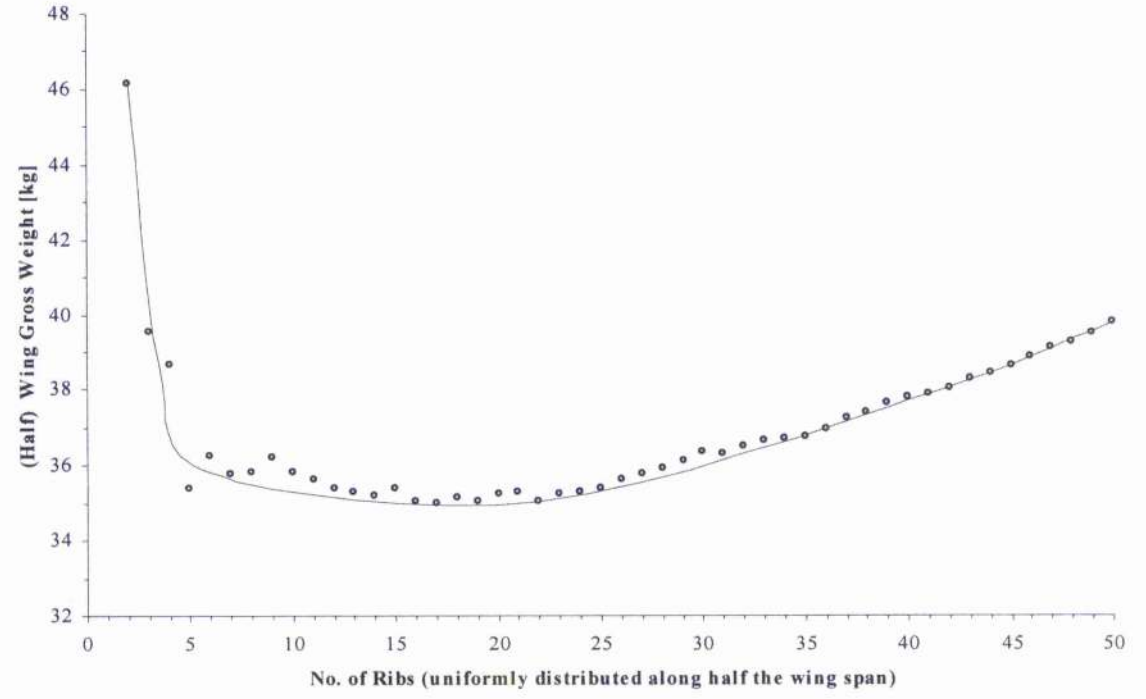

Figure 9.20 - Effect of number of uniformly distributed ribs on the gross weight of the wing model. (Spar load ratio 2:1; Boom dimensions ratio h/H = 0.95; practical dimensions)

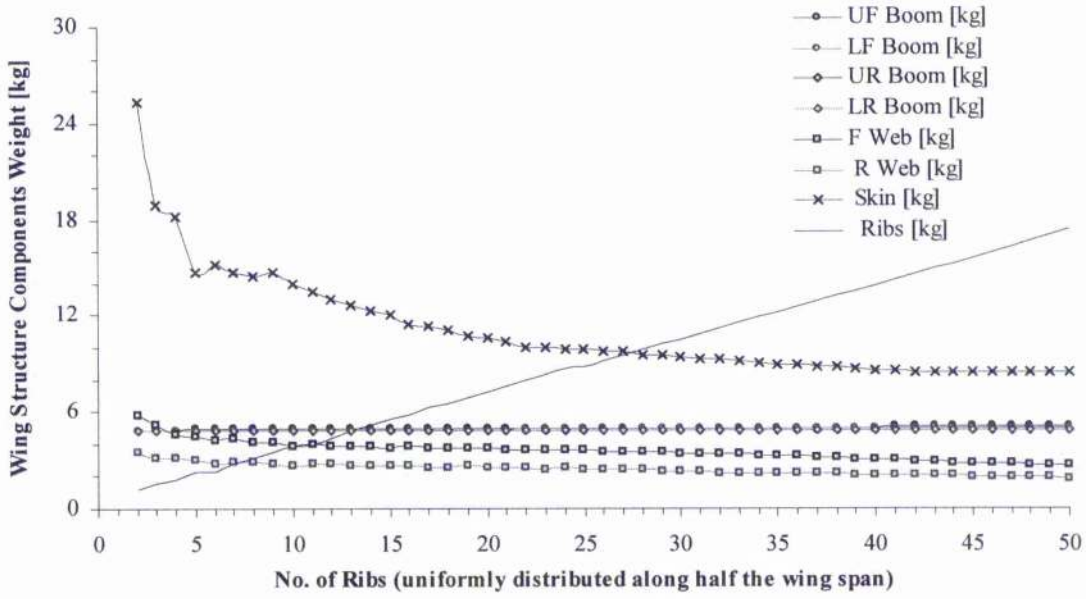

Figure 9.21 - Effect of number of uniformly distributed ribs on the weight of the wing model's components. (Spar load ratio 3:1; Boom dimensions ratio h/H = 0.85; practical dimensions)

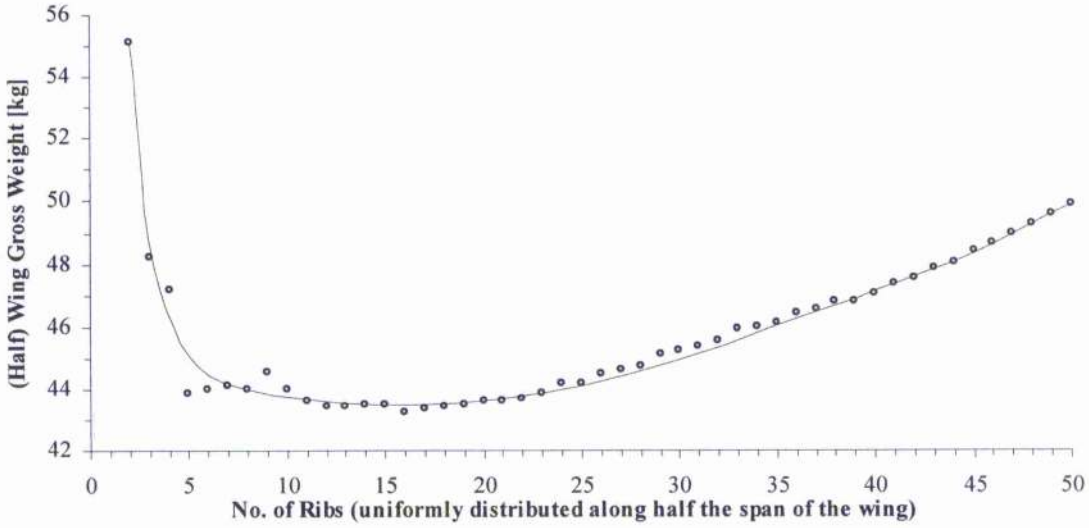

Figure 9.22 - Effect of number of uniformly distributed ribs on the gross weight of the wing model. (Spar load ratio 3:1; Boom dimensions ratio h/H = 0.85; practical dimensions)

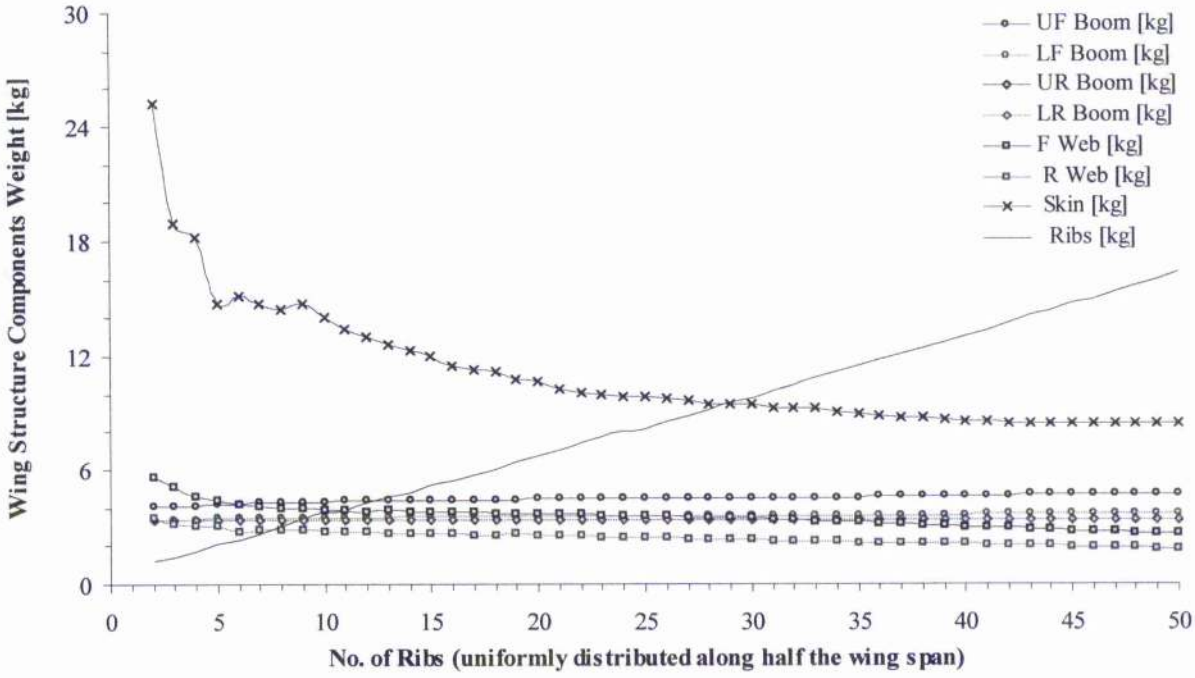

Figure 9.23 - Effect of number of uniformly distributed ribs on the weight of the wing model's components. (Spar load ratio 3:1; Boom dimensions ratio h/H = 0.9; practical dimensions)

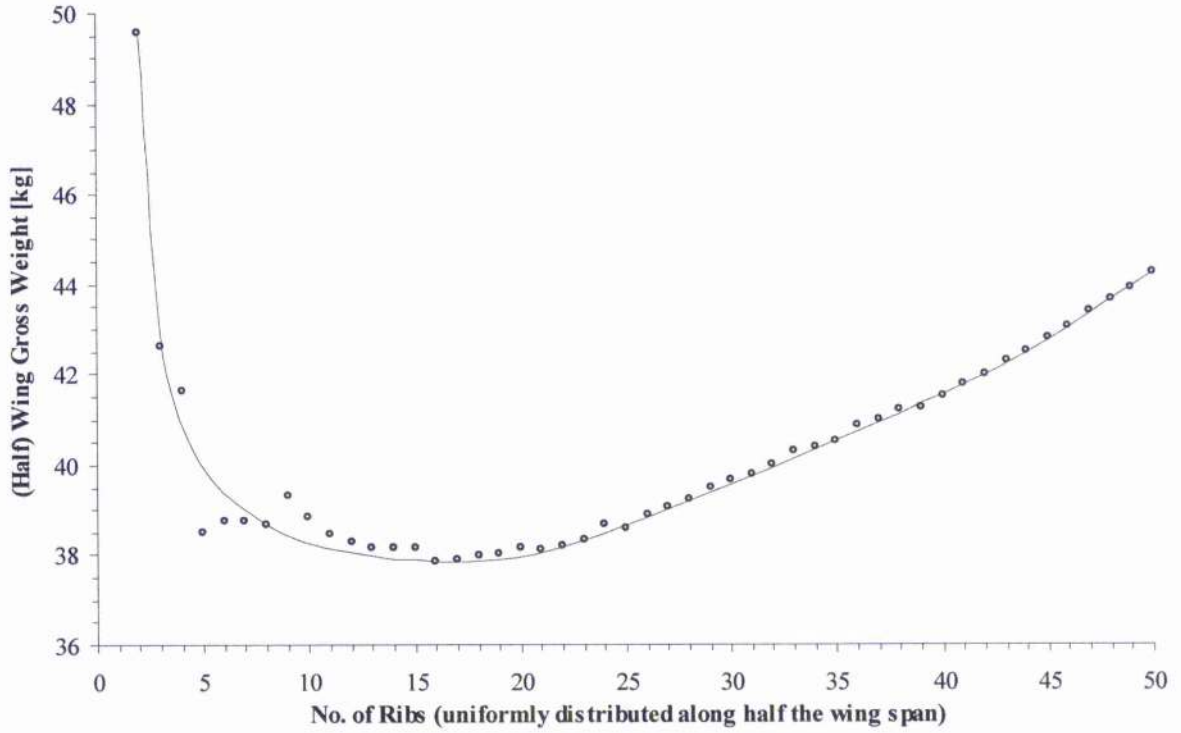

Figure 9.24 - Effect of number of uniformly distributed ribs on the gross weight of the wing model. (Spar load ratio 3:1; Boom dimensions ratio h/H = 0.9; practical dimensions)

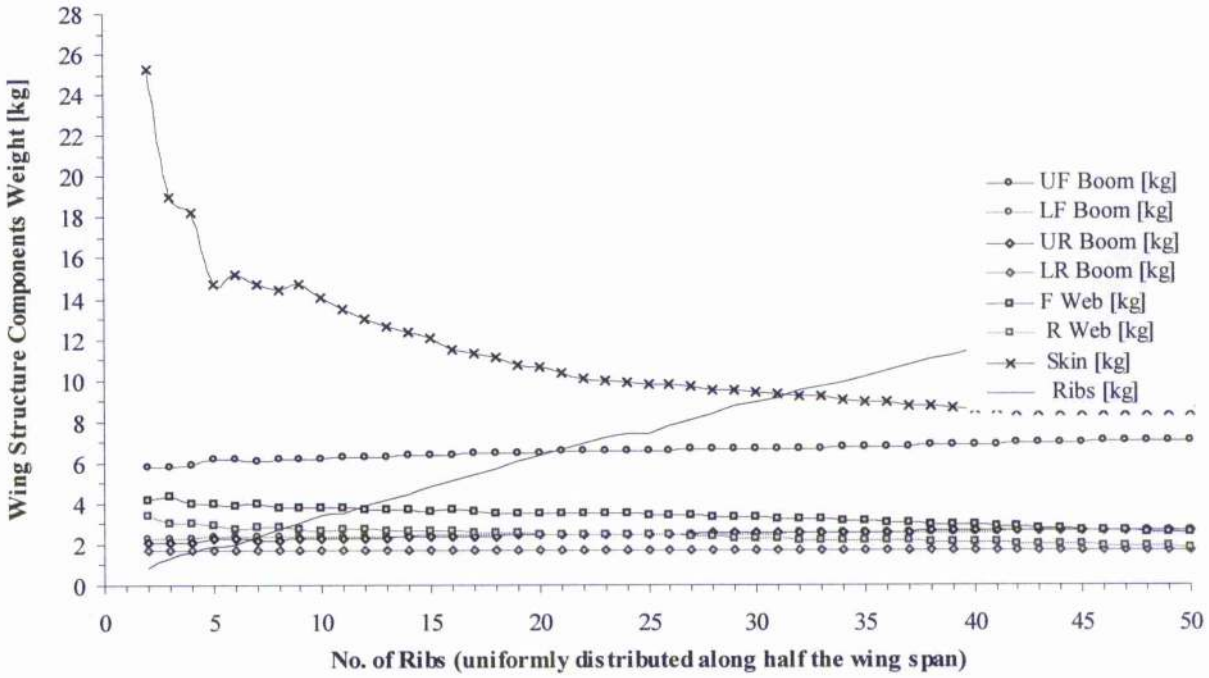

Figure 9.25 - Effect of number of uniformly distributed ribs on the weight of the wing model's components. (Spar load ratio 3:1; Boom dimensions ratio h/H = 0.95; practical dimensions)

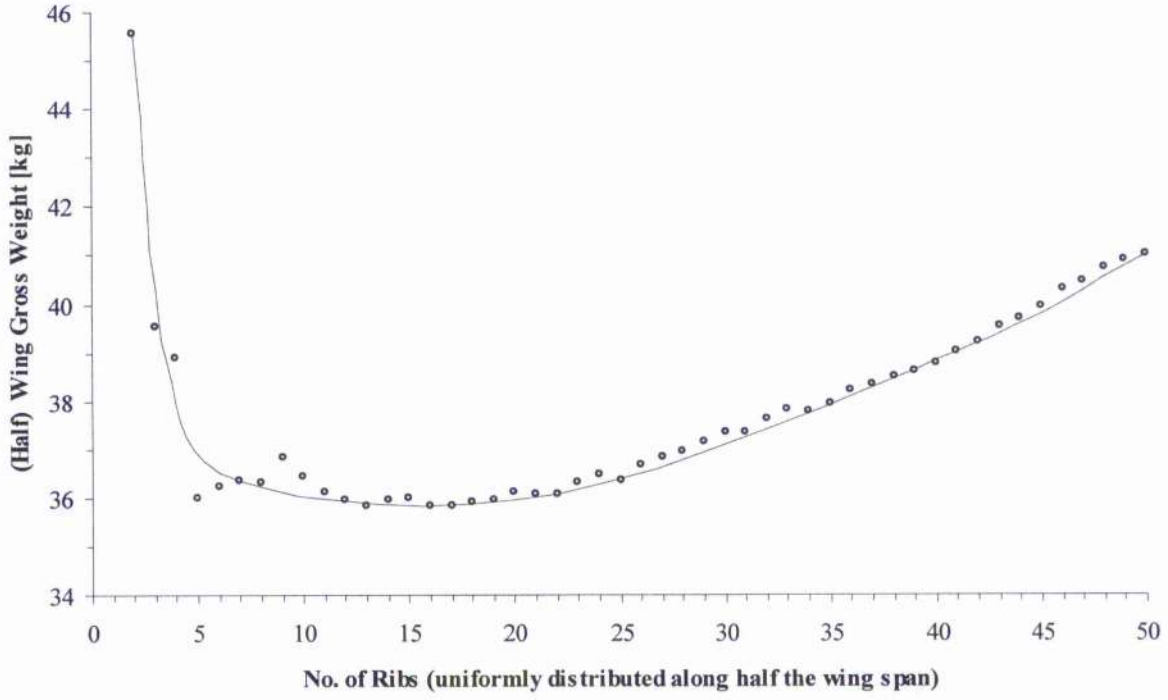

Figure 9.26 - Effect of number of uniformly distributed ribs on the gross weight of the wing model. (Spar load ratio 3:1; Boom dimensions ratio h/H = 0.95; practical dimensions)

Notation:

ts	- Skin Thickness [mm]
h_ef_F	- Effective Hight of the Front Spar [mm]
twF	- Thickness of the Front Web [mm]
HHF	- Dimension [H] of Front Spar Upper Boom [mm]
hHF	- Dimension [h] of Front Spar Upper Boom [mm]
HDF	- Dimension [H] of Front Spar Lower Boom [mm]
hDF	- Dimension [h] of Front Spar Lower Boom [mm]
h_ef_R	- Effective Hight of the Rear Spar [mm]
twR	- Thickness of the Rear Web [mm]
HHR	- Dimension [H] of Rear Spar Upper Boom [mm]
hHR	- Dimension [h] of Rear Spar Upper Boom [mm]
HDR	- Dimension [H] of Rear Spar Lower Boom [mm]
hDR	- Dimension [h] of Rear Spar Lower Boom [mm]
trw	- Rib's Web Thickness [mm]
trFU	- Rib's Upper Flange Thickness [mm]
trFL	- Rib's Lower Flange Thickness [mm]

Spar load ratio 3:1; boom dimension ratio h/H = 0.85

Bay	ts	h_ef_F	twF	HHF	hHF	HDF	hDF	h_ef_R	twR	HHR	hHR	HDR	hDR	trw	trFU	trFL
1	0.4	159.59	0.8	25	21	25	21	159.59	0.6	25	21	25	21	0.6	0.6	1.2
2	0.4	159.59	1	25	21	25	21	159.59	0.8	25	21	25	21	0.8	0.8	1.5
3	0.4	159.59	1.2	25	21	25	21	159.59	0.8	25	21	25	21	0.8	0.8	1.5
4	0.4	159.59	1.5	25	21	25	21	159.59	1	25	21	25	21	0.8	0.8	1.5
5	0.4	159.59	1.5	25	21	25	21	159.59	1	25	21	25	21	1	1	2
6	0.4	159.59	1.5	25	21	25	21	159.59	1	25	21	25	21	1	1	2
7	0.6	159.59	1.5	25	21	25	21	159.59	1.2	25	21	25	21	1	1	2
8	0.6	159.59	2	25	21	25	21	159.59	1.2	25	21	25	21	1	1	2
9	0.6	159.59	2	25	21	25	21	159.59	1.2	25	21	25	21	1	1	2
10	0.6	159.59	2	25	21	25	21	159.59	1.2	25	21	25	21	1.2	1.2	2.5
11	0.8	159.59	2	25	21	25	21	159.59	1.5	25	21	25	21	1.2	1.2	2.5
12	0.8	159.59	2	25	21	25	21	159.59	1.5	25	21	25	21	1.2	1.2	2.5
13	0.8	159.29	2	26.19	22.19	25	21	159.59	1.5	25	21	25	21	1.2	1.2	2.5
14	0.8	157.88	2	28.94	23.94	26.44	22.44	159.59	1.5	25	21	25	21	1.2	1.2	2.5

Figure 9.27 - Adjusted Structure component dimensions of wing with fifteen ribs

Notation:

ts	- Skin Thickness [mm]	twR	- Thickness of the Rear Web [mm]
h_ef_F	- Effective Hight of the Front Spar [mm]	HHR	- Dimension [H] of Rear Spar Upper Boom [mm]
twF	- Thickness of the Front Web [mm]	hHR	- Dimension [h] of Rear Spar Upper Boom [mm]
HHF	- Dimension [H] of Front Spar Upper Boom [mm]	HDR	- Dimension [H] of Rear Spar Lower Boom [mm]
hHF	- Dimension [h] of Front Spar Upper Boom [mm]	hDR	- Dimension [h] of Rear Spar Lower Boom [mm]
HDF	- Dimension [H] of Front Spar Lower Boom [mm]	trw	- Rib's Web Thickness [mm]
hDF	- Dimension [h] of Front Spar Lower Boom [mm]	trFU	- Rib's Upper Flange Thickness [mm]
h_ef_R	- Effective Hight of the Rear Spar [mm]	trFL	- Rib's Lower Flange Thickness [mm]

Spar load ratio 3:1; boom dimension ratio h/H = 0.9

Bay	ts	h_ef_F	twF	HHF	hHF	HDF	hDF	h_ef_R	twR	HHR	hHR	HDR	hDR	trw	trFU	trFL
1	0.4	160.66	0.8	25	22.5	25	22.5	160.66	0.6	25	22.5	25	22.5	0.6	0.6	1.2
2	0.4	160.66	1	25	22.5	25	22.5	160.66	0.8	25	22.5	25	22.5	0.8	0.8	1.5
3	0.4	160.66	1.2	25	22.5	25	22.5	160.66	0.8	25	22.5	25	22.5	0.8	0.8	1.5
4	0.4	160.66	1.5	25	22.5	25	22.5	160.66	1	25	22.5	25	22.5	0.8	0.8	1.5
5	0.4	160.66	1.5	25	22.5	25	22.5	160.66	1	25	22.5	25	22.5	1	1	2
6	0.4	160.66	1.5	25	22.5	25	22.5	160.66	1	25	22.5	25	22.5	1	1	2
7	0.6	160.66	2	25	22.5	25	22.5	160.66	1.2	25	22.5	25	22.5	1	1	2
8	0.6	160.66	2	25	22.5	25	22.5	160.66	1.2	25	22.5	25	22.5	1	1	2
9	0.6	160.66	2	25	22.5	25	22.5	160.66	1.2	25	22.5	25	22.5	1	1	2
10	0.6	159.76	2	27.87	24.87	25	22.5	160.66	1.2	25	22.5	25	22.5	1.2	1.2	2.5
11	0.8	158.57	2	31.17	27.17	25	22.5	160.66	1.5	25	22.5	25	22.5	1.2	1.2	2.5
12	0.8	157.12	2	35.2	31.2	26.02	23.02	160.66	1.5	25	22.5	25	22.5	1.2	1.2	2.5
13	0.8	155.31	2	39.25	35.25	29.21	26.21	160.66	1.5	25	22.5	25	22.5	1	1	2
14	0.8	152.72	2	43.43	38.43	32.48	28.48	160.66	1.5	25	22.5	25	22.5	1	1	2

Spar load ratio 3:1; boom dimension ratio h/H = 0.95

Bay	ts	h_ef_F	twF	HHF	hHF	HDF	hDF	h_ef_R	twR	HHR	hHR	HDR	hDR	trw	trFU	trFL
1	0.4	161.39	0.8	25	23.5	25	23.5	161.39	0.6	25	23.5	25	23.5	0.6	0.6	1.2
2	0.4	161.39	1	25	23.5	25	23.5	161.39	0.8	25	23.5	25	23.5	0.8	0.8	1.5
3	0.4	161.39	1.2	25	23.5	25	23.5	161.39	0.8	25	23.5	25	23.5	0.8	0.8	1.5
4	0.4	161.39	1.5	25	23.5	25	23.5	161.39	1	25	23.5	25	23.5	0.8	0.8	1.5
5	0.4	161.39	1.5	25	23.5	25	23.5	161.39	1	25	23.5	25	23.5	1	1	2
6	0.4	160.33	1.5	29.22	27.72	25	23.5	161.39	1	25	23.5	25	23.5	1	1	2
7	0.6	158.57	1.5	35.52	33.52	25	23.5	161.39	1.2	25	23.5	25	23.5	1	1	2
8	0.6	157.12	2	40.59	38.09	25	23.5	161.39	1.2	25	23.5	25	23.5	1	1	2
9	0.6	155.19	2	48.3	45.8	25	23.5	161.16	1.2	25.9	24.4	25	23.5	1	1	2
10	0.6	152.01	2	56.19	53.19	29.09	27.59	159.67	1.2	31.11	29.11	25	23.5	1	1	2
11	0.8	148.71	2	63.31	59.31	32.95	30.95	159.65	1.5	31.22	29.22	25	23.5	1	1	2
12	0.8	145.45	2	71.46	67.46	37.82	35.82	158.33	1.5	36.49	34.49	25	23.5	1	1	2
13	0.8	141.95	2	79.8	75.8	42.75	40.25	156.86	1.5	41.61	39.11	25	23.5	0.8	0.8	2
14	0.8	138.32	2	88.12	83.12	47.45	44.95	156.08	1.5	44.73	42.23	25	23.5	0.8	0.8	2

Figure 9.28 - Comparison of wing structure dimensions according to the ratio [h/H]
(the boom dimension ratio h/H = 0.85 see Figure 11.26)

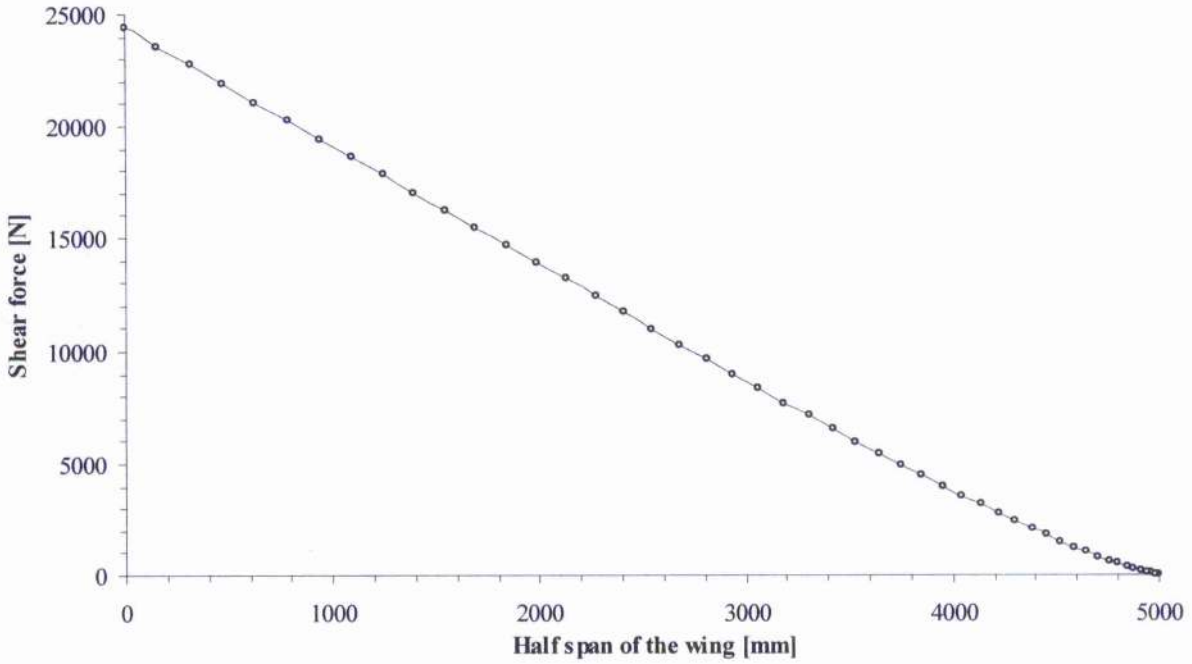

Figure 9.29 – The shear force distribution along half the span of the wing (Aircraft Weight 800 kg)

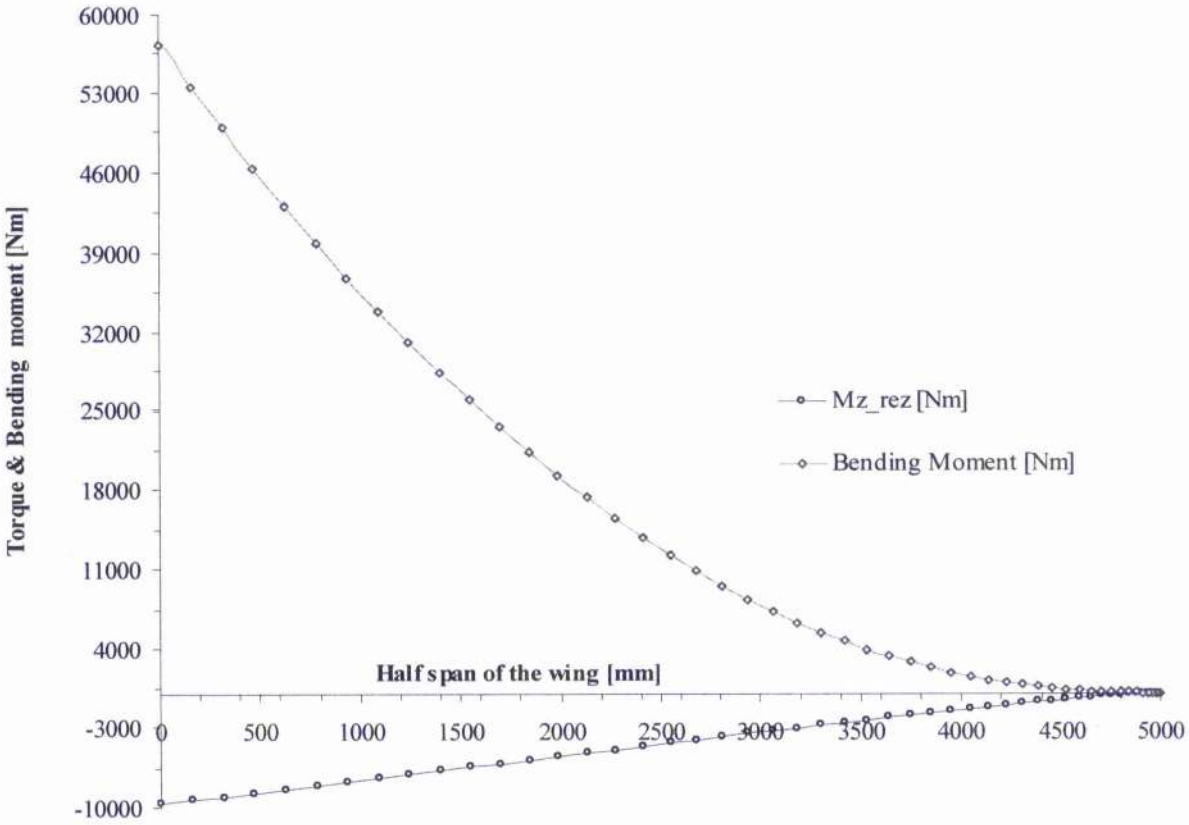

Figure 9.30 – The bending and torque moment distribution along half the span of the wing (Aircraft Weight 800 kg)

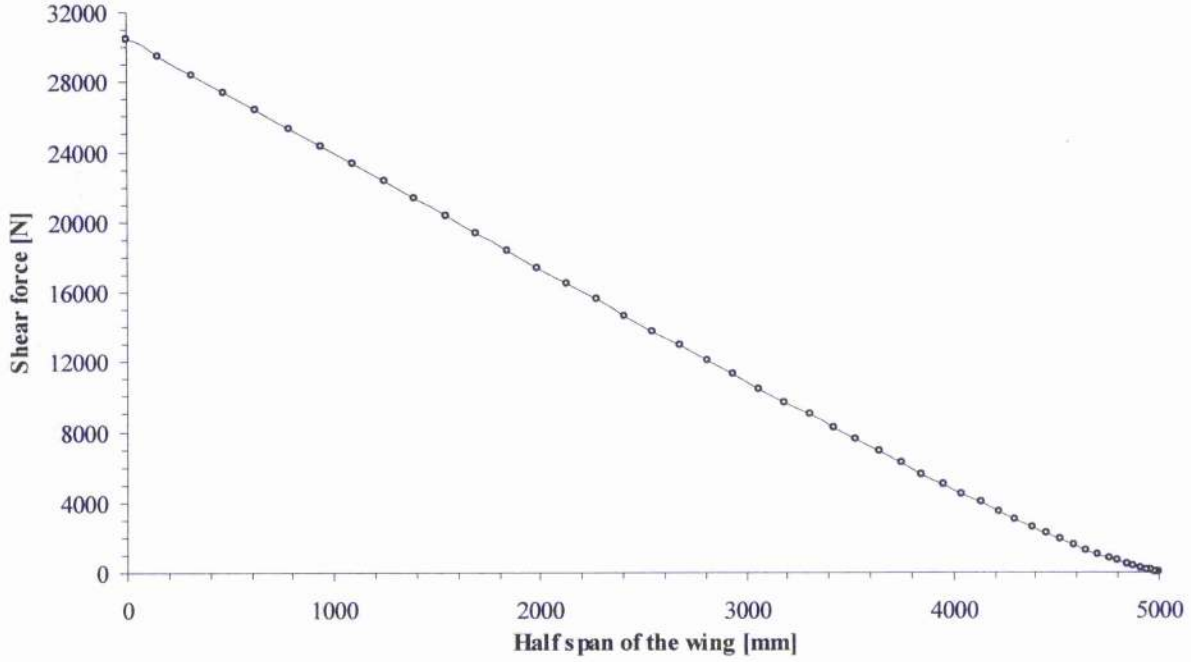

Figure 9.31 – The shear force distribution along half the span of the wing (Aircraft Weight 1000kg)

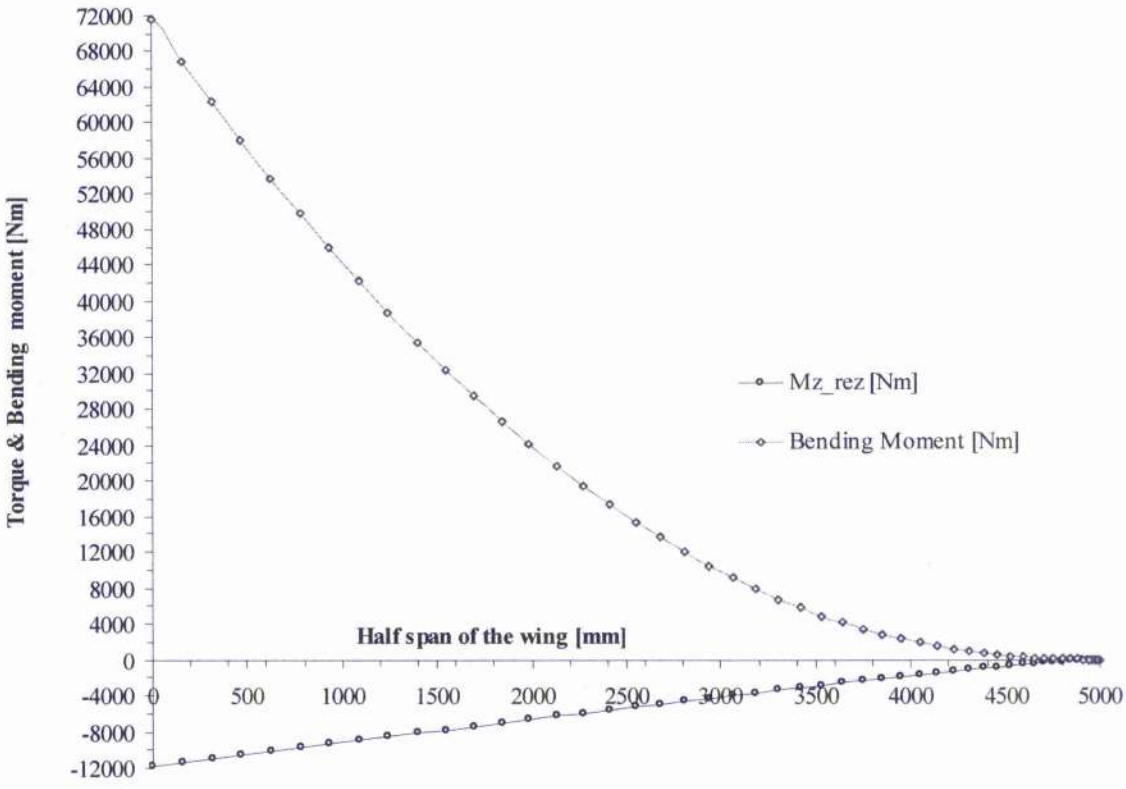

Figure 9.32 – The bending and torque moment distribution along half the span of the wing (Aircraft Weight 1000 kg)

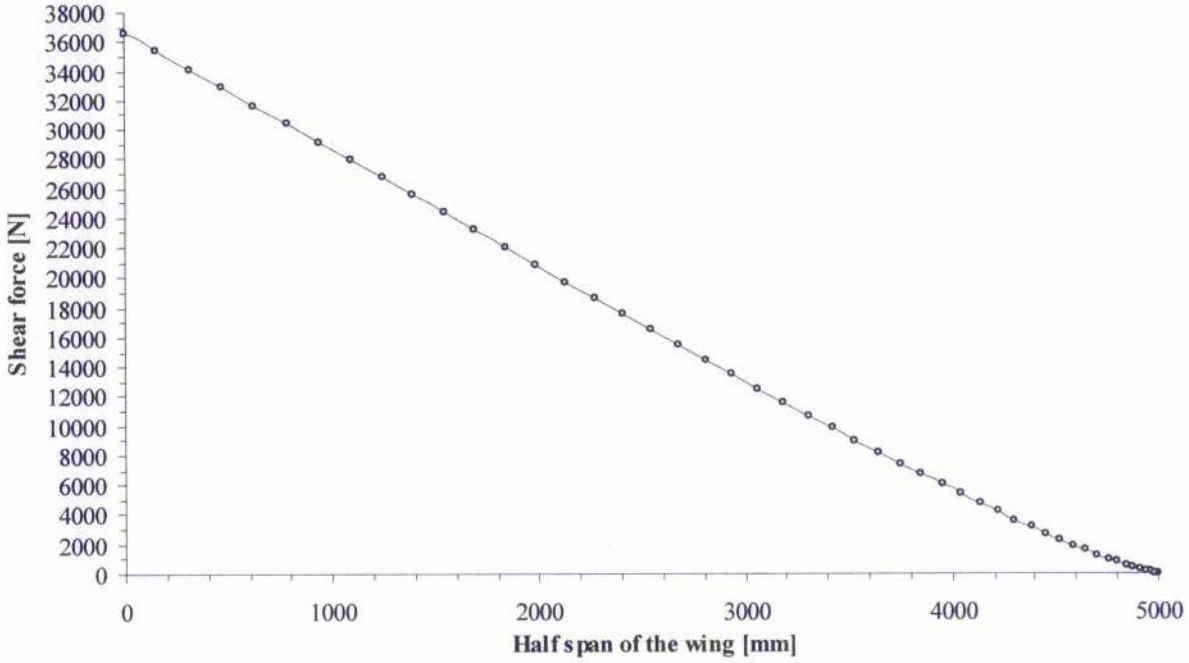

Figure 9.33 – The shear force distribution along half the span of the wing (Aircraft Weight 1200 kg)

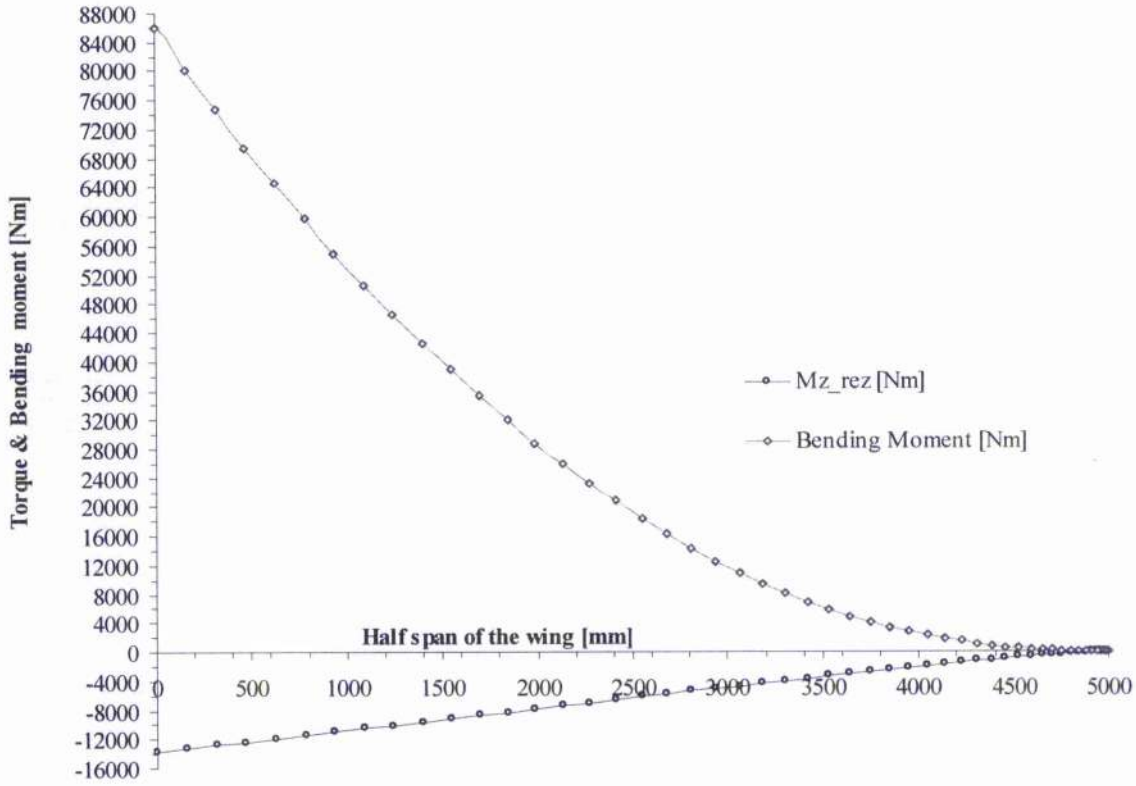

Figure 9.34 – The bending and torque moment distribution along half the span of the wing (Aircraft Weight 1200 kg)

I_z = 3.73E-06 m^4
L = 0.111111 m
E = 7.20E+10 Pa

Displacements Front Upper Boom		
Nod	9	105
u_x [m]	0.00E+00	3.49E-06
u_y [m]	0.00E+00	6.91E-05
u_z [m]	0.00E+00	-5.95E-05
φ_x [Rad]	0.00E+00	-1.23E-03
φ_y [Rad]	0.00E+00	6.02E-05
φ_z [Rad]	0.00E+00	1.63E-03

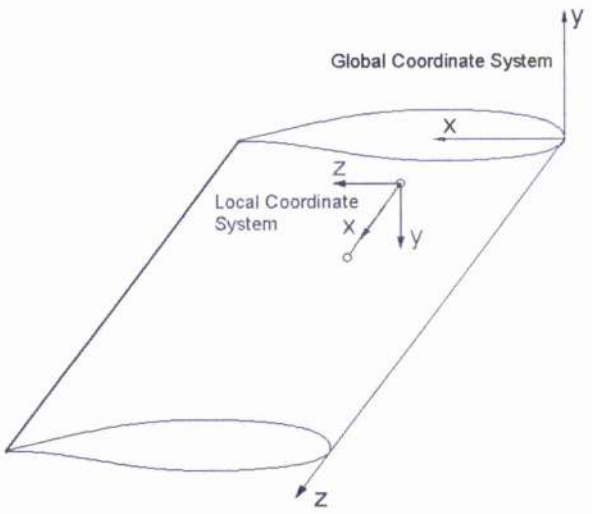

Model of the front upper boom at the root of the wing:

Member Stiffness Matrix $\mathbf{k}^*$

$$\mathbf{k}^* = EI/L^3 \begin{pmatrix} -12 & -6L & 12 & -6L \\ -6L & 4L^2 & -6L & 2L^2 \\ 12 & -6L & 12 & -6L \\ -6L & 2L^2 & -6L & -4L^2 \end{pmatrix}$$

Front Spar, Upper boom:

EI/L^3 = 5.14E+08

Nod [i]: 9
Nod [j]: 105

-6.2E+09	-3.4E+08	6.17E+09	-3.4E+08
3.43E+08	25389365	-3.4E+08	12694683
-6.2E+09	-3.4E+08	6.17E+09	-3.4E+08
-3.4E+08	-1.3E+07	3.43E+08	-2.5E+07

$\mathbf{u}^*$
u_y; φ_z
0.00E+00
0.00E+00
-6.91E-05
-1.23E-03

f^* LOCAL COOR. SYS	
$F_{H(9)}$ =	**-5517.69** N
M_9 =	**8094.73** Nm
$F_{H(105)}$ =	**-5517.69** N
M_{105} =	**7481.65** Nm

Figure 9.35 – Boom Axial Force recovery from the FEM Analysis